energies

MDPI

Review

Predicting CO_2 and H_2 Solubility in Pure Water and Various Aqueous Systems: Implication for CO_2–EOR, Carbon Capture and Sequestration, Natural Hydrogen Production and Underground Hydrogen Storage

Promise O. Longe [1,2], David Kwaku Danso [1,2], Gideon Gyamfi [1], Jyun Syung Tsau [1,2], Mubarak M. Alhajeri [3], Mojdeh Rasoulzadeh [4], Xiaoli Li [1] and Reza Ghahfarokhi Barati [1,2,*]

1 Department of Chemical and Petroleum Engineering, University of Kansas, Lawrence, KS 66045, USA; longe.promise@ku.edu (P.O.L.); kwakudanso@ku.edu (D.K.D.); gyamfigideon@ku.edu (G.G.); tsau@ku.edu (J.S.T.); li.xiaoli@ku.edu (X.L.)
2 Tertiary Oil Recovery Program (TORP), University of Kansas, Lawrence, KS 66045, USA
3 Public Authority for Applied Education & Training (PAAET), Shuwaikh 70654, Kuwait; mm.alhajeri@paaet.edu.kw
4 Department of Mathematics, University of Alabama, Tuscaloosa, AL 35487, USA; mrasoulzadeh@ua.edu
* Correspondence: rezab@ku.edu

Abstract: The growing energy demand and the need for climate mitigation strategies have spurred interest in the application of CO_2–enhanced oil recovery (CO_2–EOR) and carbon capture, utilization, and storage (CCUS). Furthermore, natural hydrogen (H_2) production and underground hydrogen storage (UHS) in geological media have emerged as promising technologies for cleaner energy and achieving net–zero emissions. However, selecting a suitable geological storage medium is complex, as it depends on the physicochemical and petrophysical characteristics of the host rock. Solubility is a key factor affecting the above–mentioned processes, and it is critical to understand phase distribution and estimating trapping capacities. This paper conducts a succinct review of predictive techniques and present novel simple and non–iterative predictive models for swift and reliable prediction of solubility behaviors in CO_2–brine and H_2–brine systems under varying conditions of pressure, temperature, and salinity (T–P–m salts), which are crucial for many geological and energy–related applications. The proposed models predict CO_2 solubility in CO_2 + H_2O and CO_2 + brine systems containing mixed salts and various single salt systems (Na^+, K^+, Ca^{2+}, Mg^{2+}, Cl^-, $SO_4{}^{2-}$) under typical geological conditions (273.15–523.15 K, 0–71 MPa), as well as H_2 solubility in H_2 + H_2O and H_2 + brine systems containing NaCl (273.15–630 K, 0–101 MPa). The proposed models are validated against experimental data, with average absolute errors for CO_2 solubility in pure water and brine ranging between 8.19 and 8.80% and for H_2 solubility in pure water and brine between 4.03 and 9.91%, respectively. These results demonstrate that the models can accurately predict solubility over a wide range of conditions while remaining computationally efficient compared to traditional models. Importantly, the proposed models can reproduce abrupt variations in phase composition during phase transitions and account for the influence of different ions on CO_2 solubility. The solubility models accurately capture the salting–out (SO) characteristics of CO_2 and H_2 gas in various types of salt systems which are consistent with previous studies. The simplified solubility models for CO_2 and H_2 presented in this study offer significant advantages over conventional approaches, including computational efficiency and accuracy across a wide range of geological conditions. The explicit, derivative–continuous nature of these models eliminates the need for iterative algorithms, making them suitable for integration into large–scale multiphase flow simulations. This work contributes to the field by offering reliable tools for modeling solubility in various subsurface energy and environmental–related applications, facilitating their application in energy transition strategies aimed at reducing carbon emissions.

Keywords: CO_2 solubility; H_2 solubility; geologic carbon storage; underground hydrogen storage; natural hydrogen production; experimental data; predictive models

Citation: Longe, P.O.; Danso, D.K.; Gyamfi, G.; Tsau, J.S.; Alhajeri, M.M.; Rasoulzadeh, M.; Li, X.; Barati, R.G. Predicting CO_2 and H_2 Solubility in Pure Water and Various Aqueous Systems: Implication for CO_2–EOR, Carbon Capture and Sequestration, Natural Hydrogen Production and Underground Hydrogen Storage. *Energies* **2024**, *17*, 5723. https://doi.org/10.3390/en17225723

Academic Editor: Nikolaos Koukouzas

Received: 11 September 2024
Revised: 27 October 2024
Accepted: 7 November 2024
Published: 15 November 2024

1. Introduction

Mitigating CO_2 emissions through carbon capture and storage (CCS) and carbon capture, utilization, and storage (CCUS) is an increasingly promising approach to curbing the rise of temperature on earth [1–3]. Geologic formations such as deep saline aquifers [4], depleted oil and gas reservoirs [5–7] and unmineable coal seams are examples of structures viable for CO_2 storage [8]. Among these, deep saline aquifers have the most significant storage potential. Carbon capture and storage (CCS) in saline aquifers depends on four fundamental mechanisms: structural/stratigraphic, dissolution/solubility, capillary/residual, and mineral trapping [9]. Dissolution trapping involves CO_2 dissolving into the brine, which decreases its buoyancy, whereas capillary trapping holds CO_2 in rock pores [10]. Mineral trapping occurs when CO_2 reacts with minerals to form stable carbonates that ensure long–term storage [11]. When CO_2 is injected into a geological formation, it dissolves into the reservoir brine, increasing the brine density and creating a density gradient [12]. This gradient induces convective mixing, which speeds up the dissolution of CO_2 and enhances solubility trapping. The effectiveness of dissolution trapping is crucial for successful geological carbon storage. Furthermore, the interaction between CO_2 and brine solubility significantly impacts long–term storage security and the reservoir's complex physical and chemical interactions among minerals and fluids. To accurately evaluate these effects and optimize carbon storage, a reliable model for predicting CO_2 solubility in reservoir brines under geological conditions is essential [13].

Predictive solubility models are essential not only for CO_2 storage but also for CO_2 utilization in enhanced oil recovery (EOR) projects [5,14–16]. These models are crucial in determining the amount of CO_2 that can be stored during EOR and the volume of CO_2 that is miscible with the oil front for improved recovery—for instance, Pi et al. [17] observed a decrease in the pH of formation water during CO_2 flooding in rock cores. They also recorded a reduction in the minimum miscibility pressure as the salinity of connate water in rock cores increased. This indicates changes in CO_2 concentration within the porous media at lower salinity levels of connate water. When modeling CO_2–EOR, it is essential to have reliable CO_2 dissolution models to accurately represent the amounts of CO_2 available for compositional interaction with the oil front. Similarly, during water–alternating–gas (WAG) injection, the salinity of injected water has been noted as a critical factor in creating optimal miscible flood fronts [18]. For example, saline–injected water with 1–2 wt.% showed good synergy and improved oil recovery. These solubility predictive models can also provide insight into the concentration or volume of CO_2 available for miscibility with oil front. Another scenario in which predictive models are essential is during the drilling of acid gas reservoirs. Acid gas reservoirs contain high amounts of CO_2, which have the potential to dissolve in water–based or oil–based drilling fluid [19,20]. The dissolution degree depends on the drilling fluid downhole salinity, pressure, and temperature. Near the wellhead, the dissolved gas will separate from the aqueous phase and expand rapidly due to a decrease in gas solubility. Therefore, the gas kick commonly exhibits the characteristics of early latency and late burst, which brings significant challenges to the safety of well control [21]. To improve safety, CO_2 predictive models can help understand the degree of solubility and well control choking required for the wellhead's safety.

In UHS, hydrogen is stored within geological formations, with its capacity and security maintained by specific trapping mechanisms akin to those used for CO_2 storage. These mechanisms include (a) structural or stratigraphic trapping [22,23], (b) residual or capillary trapping [6,24], (c) mineral trapping, (d) dissolution trapping [25], and (e) the more recently studied adsorption trapping potential of coal seams [26,27] or shale [28]. A graphical illustration of these mechanisms is shown in Figure 1. Among these trapping phenomena, trapping by solubility in aqueous media offers the highest efficiency because it requires minimal monitoring and maintenance compared to capillary trapping, which requires close monitoring. Unfortunately, storing hydrogen at surface facilities is challenging because

of its low density, thereby requiring high pressures to adequately compress it due to its high diffusivity [29]. Furthermore, H_2 has a low ignition temperature that makes it highly inflammable. Hence, the safest place to store H_2 is likely underground [30,31]. The storage of H_2 in geologic structures is regarded as the most feasible option for large–scale energy storage on a global basis, mimicking the carbon capture and utilization of the storage industry. In particular, salt caverns previously used for hydrocarbon storage are promising geologic candidates for UHS [32]. The interest in salt caverns is primarily due to the high capacity, rapid operation, and minimal contamination risk. However, cavern storage may be constrained by geography and transportation costs. Alternatively, depleted hydrocarbon reservoirs provide established infrastructure and proven containment capabilities for hydrogen storage. However, there are concerns about H_2 mixing with the residual hydrocarbons or reacting with underground minerals. Saline aquifers trap CO_2 effectively in CCUS but need more study for H_2 storage due to potential interactions with brine and rock minerals. Further, hard rock caverns (e.g., granite) offer stability but are costly to develop and may leak if not sealed properly.

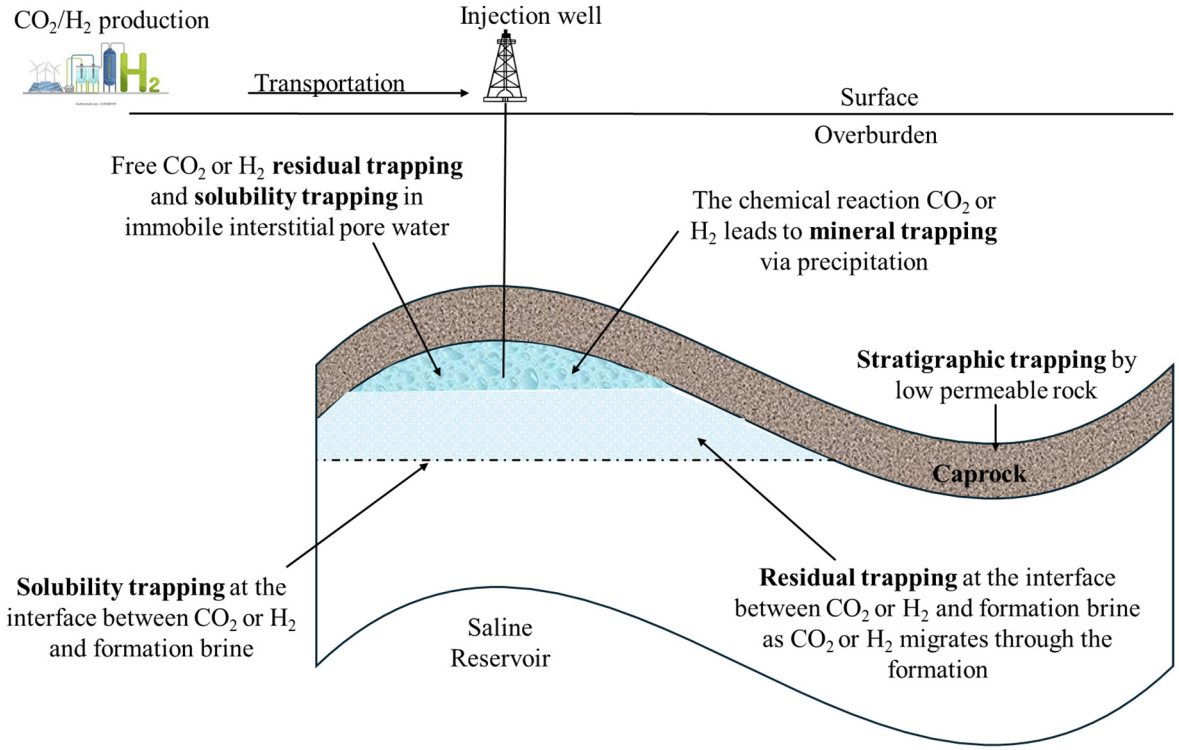

Figure 1. A diagram showing the working gas (CO_2 or H_2) of underground gas storage (UGS) in the subsurface formation. (Adapted and modified from Muhammed et al. [30]).

Raza et al. [33] conducted a review on underground hydrogen storage, and they concluded that the accurate prediction of H_2 solubility across a wide range of geographical depth–dependent temperatures, pressures, and salinities (T–P–S) is vital for assessing the feasibility of storing hydrogen in geological formations such as aquifers depleted oil and gas fields, and salt caverns [30,32,34]. This understanding is essential not only for determining the storage capacity and retention potential but also for evaluating the risks of hydrogen loss due to dissolution into formation waters or reactions with minerals [35].

Secondly, evaluating the natural production of hydrogen requires knowledge of the solubility of H_2 in the subterranean environment, particularly from serpentinization processes. Serpentinization is a metamorphic process in which mainly ultramafic rocks are oxidized by water into serpentine, producing hydrogen [36]. A typical ultramafic rock is a peridotite, which contains olivine and fayalite minerals that undergo oxidation to release H_2 into brines at temperatures between 200 to 300 °C. Pressure has also been reported to

increase the rate of peridotite serpentinization [37]. The salinity of the water is a crucial factor in the serpentinization process, as reported by [38]. The authors reported a decrease in serpentinization rates as salinity and concentration of dissolved Mg increase. Hence, predictive models that can estimate H_2 solubility may be vital in evaluating the H_2–producing potential of target ultramafic rocks. These factors influence the solubility and subsequent migration of hydrogen in subsurface environments [39]. The solubility of hydrogen in these settings can control the concentration of hydrogen that accumulates in fractures and pores, ultimately affecting the efficiency of hydrogen extraction [40].

Critical factors influencing geological carbon storage (GCS) and underground hydrogen storage (UHS) can be broadly categorized into solid, fluid, and solid–fluid interaction factors [30]. Solid factors include absolute permeability and effective porosity, which dictate the capacity and efficiency of the storage formations. Fluid factors such as fluid density, viscosity, solubility, and diffusivity govern the behavior and movement of the gases within the storage medium. Meanwhile, solid–fluid interaction factors like wettability, solid–fluid interfacial tension, capillary pressure, relative permeability, mobility ratio, and adsorption–desorption processes play crucial roles in determining the ease with which gases can be injected, stored, and retained within the geological formations. Figure 2 presents the classifications of the parameters influencing the storage of hydrogen gas in subsurface formation. Understanding these parameters is essential for optimizing storage strategies and ensuring the long–term stability and safety of CO_2 and H_2 storage. Solubility is a key parameter that impacts several of the other parameters significantly.

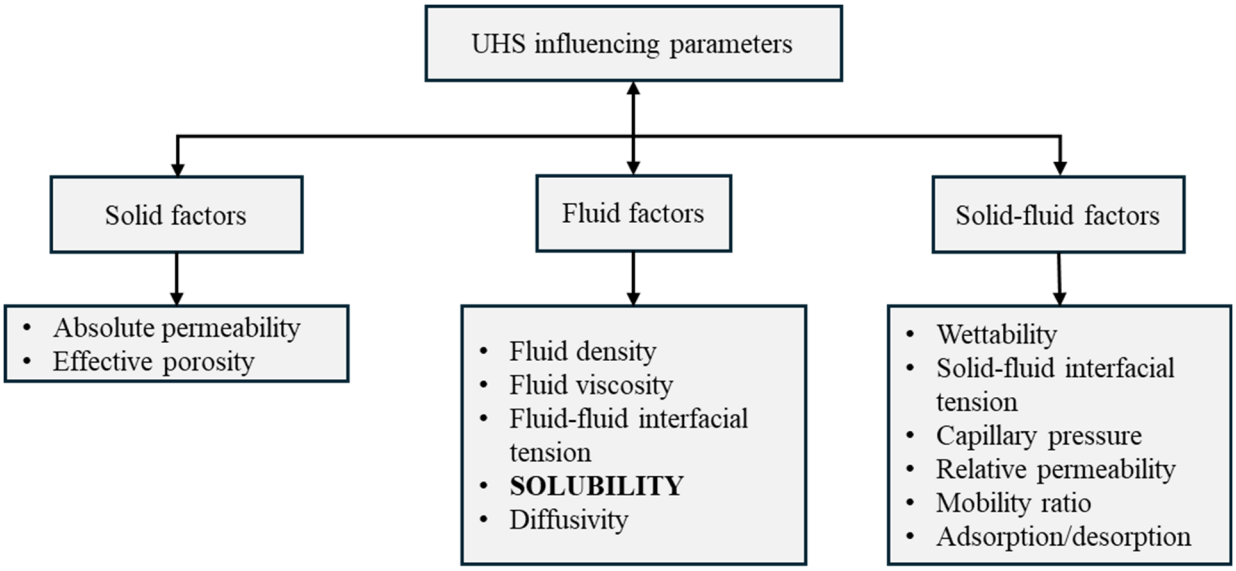

Figure 2. Hydrodynamic parameters influencing GCS and UHS (Adapted and modified from Muhammed et al. [30]).

Given the complexity and the plethora of parameters influencing GCS, UHS, and natural hydrogen production, this paper focuses on the solubility factors of CO_2 and H_2 in water and saline systems, which are pivotal for various subsurface and industrial applications. The solubility of CO_2 and H_2 in solvent directly affects the capacity and stability of the stored gases, influencing how CO_2 and H_2 interact with the storage medium at a molecular and pore–scale level. The critical review of techniques for predicting CO_2 solubility and H_2 solubility, concludes that currently available predictive models employed in predicting CO_2 solubility and H_2 solubility from equation of state (EoS) to machine learning models (ML) have the following limitations: EoS modelling [41–53] involve iterative approach that might have convergence problems, most of published empirical models [54–59] also involve iterative method and many parameters, Molecular dynamic simulation [44,60–65] require additional parameter and high computation costs, and ML

models [66–72] lack interpretability. Therefore, we proposed simple, non–iterative and reliable models to accurately predict CO_2 solubility and H_2 solubility in pure water and various salt systems. This paper contributes to the body of knowledge by enhancing the understanding of CO_2 solubility in natural formation brines, aiding in the assessment of CO_2 and H_2 storage capacity and the long–term behavior of CO_2 and H_2 at storage sites in the context of GCS, UHS, and natural hydrogen production.

The rest of the paper's sections following the introduction are outlined as follows: Section 2 provides a concise review of the progress of experimental work and different techniques of modeling the solubility of CO_2 and H_2 in water and saline systems. Section 3 focuses on analyzing the collected CO_2 and H_2 solubility data and developing CO_2 and H_2 correlations. Section 4 presents the validation and evaluation of the predicted performance of the developed CO_2 and H_2 solubility correlations. Also, discusses the salting out characteristics of CO_2 and H_2 in various brine solutions. Lastly, Section 5 provides major findings and limitations of the study.

2. Literature Review

This section briefly reviews the state–of–the–art techniques on CO_2 and H_2 solubility determination in various pure water and aqueous systems. The techniques include experimental works, equation of state (EoS) models, empirical correlations, molecular dynamics simulations (MDS), and machine learning (ML) techniques. Each approach offers unique insights and advantages that contribute to a deeper understanding of gas solubility under diverse conditions with implications for both large–scale industrial applications and scientific research.

2.1. Carbon Dioxide (CO_2)

Knowledge of CO_2 solubility in geological fluids is essential for studying fluid inclusions [73], carbonate precipitation [74–76], and the global carbon cycle. Despite extensive research, accurately predicting CO_2 solubility across different temperatures, pressures, and ionic strengths remains a challenge. Researchers have primarily focused on CO_2 solubility in water and NaCl solutions, which are common in geological fluids [73]. Among potential long–term CO_2 storage sites, deep saline aquifers stand out, with an estimated storage capacity of 2400 to 21,600 billion metric tons [77]. To estimate this storage potential accurately, it is crucial to evaluate the pore volume available for supercritical CO_2 storage and the capacity for CO_2 to dissolve into the brine. Understanding how CO_2 dissolves in brine and groundwater helps predict possible migration pathways and environmental impacts, especially in the event of a leak. CO_2 solubility is influenced by factors like temperature, pressure, and solute concentrations, which can vary both between and within different formations [13,78].

2.1.1. CO_2 Solubility–Experimental Works

Carbon dioxide (CO_2) solubility in water has been extensively studied over the years due to its relevance in various industrial and environmental applications, including carbon sequestration, enhanced oil recovery, and understanding natural carbon cycles. Various experimental techniques have been employed to explore CO_2 solubility in water under different conditions (see Table 1). Among the earliest and most influential studies were those by Wiebe and Gaddy [79], who investigated the CO_2 solubility in water at temperatures ranging from 323 to 373 K and pressures approaching 71 MPa. Their work has provided foundational data for the study of CO_2 behavior under sequestration conditions. In the literature, the highest pressure at which CO_2 solubility in water has been experimentally measured is around 350 MPa, according to studies by Todheide and Franck [80], and later by Takenouchi and Kennedy [81,82]. These works significantly expanded the understanding of CO_2 solubility across a wide range of temperatures (323 to 623 K) and pressures (up to 350 MPa), offering critical insights into CO_2 behavior in deep geological formations. Finally, the study of CO_2 solubility in water and aqueous salt solutions has made consid-

erable progress, with a rich database of experimental data now available for modeling efforts. However, the field still faces challenges, particularly in obtaining high–quality data for mixed–salt solutions and under extreme conditions. Continued experimental and theoretical work is necessary to build refined models and enhance the understanding of CO_2 behavior in these complex systems.

Table 1. Published experimental studies of CO_2 solubility in water and aqueous systems in the compiled database.

References	Data Points	T_{min} (K)	T_{max} (K)	P_{min} (MPa)	P_{max} (MPa)	S_{min} (mol/kg)	S_{max} (mol/kg)	Systems
Hou et al. (b) [46] *	71	323.15	423.15	2.6	18.2	2.50	4.00	KCl, NaCl
Todheide and Franck [80] *	104	323.15	623.15	10.0	350.0	0.00	0.00	H_2O
Takenouchi and Kennedy (b) [81] *	21	423.15	723.15	10.0	140.0	0.00	4.28	H_2O, NaCl
Takenouchi and Kennedy (a) [82] *	116	383.15	573.15	10.0	150.0	0.00	0.00	H_2O
King et al. [83]*	28	288.15	298.15	6.1	24.3	0.00	0.00	H_2O
Ahmandi and Chapoy [84] *	29	300.95	423.48	1.3	42.1	0.00	0.00	H_2O
Al Ghafri, S.Z.S. [85] *	8	323.15	323.15	2.1	18.7	0.00	0.00	H_2O
Anderson, G.K. [86] *	54	274.15	288.15	0.1	2.2	0.00	0.00	H_2O
Bamberger et al. [87] *	29	323.20	353.10	4.1	14.1	0.00	0.00	H_2O
Bando et al. [88] *	45	303.15	333.15	10.0	20.0	0.00	0.55	H_2O, NaCl
Bastami et al. [89] *	32	328.15	375.15	6.9	20.7	0.00	4.80	H_2O, $CaCl_2$
Bermejo et al. [90] *	92	286.97	368.81	2.0	13.1	0.25	0.99	Na_2SO_4
Bo liu et al. [91] *	538	298.00	373.00	0.1	20.3	0.00	0.26	$CaCl_2$, H_2O, $MgCl_2$, ($MgCl_2$ + $CaCl_2$)
Campos et al. [92]	50	298.20	323.20	0.1	0.5	0.00	0.00	H_2O
Carvalho et al. [93]	107	283.24	363.42	0.3	40.0	0.00	2.00	H_2O, NaCl
Chapoy et al. [94]	27	274.14	351.31	0.2	9.3	0.00	0.00	H_2O
Corti et al. [95]	10	323.15	348.15	3.8	14.5	0.96	2.72	Na_2SO_4
Dalmolin et al. [96]	49	288.00	323.00	0.1	0.5	0.00	0.00	H_2O
Dell'Era, C. et al. [97]	7	298.48	298.63	0.3	0.7	0.00	0.00	H_2O
dos Santos et al. [98]	62	303.15	423.15	1.5	20.3	1.00	6.00	$MgCl_2$, NaCl, (NaCl + Na_2SO_4)
Ellis and Golding [99]	54	445.15	607.15	1.6	9.3	0.00	2.00	H_2O, NaCl
Gilbert et al. [100]	35	308.15	413.15	1.9	35.8	0.00	3.40	$CaCl_2$, H_2O, Na_2SO_4, NaCl, $NaHCO_3$
Guo et al. [101] *	168	273.15	453.15	10.0	40.0	1.00	5.00	NaCl
Han et al. [102] *	75	313.00	333.00	0.3	2.0	0.00	1.00	$NaHCO_3$
Han Ji et al. [103] *	28	313.20	343.20	4.3	18.3	0.00	0.00	H2O
He and Morse [104]	157	298.15	363.18	0.0	0.1	0.02	6.14	$CaCl_2$, K_2SO_4, KCl, $MgCl_2$, $MgSO_4$, Na_2SO_4, NaCl
He et al. [105]	35	293.15	348.15	5.2	38.3	0.00	2.70	H_2O, NaCl
Hoballah [106] *	12	348.15	398.15	5.0	50.0	0.80	0.80	$NaHCO_3$
Hou et al. (a) [107] *	41	298.15	448.15	1.1	17.6	0.00	0.00	H_2O
Kamps et al. [108] *	138	313.10	433.10	0.3	9.4	0.43	4.05	K_2CO_3, KCl
Kiepe et al. [109] *	190	313.16	393.17	0.1	10.5	0.00	4.34	H_2O, KCl, NaCl
Koschel et al. [110] *	49	323.00	423.00	5.0	20.2	0.33	4.50	KCl, $MgCl_2$, NaCl
Malinin and Kurovskaya [111]	25	298.15	348.15	4.8	4.8	0.36	5.21	$CaCl_2$
Malinin and Kurovskaya [111]	27	298.15	423.15	4.8	4.8	0.32	1.91	NaCl
Martin et al. [112] *	5	353.00	393.00	10.0	30.0	0.00	0.00	H_2O
Messabeb et al. [113] *	40	323.15	423.15	5.0	20.2	0.00	6.00	H_2O, NaCl
Mohammadian et al. [114] *	68	333.15	353.15	0.1	21.3	0.00	0.26	H_2O, NaCl
Muromachi et al. [115] *	17	286.15	298.15	0.2	4.0	0.00	0.00	H_2O
Nighswander et al. [116]	33	353.00	473.65	4.1	100.3	0.17	0.17	NaCl
Portier and Rochelle [117] *	35	291.15	353.15	8.0	12.0	0.38	0.38	NaCl, KCl, $MgCl_2$, $CaCl_2$, $NaHCO_3$
Poulain et al. [118] *	48	323.00	423.00	1.0	20.0	1.40	1.50	NaCl, $CaCl_2$, KCl
Prutton and Savage [119]	139	348.65	394.15	1.5	71.2	0.00	3.90	$CaCl_2$, H_2O
Qin et al. [120] *	7	323.60	375.80	10.6	49.9	0.00	0.00	H_2O
Ruffine and Trusler [121] *	3	333.00	333.00	4.9	11.5	0.00	0.00	H_2O
Rumpf and Maurer [122]	111	313.11	433.16	0.0	9.7	0.99	2.01	Na_2SO_4
Rumpf et al. [123]	63	313.14	433.08	0.5	9.6	4.00	6.00	NaCl
Sako et al. [124]	7	348.30	421.40	10.2	19.7	0.00	0.00	H_2O
Serpa et al. [125] *	9	298.00	323.00	0.1	0.4	0.00	0.00	H_2O
Servio and Englezos [126] *	6	278.05	283.15	2.0	3.7	0.00	0.00	H_2O
Tang et al. [127] *	70	308.15	408.15	8.0	40.0	0.00	1.41	H_2O, NaCl, $CaCl_2$, $MgCl_2$, $NaHCO_3$
Tong et al. [128] *	94	308.00	424.68	1.1	38.0	0.00	5.00	$CaCl_2$, H_2O, $MgCl_2$, NaCl, KCl
Valtz et al. [129] *	47	278.22	318.23	0.5	8.0	0.00	0.00	H_2O
Wiebe [130] *	73	273.15	373.15	2.5	70.9	0.00	0.00	H_2O
Wiebe and Gaddy [131]*	29	323.15	373.15	2.5	70.9	0.00	0.00	H_2O
Y. Liu et al. (a) [132] *	154	308.15	328.15	1.3	16.0	0.00	1.90	$CaCl_2$, KCl, NaCl,
Y. Liu et al. (b) [133] *	6	308.15	318.15	8.0	16.0	0.00	0.00	H_2O
Yan et al. [134] *	54	323.20	413.20	5.0	40.0	0.00	5.00	H_2O, NaCl
Zhao et al. (b) [135] *	70	323.00	423.00	15.0	15.0	0.33	4.50	$CaCl_2$, KCl, $MgCl_2$, Na_2SO_4
Zhao et al. (a) [136] *	21	323.15	423.15	15.0	15.0	0.00	6.00	H_2O, NaCl

* Experimental CO_2 solubility data were used in the regression of this study model.

2.1.2. CO_2 Solubility–Equation of State

Generally, Peng Robinson Equation of State, PR (EoS) [137,138] have been commonly used to describe the phase behavior of pure components and mixtures in the gas, liquid, and supercritical fluid states. The traditional PR (EoS) model often results in significant errors, particularly in predicting gas solubility in aqueous phases. It struggles to account for the effects of salts like NaCl, leading to underestimation of the salting–out effect and inaccurate phase behavior predictions in subsurface engineering simulations. To enhance the prediction of CO_2 solubility in brine and hydrocarbon systems, Søreide and Whitson [139] introduced a tailored α–term to the PR (EoS) [137,138]. Other authors have expanded on this work, Duan and Sun [52] extended the pressure (0 to 200 MPa), temperature (273 to 533 K), and ionic strength up to 4.3 M using specific particle interaction theory for the liquid phase. Duan et al. [53] introduced Pitzer's specific interaction model to calculate the chemical potential of CO_2 in the vapor phase. Advancing on earlier works, various authors [46–51,140] have contributed to the modeling of CO_2 solubility in water and saline systems.

2.1.3. CO_2 Solubility–Empirical Correlations

Despite the advantage of EoS modeling being fast and requiring less computing power compared to molecular dynamics, the application of this method to estimate CO_2 solubility in brine, particularly under extreme subsurface injection conditions, remains challenging. These EoS models are usually accurate within a given constraint of pressure and temperature [139]. In addition, EoS can sometimes be computationally extensive, hence the need for accurate, fast, and cheap empirical models. In an earlier study, Darwish [55] developed an extension of the Setschenov model to predict CO_2 solubility in the H_2O–NaCl system under geological sequestration conditions, spanning temperatures from 300 to 500 K, pressures from 5 to 200 MPa, and salt concentrations of 1 to 4 mol/kg. Barta and Bradley [56] applied an interaction model to study gas solubility in high ionic strength and high–temperature aqueous salt solutions, focusing on CO_2, H_2O, and CH_4 in aqueous NaCl up to 6 molar, 623.15 K and 15.19 MPa. Furthermore, to accurately correlate CO_2 solubility in water by analyzing 110 data points from literature covering a temperature range of 298 to 523 K and a pressure range of 3.4 to 72.41 MPa, Enick and Klara [58] employed Henry's law to model CO_2 solubility in pure water, utilizing an equation of state for hydrocarbon phase equilibria. Diamond and Akinfiev [141] present a detailed evaluation of the solubility of carbon dioxide in pure water over a temperature range of 271.65 to 373.15 K and pressures between 0.1 and 100 MPa. Sun et al. [57] developed a simple model for the prediction of mutual solubility in CO_2 + H_2O and CO_2 + Brine systems that cover 0–250 °C, 0–200 MPa and brines containing Na^+, K^+, Ca^{2+}, Mg^{2+}, Cl^-, and $SO_4{}^{2-}$.

2.1.4. CO_2 Solubility–Molecular Dynamics Studies

MDS and other atomistic techniques like Monte Carlo (MC) simulations have become essential for exploring the molecular foundations of various phase behavior and geochemical processes. These simulations offer a unique capability to study the behavior of individual atoms, providing insights that are often challenging to obtain through experimental approaches, which typically capture the average behavior of large molecular groups. The versatility of MDS, which can examine a wide range of length and time scales —from angstroms to nanometers and from femtoseconds to microseconds—makes them particularly effective in understanding how small–scale molecular properties lead to more pr collective behaviors in geochemical systems. One significant application of these molecular simulations has been in investigating the vapor–liquid equilibrium (VLE) in H_2O–CO_2 and CO_2 –NaCl brine systems.

Liu et al. [63] examined the phase behavior of H_2O–CO_2 mixtures using histogram–reweighting Grand–Canonical Monte Carlo (GCMC) simulations over a temperature range of 323.15 to 723.15 K and pressures from 0 to 100 MPa. The study by Yasaman et al. [65] leverages comprehensive MDS with a focus on force field parameters using Large–scale

Atomic and Molecular Massively Parallel Simulator (LAMMPS) [142] to predict the equilibrium, interfacial, and transport properties of CO_2 –brine systems under realistic CO_2 storage conditions. In another study, Vorholz et al. [64] utilized Gibbs Ensemble Monte Carlo (GEMC) [143] simulations to study the VLE of water (H_2O) at temperatures between 323 and 573 K, CO_2 between 230 and 290 K, and H_2O–CO_2 mixtures between 348 and 393 K, employing both Number of Particles Volume and Temperature (NVT) and Number of Particle Pressure Temperature (NPT) ensembles. Furthering this research, Liu et al. [62] also investigated the phase behavior and interfacial tension of H_2O–CO_2 –NaCl mixtures using MDS across a temperature range of 323.15 to 523.15 K, pressures from 0 to 60 MPa, and NaCl concentrations between 1 and 4 molal. Moreover, Orozco et al. [144] applied NPT GEMC simulations to optimize intermolecular potential parameters for describing the phase behavior of H_2O–CO_2 mixtures. Similarly, Lobanova et al. [145] modeled the VLE of CO_2 –H_2O systems at 423 and 548 K using SAFT–CG Mie force fields for CO_2 and H_2O, achieving good agreement with experimental solubility data. In another article, Jiang et al. [146] studied the phase equilibria of H_2O–CO_2 and H_2O/n–alkane mixtures using GEMC simulations, covering a temperature range of 323 to 523 K and pressures from 20 to 80 MPa. Hulikal et al. [147] tackles the challenge of predicting VLE in H_2O–CO_2 and CO_2 –NaCl brine systems over a temperature range of 230 to 723.15 K and pressures up to 100 MPa using advanced methods like Gibbs Ensemble Monte Carlo (GEMC) and Grand–Canonical Monte Carlo (GCMC). Their work revealed discrepancies between simulation results and experimental data, highlighting the need for better force fields. Moreover, Adam et al. [148] utilized equilibrium MD using the LAMMPS software (23Jun22 version) to explore the solubilities of H_2 and CO_2 in brine under conditions relevant to CCUS.

2.1.5. CO_2 Solubility–Machine Learning Studies

Machine learning (ML) provides alternative and reliable techniques for predicting the solubility of CO_2 in aqueous solutions. In contrast to conventional models, which frequently rely on simplified equations with restricted variables, ML is a data–driven approach that uses readily available parameters such as temperature, pressure, and electrolyte concentration to predict solubility. Here, we present a succinct review of ML studies to estimate CO_2 solubility in water and brine systems, particularly under subsurface processes.

Menad et al. [67] applied machine learning to model CO_2 solubility in brine, utilizing Multilayer Perceptron (MLP) optimized by the Levenberg–Marquardt algorithm, and Radial Basis Function Neural Network (RBFNN) optimized using Genetic Algorithm (GA), Particle Swarm Optimization (PSO), and Artificial Bee Colony (ABC). Mohammadian et al. [68] used the Group Modeling Data Handling (GMDH) in predicting CO_2 solubility in aqueous solutions at pressures up to 400 atm and temperatures between 283 and 298 K. Continuing this research, Mohammadian et al. [149] applied four data–driven techniques—extreme gradient boosting (XGB), multilayer perceptron (MLP), K–nearest neighbor (KNN), and an in–house genetic algorithm (GA)—to estimate CO_2 solubility across a broader range of conditions (salinity 0–15,000 ppm, temperatures 298–373 K, and pressures up to 200 atm). Ratnakar et al. [150] developed a machine learning–based workflow for accurately estimating CO_2 solubility in brine for CCUS applications. In another study, Jeon and Lee [69] used an artificial neural network (ANN) to predict CO_2 solubility, utilizing 2406 experimental data points in salt–dissolved solutions across a broad range of pressures (0.92–712.31 bar), temperatures (273.15–473.65 K), concentrations of water molecules (0–90.12 mol/kg), and overall mole fractions of dissolved salts (0–25.39 mol%), including supercritical CO_2 conditions. Recently, Mahmoudzadeh et al. [70] developed two tree–based models, LightGBM and GBoost, to predict CO_2 solubility in pure H_2O using a comprehensive dataset of 785 experimental data points from various sources. Pressure and temperature were the input parameters, and solubility was the output. The GBoost model outperformed LightGBM, achieving an R^2 of 0.9976 and an RMSE of 0.137 mol/kg. Similarly, Zou et al. [151] used machine learning to predict CO_2 solubility in water and brine–based on 1278 experimental data points covering temperatures from 273.15 to 453.15 K and pressures ranging from 0.06

to 100 MPa. They employed two ANNs—cascade forward neural network (CFNN) and generalized regression neural network (GRNN)—along with three optimization algorithms.

The advancement of machine learning techniques in these studies has significantly boosted the precision and reliability of CO_2 solubility predictions. Initial models encountered difficulties in formulating practical equations and handling high–pressure conditions. However, later research improved accuracy by utilizing advanced optimization algorithms, hybrid models, and thorough feature analysis. The use of extensive and diverse datasets, along with careful validation against experimental data, has been key in overcoming the shortcomings of earlier models. This has positioned data–driven approaches as a reliable alternative for estimating CO_2 solubility in brine.

2.2. Hydrogen (H_2)

The study of hydrogen (H_2) solubility is crucial for understanding various natural and engineered processes, particularly in the context of UHS and the natural production of hydrogen. There is a pressing need for more experimental and theoretical work to accurately model hydrogen solubility across the full spectrum of relevant T–P–S conditions, particularly in complex saline aquifer systems and under the high–pressure conditions found in deep geological formations [59,152]. This review of hydrogen solubility is not only fundamental for the safe and efficient design of hydrogen storage systems but also for understanding the broader implications of hydrogen in natural geochemical processes, including its role in the global hydrogen cycle and its potential as a renewable energy resource.

2.2.1. H_2 Solubility–Experimental Works

In the literature, there are numerous data on the solubility of hydrogen in pure water, the majority of which comes from very old studies. All these data are also limited to low temperature and atmospheric pressure. On the other hand, the solubility of hydrogen in various brines have been studied less than in pure water. A substantial amount of experimental data on hydrogen solubility in pure water is available in the literature. This data mainly includes volume ratio measurements, such as Ostwald, Knudsen, and Bunsen coefficients. Additionally, some data are provided as direct solubility measurements in mole fraction using PVT cells ("TPxy" data) or as Henry's constants. Some experimental data on hydrogen solubility in seawater solutions and $NaCl_{(aq)}$ are available in the literature; however, these data cover only a narrow range of temperatures and salinities. According to IUPAC's [153] evaluation of experimental data, Wiebe and Gaddy [154] data are the most reliable and largely cover the pressure and temperature range of geological storage conditions. The most significant contribution comes from Crozier and Yamamoto [155], who collected extensive data on hydrogen solubility in seawater and NaCl aqueous solutions, albeit experiments were conducted at atmospheric pressure. Conversely, the data from Braun [156] were excluded because they were found to be inconsistent with all other available data under similar conditions. Recently, Chabab et al. [59,152] carried out measurements of hydrogen solubility of the H_2 + H_2O + NaCl system, as well as data from the literature. Therefore, it is necessary to overcome data gaps, especially for the H_2 + H_2O + NaCl system, which is the most important since Na^+ and Cl^- are the predominant species in natural saline water. These experimental data on hydrogen solubility in water and salt were collected and listed in Table 2. Figures 3 and 4 show experimental data as a function of temperature and pressure.

Table 2. Published experimental studies of H_2 solubility in aqueous systems in the compiled database.

Authors	Year	Min. Temp (K)	Max. Temp (K)	Min. Press (MPa)	Max. Press (MPa)	Max. Molality (mol/kg)	Systems
Chabab et al. [59] *	2020	323.00	372.00	2.00	20.00	5.0	NaCl
Chabab et al. [152]. *	2023	298.15	373.15	10.00	20.00	4.0	NaCl
Wiebe and Gaddy [154]	1934	273.15	373.15	2.53	101.33	0.0	H_2O
Crozier and Yamamoto [155] *	1974	274.60	302.47	0.10	0.10	0.0	H_2O
Crozier and Yamamoto [155] *	1974	274.03	301.51	0.10	0.10	0.5	NaCl

Table 2. *Cont.*

Authors	Year	Min. Temp (K)	Max. Temp (K)	Min. Press (MPa)	Max. Press (MPa)	Max. Molality (mol/kg)	Systems
Braun [156]	1900	278.15	298.15	1.022	1.045	0.0	H_2O
Braun [156]	1900	278.15	298.15	1.022	1.045	1.1	NaCl
Torin–Oilarves and Trusler [157] *	2021	323.00	323.00	12.00	39.40	2.5	NaCl
Bunsen [158]	1855	277.15	296.75	0.10	0.10	0.0	H_2O
Bohr and Bock [159]	1891	273.20	373.15	0.10	0.20	0.0	H_2O
Winkler [160]	1891	273.65	323.25	0.10	0.11	0.0	H_2O
Steiner [161] *	1894	288.20	288.20	0.10	0.10	0.0	H_2O
Steiner [161] *	1894	286.32	286.95	0.10	0.10	5.3	NaCl
Steiner [161]	1894	291.77	292.38	0.10	0.10	4.0	KCl
Steiner [161]	1894	290.83	291.67	0.10	0.10	3.2	$CaCl_2$
Steiner [161]	1894	291.56	291.72	0.10	0.10	1.4	Na_2SO_4
Steiner [161]	1894	290.25	291.41	0.10	0.10	2.6	$MgSO_4$
Geffcken [162] *	1904	288.15	298.15	0.10	0.10	0.0	H_2O
Knopp [163] *	1904	293.15	293.15	0.10	0.10	0.0	H_2O
Knopp [163]	1904	293.15	293.15	0.10	0.10	2.1	KCl
Huefner [164] *	1907	293.15	293.34	0.10	0.10	0.0	H_2O
Findlay and Shen [165]	1912	298.15	298.15	0.10	0.18	0.0	H_2O
Muller [166]	1913	289.35	290.35	0.10	0.10	0.0	H_2O
Ipatiew et al. [167]	1932	273.65	318.15	2.03	14.19	0.0	H_2O
Morrison and Billett [168] *	1952	285.65	345.65	0.10	0.14	0.0	H_2O
Pray et al. [169] *	1952	324.82	588.71	0.69	2.42	0.0	H_2O
Zoss [170] *	1952	273.15	606.48	3.45	20.70	0.0	H_2O
Stephan et al. [171]	1953	373.15	435.93	1.41	10.03	0.0	H_2O
Wet [172] *	1964	291.65	304.55	0.10	0.11	0.0	H_2O
Ruetschi and Amlie [173] *	1966	303.15	303.15	0.11	0.11	0.0	H_2O
Shoor et al. [174]	1969	298.15	333.15	0.10	0.12	0.0	H_2O
Longo et al. [175] *	1970	310.15	310.15	0.11	0.11	0.0	H_2O
Power and Stegall [176]	1970	310.15	310.15	0.11	0.11	0.0	H_2O
Gerecke and Bittrich [177] *	1971	298.15	298.15	0.10	0.10	0.0	H_2O
Gerecke and Bittrich [177] *	1971	288.15	298.15	0.10	0.10	4.3	NaCl
Gerecke and Bittrich [177] *	1971	288.15	288.15	0.10	0.10	1.0	KCl
Jung et al. [178]*	1971	373.15	423.15	1.00	8.58	0.0	H_2O
Schroder [179]	1973	298.15	373.15	10.13	10.13	0.0	H_2O
Gordon et al. [180] *	1977	273.29	302.40	0.10	0.10	0.0	H_2O
Devaney [181] *	1978	366.48	588.7	1.38	11.03	0.0	H_2O
Cargill [182]	1978	277.70	344.83	0.10	0.14	0.0	H_2O
Meyer et al. [183] *	1980	310.15	310.15	0.10	0.10	0.0	H_2O
Gillespie and Wilson [184] *	1980	310.93	588.71	0.35	13.80	0.0	H_2O
Choudhary et al. [185]	1982	323.15	373.15	2.53	10.13	0.0	H_2O
Dohrn and Brunner [186]	1986	473.15	623.15	10.00	30.00	0.0	H_2O
Alvarez et al. [187] *	1988	318.90	497.50	0.44	4.59	0.0	H_2O
Kling and Maurer [188] *	1991	323.15	423.15	3.18	15.37	0.0	H_2O
Jauregui–Hazaetal. [189]	2004	353.00	373.00	0.15	0.20	0.0	H_2O

* Experimental H_2 solubility data used in the regression of this study model.

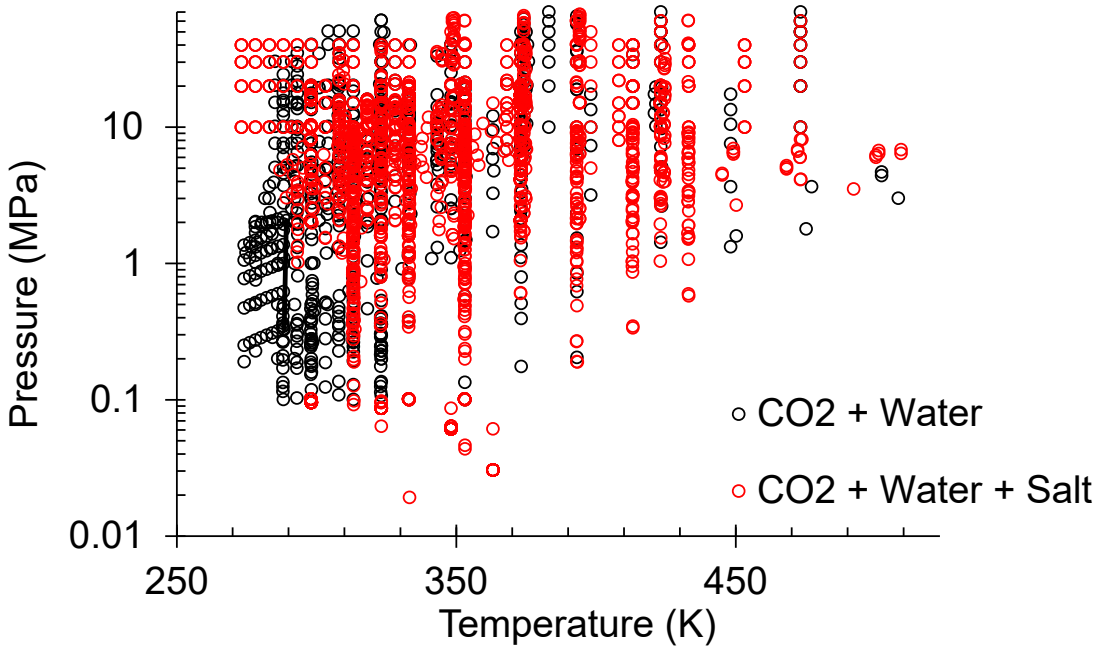

Figure 3. Pressure and temperature ranges of the selected CO_2 solubility data used in this work.

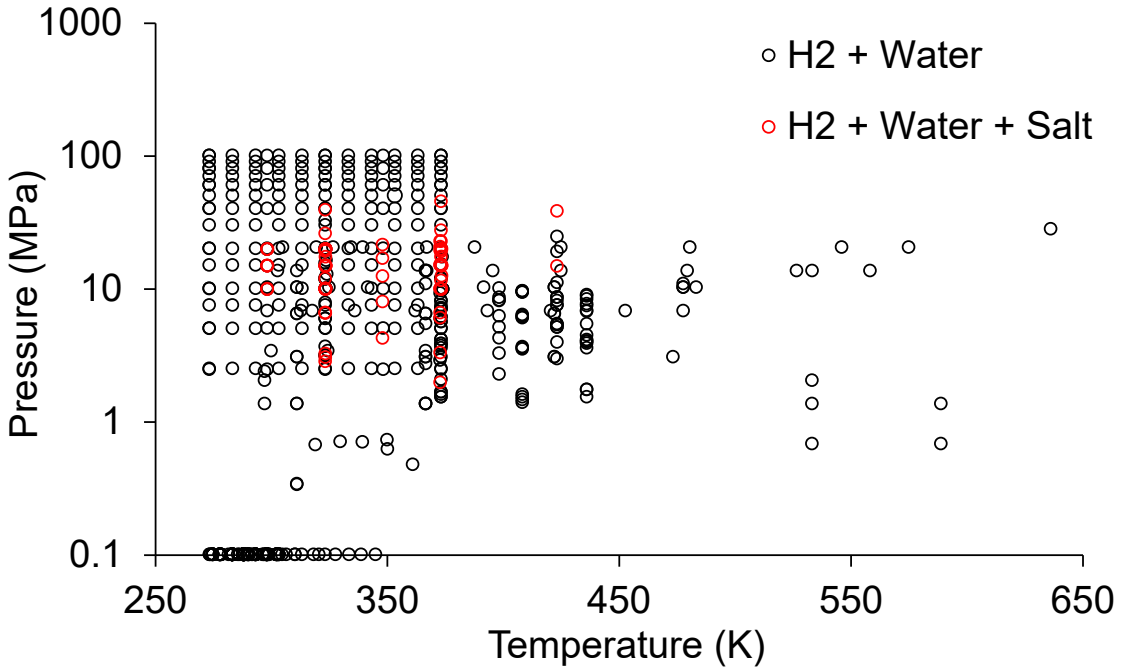

Figure 4. Pressure and temperature ranges of the selected H_2 solubility data used in this work.

2.2.2. H_2 Solubility–Equation of State

In the last few decades, several researchers have relied on the EoS to estimate hydrogen solubility in a wide variety of brine solutions [41–45]. A reliable and accurate model for hydrogen solubility was developed by Li et al. [43]. This model calculated hydrogen solubility in formation fluids and tracked changes in fluid density. It accounted for factors like system pressure, temperature, fluid salinity, molar fraction, fugacity coefficient, Henry's constant, Poynting factor, and the activity coefficient of hydrogen. The model performed well within typical geological storage conditions (273–373 K, 1–50 MPa, and 0–5 mol/kg NaCl), accurately reproducing experimental data and predicting hydrogen solubility and fluid density. Additionally, the model handled H_2–N_2 or H_2–CH_4 gas mixtures and mixed electrolyte solutions containing Na, K, Ca, Mg, Cl, or SO_4. Rahbari et al. [41] conducted thermodynamic modeling to investigate the phase coexistence of the H_2O–H_2 system at temperatures ranging from 283 K to 423 K and pressures between 10 bar and 1000 bar. The authors found that both the Peng–Robinson and Soave Redlich–Kwong equations of state, even with van der Waals mixing rules and fitted binary interaction parameters were unable to accurately predict the equilibrium compositions of the liquid and gas phases. In another study, Lopez–Lazaro [44] used Monte Carlo simulations to generate new data on hydrogen solubility in aqueous NaCl solutions across temperature and salinity ranges relevant to geological applications where experimental data are currently lacking. They fitted a binary interaction parameter for the Soreide and Whiston equation of state using the simulated data generated through molecular simulations. This model enables fast and reliable phase equilibrium calculations and was applied to scenarios pertinent to hydrogen geological storage and natural hydrogen emissions.

Sun et al. [45] applied the SAFT–LJ EoS, which incorporates a multipolar term to explicitly account for dipole–dipole, dipole–quadrupole and quadrupole–quadrupole interactions, to model the VLE of H_2O–H_2 systems. In their model, H_2 was treated as chain molecules with evenly distributed quadrupole moments. The van der Waals one–fluid mixing rule was used to calculate mixture parameters and evaluated two binary parameters for H_2O–H_2 interactions based on mutual solubility data from binary water–gas systems. When compared with experimental data, this molecular–based EoS accurately represented the VLE of H_2O–N_2 and H_2O–H_2 systems across a wide P–T range (273–623 K and 0–1000 bar). The authors concluded that this ability to account for multipolar interactions is

why the SAFT–LJ EoS can quantitatively represent the VLE of highly non–ideal water–gas systems. Ratnakar et al. [42] developed a PVT model for the H_2–H_2O system using the traditional PR EoS along with a non–classical Huron–Vidal (HV) mixing rule. Their model effectively captures molecular interactions and aligns well with available experimental data. They also established a robust workflow for determining HV parameters from binary solubility data, which was validated against experimental observations.

2.2.3. H_2 Solubility–Empirical Correlations

Various researchers developed correlations to predict the hydrogen Henry constants in pure water, comparing experimental data. The pioneered work by Harvey [190] was later refined by Fernández–Prini [191]. Trinh et al.'s developed model for estimating hydrogen Henry's constant in oxygenated solvents [192] and adjusted by Lopez–Lazaro et al. [44] for water. Akinfiev and Diamond's utilize a virial–like equation of state to describe the properties of aqueous nonelectrolytes at infinite dilution [193]. Li et al. [43] and Torín–Ollarves and Trusler [157] empirical models were calibrated using high–pressure H_2 solubility data in water. Chabab et al. [59] presented an empirical correlation to predict H_2 solubility in pure H_2O and brine. The correlation considers the effects of temperature, pressure, and molal concentration (mol/kg of NaCl). Although Chabab et al.'s correlation provides a useful tool for predicting hydrogen solubility in pure water and NaCl–brine systems, its limitations make it less applicable to more complex or mixed brine environments commonly encountered in natural hydrogen production and UHS scenarios. The correlation does not account for these interactions, which can lead to inaccuracies when applied to systems that are not dominated solely by NaCl. Zhu et al. [54] used a semi–empirical approach to model H_2 solubility in purified water and aqueous NaCl solutions by utilizing a high–precision equation of states and a specific particle interaction theory for the liquid and vapor phases of H_2, respectively. Although the model effectively predicts H_2 solubility in pure water and NaCl solutions, its application is limited by its calibration range, which has a maximum temperature of 373.15 K (100 °C). This limitation restricts its use in high–temperature environments like natural hydrogen production, where temperatures often exceed this range.

2.2.4. H_2 Solubility–Molecular Dynamics Studies

Molecular dynamics studies are increasingly being used to model the solubility behavior of fluid systems, particularly for H_2 in brine, due to the complexities associated with its very low solubility, as well as the high costs and hazards posed by experimental measurements under extreme conditions (e.g., high pressure, flammability of H_2, and the corrosive nature of salt). While these simulations are invaluable, experimental measurements remain essential for validating and refining models used in classical and statistical thermodynamics. Additionally, molecular simulations complement experimental work by offering deeper insights into the underlying physical mechanisms, generating vapor–liquid equilibrium data under severe conditions (such as high temperature, pressure, and salinity), and aiding in the development of consistent and reliable models for predicting solubility.

MDS application to H_2 solubility in pure water and brine is relatively recent and limited, likely due to the low solubility of H_2, which poses significant statistical challenges [44,61]. Rahbari et al. [41] used molecular simulations to study the phase coexistence of the H_2O–H_2 system across temperatures from 283 K to 423 K and pressures between 10 and 1000 bar. They found that force–field–based molecular simulations could predict the solubility of water in compressed hydrogen. Lopez–Lazaro et al. [44] applied this indirect method to calculate Henry's constant for H_2 in brine and used it to calibrate the Søreide and Whitson equation of state for predicting solubilities at high pressures. Recently, Kerkache et al. [60] employed both direct and indirect molecular dynamic approaches to calculate H_2 solubility in water and brine, demonstrating the applicability of these approaches under various conditions. Similarly, van Rooijen et al. [61] used this method to estimate H_2 solubility at pressures up to 10 MPa, noting that Henry's law requires correction beyond

this pressure. In NaCl brine, a significant lack of experimental data has resulted in few recent molecular dynamic studies [44,60,61] on high–pressure H_2 solubility. These sources show notable discrepancies, particularly in the salt–free molar fraction ($x'H_2$). This inconsistency highlights the variations between the experimental and simulation results, underscoring the need for further investigation to reconcile these differences. Although molecular dynamic techniques are powerful tools, they are computationally intensive and necessitate additional parameters that are often challenging to obtain. This complexity increases significantly when transitioning from simpler systems like pure water to more complex ones involving mixed salts, making the modeling process even more resource demanding and less accessible for practical applications.

2.2.5. H_2 Solubility–Machine Learning Studies

Machine learning offers a robust approach to predicting hydrogen solubility in aqueous solutions, especially underground hydrogen storage conditions. Unlike traditional models that rely on simplified equations with limited variables like temperature and pressure [194], machine learning can incorporate a wider range of input variables that includes the chemical properties of other solutes [195]. This broader analysis significantly improves the accuracy and reliability of predictions. Recent studies have successfully applied machine learning techniques to predict hydrogen solubility in various mediums [196–198], demonstrating their effectiveness in complex systems where conventional models may fall short.

Various machine learning algorithms have been widely used to predict hydrogen solubility. Lv et al. [71] employed advanced models including adaptive boosting decision tree (AdaBoost–DT), adaptive boosting support vector regression (AdaBoost–SVR), gradient boosting decision tree (GB–DT), gradient boosting support vector regression (GB–SVR), and k–nearest neighbors (KNN) to estimate H_2 solubility in both pure and saline water. Similarly, Zhu et al. [66] used a wavelet neural network that combines ANN with wavelet transform to model hydrogen storage in saline water under real–world conditions. Vo Thanh et al. [72] also investigated hydrogen solubility in aqueous systems using various machine learning models such as adaptive gradient boosting (AdaBoost), gradient boosting, random forest, and extreme gradient boosting, confirming their effectiveness. Recently, various authors [199–202] have contributed to the machine learning modeling of H_2 solubility in water and saline systems.

The application of machine learning to predict hydrogen solubility in aqueous solutions marks a significant advancement over traditional methods; however, the current approaches are constrained by the major limitations of the lack of an extensive experimental database. To improve the accuracy and reliability of these predictions, future research should focus on expanding the datasets to cover a wider range of conditions relevant to both underground hydrogen storage and natural hydrogen production. Additionally, integrating more comprehensive data could help mitigate the risks of overfitting and enhance the generalizability of these models to diverse real–world scenarios.

3. Methodology

Here, we present a detailed analysis of the CO_2 and H_2 solubility data, encompassing various stages from data collection and characterization to model development and performance evaluation. We begin by discussing the methodologies employed in gathering and processing the data, which form the foundation for subsequent empirical model development. The focus then shifts to the formulation and development of predictive correlations fitted from the experimental data, specifically tailored for CO_2 and H_2 solubility under varying conditions. Finally, we assess the accuracy and reliability of these models through statistical evaluation, providing insights into their predictive capabilities and limitations.

3.1. Data Collection and Characterization

To develop a robust and quick predictive model that can accurately predict CO_2 and H_2 solubility in aqueous systems for subsurface applications, reliable and consistent database is essential. In light of this, we collected experimental data points for CO_2 and H_2 solubility from published studies (see Tables 1 and 2). Because most experimental data are published in different measurement units, a conversion was conducted for all measured data to establish a consistent data unit system. All pressure data was converted to megapascals (MPa), temperature to Kelvin (K), salinity to molality (mol/kg) and solubility to moles per kilogram of water (mol/kg). These datasets cover diverse aqueous systems with three main input variables, including temperature, pressure and salinity (mol/kg). The objective of the section was to gather consistent experimental data and develop swift and accurate correlations to predict CO_2 and H_2 solubility as a function of pressure, temperature and salinity in terms of ionic strength. They are formulated as follows:

$$Solubility = f(P,\ T,\ and\ IS) \tag{1}$$

Furthermore, the salinity of all experimental data was converted into ionic strength (*IS*), expressed in mol/kg, using the Debye–Hückel [203] model expressed by Equation (2). The Debye–Hückel model presents an easy approach to determining ionic strength. However, its limitation is that it does not consider the impact of ion interaction.

$$IS = \frac{1}{2}\sum m_i z_i^2 \tag{2}$$

where m_i and z_i represent the molality (mol/kg) and charge of the ion, respectively.

In the context of the experimental measurement unit, Equation (3) can be used to convert the molality and weight fraction of ions to total dissolved salt (TDS). Alternatively, TDS can be calculated from the weight fraction of the ion using Equation (4).

$$TDS = m_{ion} \times M_{ion} \times 1000 \tag{3}$$

$$TDS = \frac{\left(\frac{wt\%_{ion}}{MM_{ion}} \times 100\right)}{(100 - wt\%_{ion}) \times 10^3 \times M_{ion}} \tag{4}$$

where $wt\%_{ion}$ = weight fraction of ion, M_{ion} = molar mass of ion, and m_{ion} = mole concentration of ion.

Because most industrial applications measure brine salinity in terms of TDS, mostly in parts per million (ppm), it is essential to capture this rationale in our empirical correlation. Electrical conductivity, salinity, and TDS measurements are often used to quantify the ionic strength of water. These measurements typically show good correlation with the concentration of ions. Therefore, we introduce Langelier et al. [204] correlation to estimate ionic strength based on TDS. The empirical correlation (Equation (5)) with the assumption that the relative composition of natural waters is fairly constant. The correlation is expressed as:

$$IS = 2.5 \times 10^{-5} \times TDS \tag{5}$$

Furthermore, these equations were employed to ensure accurate conversions between salinity, ionic strength, and TDS, facilitating a comprehensive analysis of the experimental data.

Next, we collected and compiled CO_2 solubility data. The dataset includes solubility measurements under a wide range of conditions, with maximum values reaching 71 MPa for pressure, 523 K for temperature, and 6.14 mol/kg for salinity. Table 1 outlines the specific experimental conditions under which the CO_2 solubility data was collected. In this study, the oriented temperature and pressure range is 273.15–523.15 °K and 0–71 MPa, respectively and across all salinity levels in which the CO_2–rich and water–rich phases are commonly immiscible. The chosen pressure range covers the domain of applicability for CO_2–EOR and geologic carbon storage. From Figure 3 it is evident that most data

points are concentrated between temperatures of 280 K to 350 K and pressures ranging from 0 to 30 MPa. There is a notable concentration of data within the lower temperature (below 350 K) and low–to–medium pressure ranges (0 to 20 MPa), particularly for the CO_2–H_2O–salt system. These temperatures and pressure conditions are typical of CO_2–EOR studies. However, as temperatures rise above 350 K and pressures exceed 30 MPa, the data points become sparse, indicating less experimental coverage in these regions. This suggests that the region between 350 K to 500 K and 20 MPa to 70 MPa lacks sufficient data, which may be critical for understanding CO_2 solubility under conditions of injection into deep saline aquifer. This gap highlights the need for additional experimental studies to extend the coverage to more extreme conditions, thereby improving the reliability of CO_2 solubility predictions for these important applications.

Similarly, for H_2 solubility data, available published data were collected and compiled into a databank. H_2 solubility data were collected. The dataset includes solubility measurements under a wide range of conditions, with maximum values reaching 101.3 MPa for pressure, 636.1 K for temperature, and 5.0 mol/kg for salinity. Notably, most of the available solubility data is from pure water systems. For more detailed information, please refer to Table 2, which outlines the specific experimental conditions under which the H_2 solubility data was collected. Finally, a total number of 438 experimental data records were filtered and selected from our preliminary database. The final dataset comprises solubility data in water and NaCl brine. From Figure 4, it is evident that most data points are concentrated within the temperature range of 250 K to 400 K and pressure range of 0 to 40 MPa. There is a noticeable clustering of data in the lower to medium temperature range, particularly between 250 K and 350 K, and pressures between 0 and 20 MPa. This suggests that the data coverage is quite robust in these regions, which may be relevant for standard conditions encountered in underground hydrogen storage applications. However, there is a significant lack of data at higher temperatures (above 400 K) and higher pressures (above 40 MPa), with very few data points extending up to 640 K and 100 MPa. This indicates that the data coverage is sparse in these high–temperature and high–pressure regions, which are critical for understanding H_2 solubility under extreme conditions like those encountered in natural hydrogen production. The limited data in these regions suggests that more experimental studies are needed to explore and accurately model H_2 solubility under such conditions. Details of the final datasets for CO_2 and H_2 solubility that were used for CO_2 and H_2 correlation development are provided in Tables 1 and 2.

Although other contaminants do not significantly affect solubility, Na and Cl are often the primary species taken into account when analyzing brines in aquifers [59,152] Commonly for thermodynamic characteristics, most subsurface brines are treated as NaCl brine, and the other species are either ignored or converted to NaCl equivalents [205]. Chemical reactivity, however, requires considering actual existent species rather than assimilating them to NaCl.

3.2. Development of CO_2 Solubility Correlations

Various experimental methods were used to obtain these measurements, including water-trapping [81,87,111], gas chromatography [107,124,129], volumetric expansion [116,135], synthetic methods. [94,108], Raman spectroscopy [206,207], calorimetric [110], and potentiometric techniques [91]. Overall, most of the data is consistent across a broad range of temperatures and pressures. The reliability and consistency of these measurements have been extensively analyzed in previous studies [49,53,141] which is beyond the scope of this work. Table 1 provides details of the databank for the CO_2 + water system.

An accurate model of CO_2 solubility should not only reflect the overall trends across a wide range of temperatures and pressures but also account for abrupt local changes under specific thermodynamic conditions. Traditional models often address this by using different parameters for various CO_2 phases or temperature–pressure ranges [49]. However, this approach can disrupt the smoothness and continuity of the function's derivative, potentially causing issues like an ill–conditioned Jacobian matrix in large–scale multiphase

flow simulations [208,209]. A simple model is proposed to maintain continuity in both the function and its gradient. Herein, the focus is on a temperature range of 273.15–523.15 °K and a pressure range of 0–71 MPa, where the CO_2–rich and water–rich phases are generally immiscible. Due to the strongly non–ideal nature of the CO_2 and water mixture, the composition of different phases varies in a complex manner with changes in pressure and temperature [49,118,128].

In this section, we use our compiled and filtered data to develop mathematical correlations to predict CO_2 solubility in water and various brine systems. These empirical correlations consider temperature and pressure for a CO_2–water system and temperature, pressure, and salinity in terms of ionic strength for CO_2+water+salt systems. The developed correlations were adapted and formulated from the work of Chen et al. [210]. Due to the complex behavior of CO_2 solubility in different aqueous systems, we further separated the entire data into various subsets, namely pure water, mixed salt, monovalent, and divalent single salt systems. Table 3 provides a summary of the dataset used to develop correlations between CO_2–water and CO_2–water–salt systems.

Table 3. Description of the experimental data used for developing the CO_2 and H_2 solubility models.

Correlation	Systems	Data Points	T Min (K)	T Max (K)	P Min (MPa)	P Max (MPa)	IS Min mol/kg)	IS Max (mol/kg)
CO_2–Water	—	926	274.14	523.15	0.10	71	–	–
CO_2–Water–Salt	Mixed Salts (K^+, Na^+, Ca^{2+}, Mg^{2+})	391	291.15	424.67	0.10	40.0	0.024	6.00
	KCl	260	313.1	433.1	0.13	18.22	0.427	4.50
	NaCl	766	273.15	523.15	0.10	40.0	0.017	6.00
	Na_2SO_4	226	286.97	433.16	0.42	15.0	0.300	8.16
	$NaHCO_3$	75	313	398.15	0.31	50.0	0.050	1.00
	$CaCl_2$	355	298	424.64	0.10	67.4	0.027	15.63
	$MgCl_2$	223	298	424.68	0.10	34.9	0.031	15
H_2–Water	—	360	273.15	636.1	0.629	101.35	–	–
H_2–Water–Salt	NaCl	78	298.05	423.155	1.9884	45.81	1.00	5.00

The final mathematical model that describes the quantitative effects of temperature, pressure, and salinity on the solubility of CO_2 for water and different saline systems is expressed in the following equation forms:

For $CO_2 - H_2O$ system:

$$mCO_2 = (1-\varepsilon)\frac{A.\,P_r^{a1}\,T^{a2}}{B.\,P_r^{a3}\,T^{a4} + C.P_r^{a5}\,T^{a6} + D} + \varepsilon\frac{E.\,P_r^{a7}\,T^{a8}}{F.\,P_r^{a9}\,T^{a10} + G.P_r^{a11}\,T^{a12} + H} \quad (6)$$

$$\varepsilon = \frac{T - T_{min}}{T_{max} - T_{min}} \quad (7)$$

ε = weighting factor, $T_{min} = 273.15$ K and $T_{max} = 523.15$ K

$$P_r = \frac{P}{P_0} \quad (8)$$

P_r = relative pressure, P_0 is the pressure at which the variation trend of CO_2 solubility undergoes an abrupt change, MPa. In this study, the expression of P_0 was derived from Sun et al. [57] and it is expressed as:

$$P_0 = 16.2086 - \frac{12.1147}{1 + exp(0.049635 \times (T - 273.15) - 2.8034)} \quad (9)$$

Regarding the aqueous phase containing either one or a combination of Na^+, K^+, Ca^{2+}, Mg^{2+}, Cl^- HCO_3^- and SO_4^{2-}, a simple model for CO_2 solubility in salt solution is proposed:

For $CO_2 - H_2O$ salts system:

$$mCO_{2,\,salt} = mCO_2{}^0 exp(a_1 IS + a_2 IS^{a3}) \quad (10)$$

where P, T, IS, $mCO_2{}^0$ and $mCO_{2,\,salt}$ represent the pressure (MPa), temperature (K), ionic strength (mol/kg), solubility of CO_2 in pure water (mol/kg) and solubility of CO_2 in salt solution (mol/kg), respectively. Also, A, B, C, D, E, F, G, H and a_1–a_{12} are constant fitted by experimental measurements of CO_2 solubility, respectively.

3.3. Development of H_2 Solubility Correlations

Next, similar to the previous section, we utilized processed hydrogen solubility data to develop mathematical models to predict H_2 solubility in water and various brine systems. The empirical correlations consider temperature and pressure for an H_2–water system and temperature, pressure, and salinity in terms of ionic strength for H_2—water—salt systems. The developed correlations are formulated as multivariable nonlinear regression models. Table 3 provides a summary of the dataset used to develop correlations for H_2–water and H_2–water–salt systems.

The final mathematical model that describes the quantitative effects of temperature, pressure, and salinity on the solubility of H_2 for water and different saline systems is expressed in the following equation forms:

For $H_2 - H_2O$ system:

$$mH_2 = (1-\varepsilon)\frac{A.\,{P_r}^{a1}\,T^{\,a2}}{B.\,{P_r}^{a3}\,T^{\,a4} + C.{P_r}^{a5}\,T^{\,a6} + D} + \varepsilon\frac{E.\,{P_r}^{a7}\,T^{\,a8}}{F.\,{P_r}^{a9}\,T^{\,a10} + G.{P_r}^{a11}\,T^{\,a12} + H} \quad (11)$$

$$\varepsilon = \frac{T - T_{min}}{T_{max} - T_{min}} \quad (12)$$

where $T_{min} = 273.15$ K and $T_{max} = 636.1$ K

$$P_r = \frac{P}{P_0} \quad (13)$$

Regarding the aqueous phase containing Na^+ and Cl^-, a simplified model for H_2 solubility in brine is proposed:

For $H_2 - H_2O -$ salts system:

$$mH_{2,\,salt} = mH_2{}^0 exp(a_1 IS + a_2 IS^{a3}) \quad (14)$$

where P, T, IS, $mH_2{}^0$ and $mH_{2,\,salt}$ represent the pressure (MPa), temperature (K), ionic strength (mol/kg), solubility of H_2 in pure water (mol/kg) and solubility of H_2 in salt solution (mol/kg), where A, B, C, D, E, F, G, H and a_1–a_{12} are constants, fitted by experimental measurements of H_2 solubility, respectively.

3.4. Model Parameter Determination

Experimental measurements are crucial for determining model parameters in phase equilibria models, as the quality of this data directly impacts the model's accuracy [57,118]. For CO_2 systems, an updated databank has been developed, which includes 923 measurements for the CO_2–water system and 1565 measurements for the CO_2+water+salts system. In the case of the H_2 system, the databank contains 438 measurements of H_2 solubility, 360 for the H_2–water system and 78 for the H_2 + water + salt systems. The Generalized Reduced Gradient algorithm was employed to determine the model parameters using the developed experimental database [211]. Due to the uneven distribution of experimental data across the targeted temperature and pressure range, the parameters were fitted exclusively with the available data. The resulting model parameters for CO_2 and H_2 solubility models are

presented in Table 4 showing the empirical constants for the CO_2 solubility models and H_2 solubility models.

Table 4. Empirical constants of developed CO_2 and H_2 solubility models.

Constants	CO_2 Solubility Correlations								H_2 Solubility Correlations	
	CO_2–H_2O	Mixed Salts	NaCl	KCl	$CaCl_2$	$MgCl_2$	Na_2SO_4	$NaHCO_3$	H_2–Water	H_2–Water–Salts (NaCl)
A	0.284888	–	–	–	–	–	–	–	0.101466	–
B	−5.02511	–	–	–	–	–	–	–	−5.632826	–
C	4.094051	–	–	–	–	–	–	–	3.732906	–
D	0.507286	–	–	–	–	–	–	–	−0.113223	–
E	0.006187	–	–	–	–	–	–	–	0.543337	–
F	−4.164112	–	–	–	–	–	–	–	−4.379279	–
G	4.939346	–	–	–	–	–	–	–	4.570177	–
H	0.340918	–	–	–	–	–	–	–	0.136001	–
a1	0.756798	0.52944	0.26827	0.287342	1.008286	1.801932	−0.11701	1.565179	1.036691	−0.180909
a2	−0.328316	−0.72297	−0.49775	−0.43852	−1.16212	−1.94698	−0.20067	−1.69733	−0.731073	−0.066281
a3	0.144697	0.998793	0.922111	0.926434	0.987298	0.99382	0.283081	0.961564	−0.003084	−7.126735
a4	−0.182119	–	–	–	–	–	–	–	−0.069526	–
a5	0.208901	–	–	–	–	–	–	–	−0.001675	–
a6	−0.200669	–	–	–	–	–	–	–	0.010505	–
a7	0.573537	–	–	–	–	–	–	–	0.60633	–
a8	−0.097774	–	–	–	–	–	–	–	−0.429898	–
a9	0.043382	–	–	–	–	–	–	–	−0.187142	–
a10	−0.205101	–	–	–	–	–	–	–	0.110585	–
a11	0.059729	–	–	–	–	–	–	–	−0.192603	–
a12	−0.287825	–	–	–	–	–	–	–	0.102827	–

4. Results and Discussions

4.1. Validation of the Developed CO_2 Solubility Correlations

The prediction performance of the developed correlations is validated against experimentally measured data using statistical analysis and graphical plots (isotherms curves and response surface plots). The different CO_2 solubility systems studied namely are pure water, mixed salts, and seawater with ions (Na^+, K^+, Ca^{2+}, Mg^{2+}, Cl^-, HCO_3^-, SO_4^{2-}), monovalent salt (KCl, NaCl, $NaHCO_3$ and Na_2SO_4) and divalent salts ($CaCl_2$ and $MgCl_2$). The NaCl and KCl salts were separated because, at the same concentration, the solubility of CO_2 is generally greater in KCl solutions than in NaCl solutions. This is a result of the ionic interactions between the CO_2 molecules and the ions in the solutions. In contrast to Na^+ ions in NaCl, the K^+ ions in KCl have a larger ionic radius, which leads to a less structured water network and reduced hydration. This less structured water network enables a greater amount of CO_2 to dissolve in the solution [102,212]. Conversely, Na^+ ions exert a significant influence on the structure and hydration of the water molecules in their vicinity, thereby diminishing the amount of space available for the dissolution of CO_2 molecules [102,212,213].

4.1.1. CO_2 + H_2O Systems

The developed model shows strong agreement with experimental data across various isotherms. The model captures the general trend of increasing solubility, as seen in Figure 5, with rising pressure and saturation behavior at higher pressures, which is consistent with observations in the Duan and Sun [52]. Figure 5 shows the comparison of the simulated results and measured data on CO_2 solubility in the pure water system. Overall, there is a good agreement between the published experimental data and our computed data. As can be seen, the solubility of CO_2 rises gradually in a non–linear manner. A clear turning point in the upward trend occurs when the phase with a high concentration of CO_2 transitions from the gaseous phase to the liquid or supercritical phase. The suggested model can precisely quantify the impact of phase transition on the solubility of CO_2. Nevertheless, there is still some ambiguity, particularly at some temperatures such as 298 and 353 °K, due to substantial inconsistencies across the available literature sources. The inconsistencies mostly arose from variations in experimental principles, techniques, and measurement precision [193,214]. Given that other scholars [50,52,141] have extensively examined the

dependability of phase partitioning data, and doing a rigorous review of that topic is not within the scope of this article.

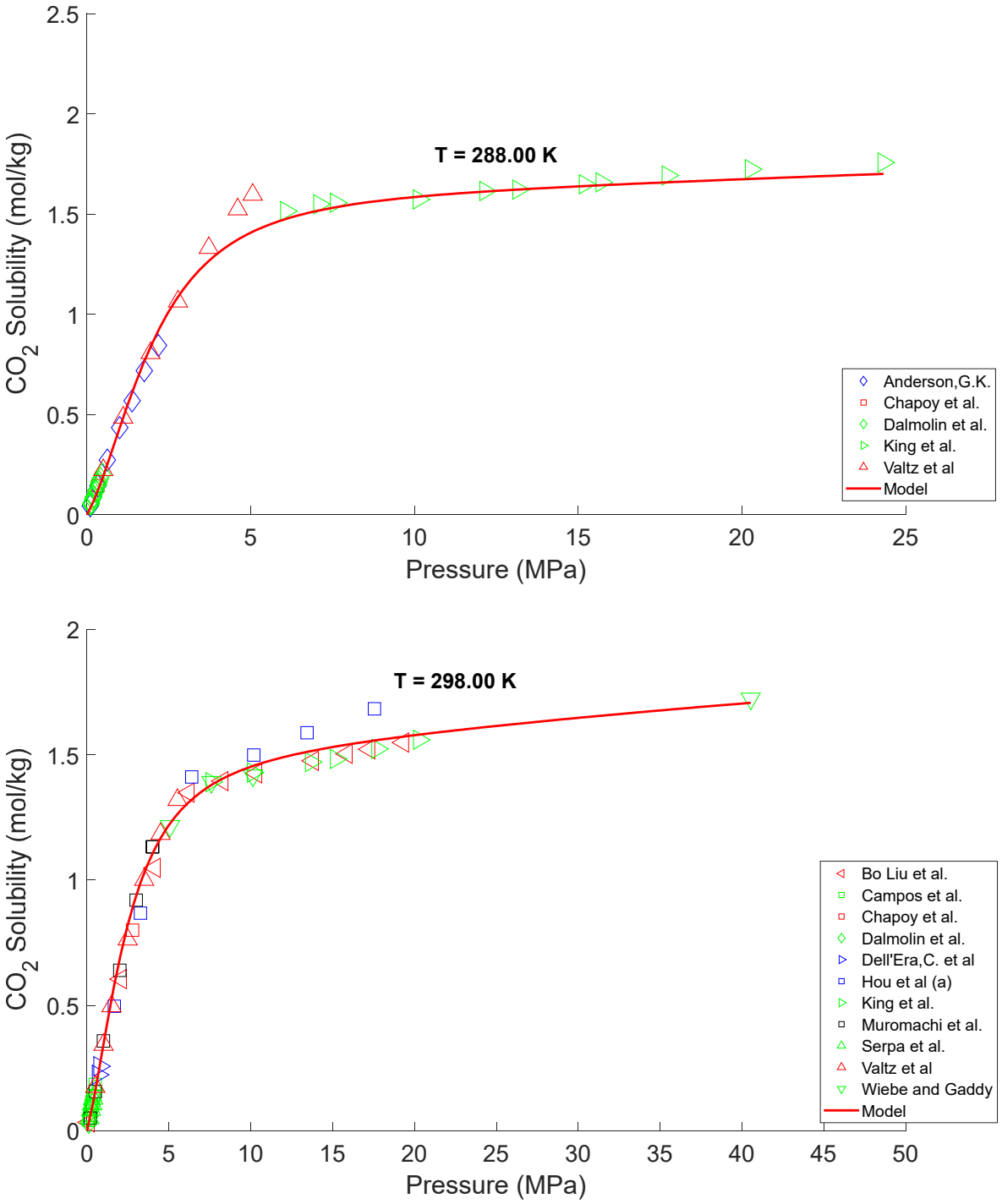

Figure 5. *Cont.*

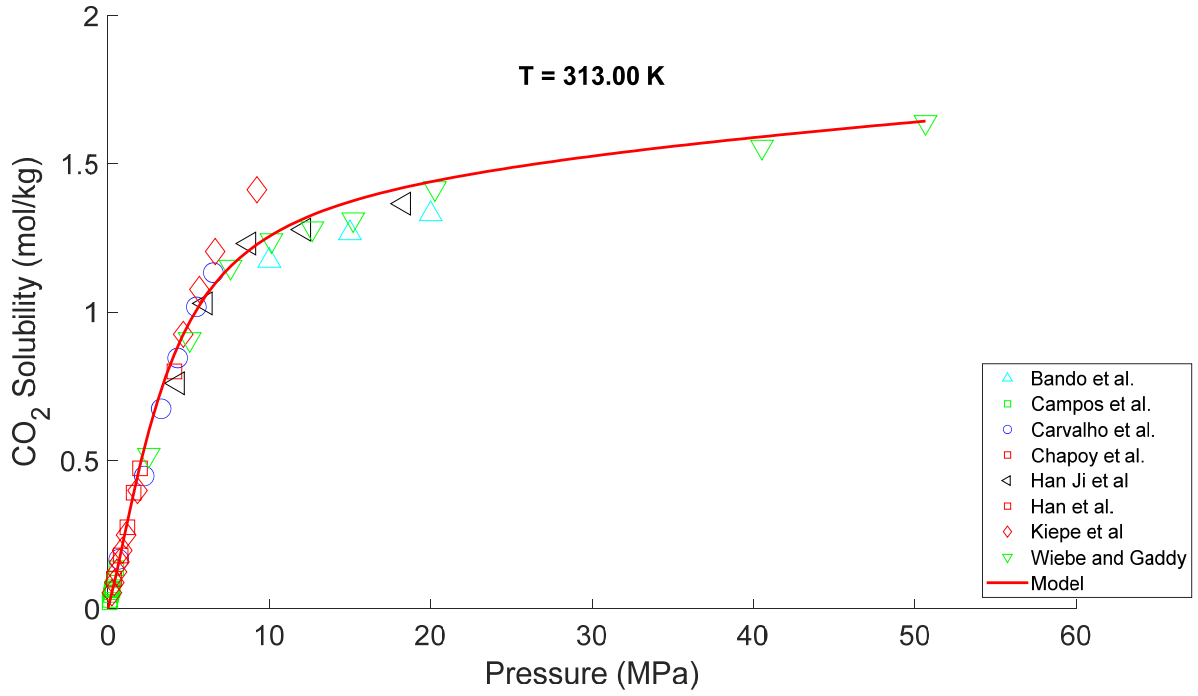

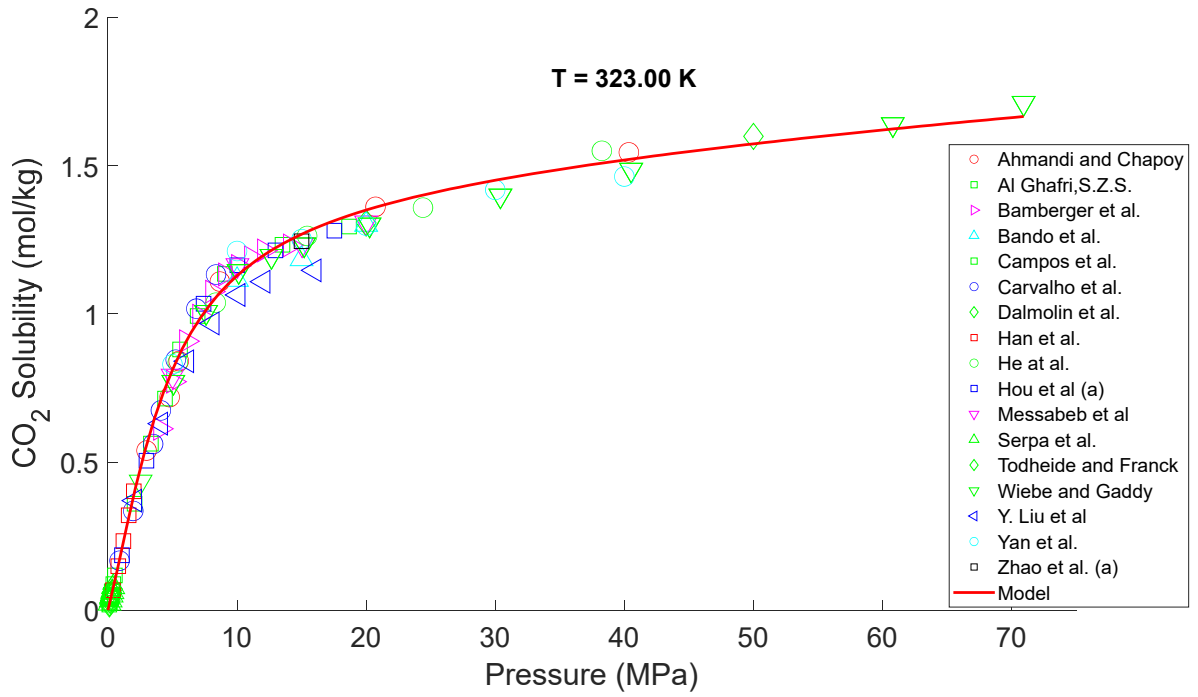

Figure 5. *Cont.*

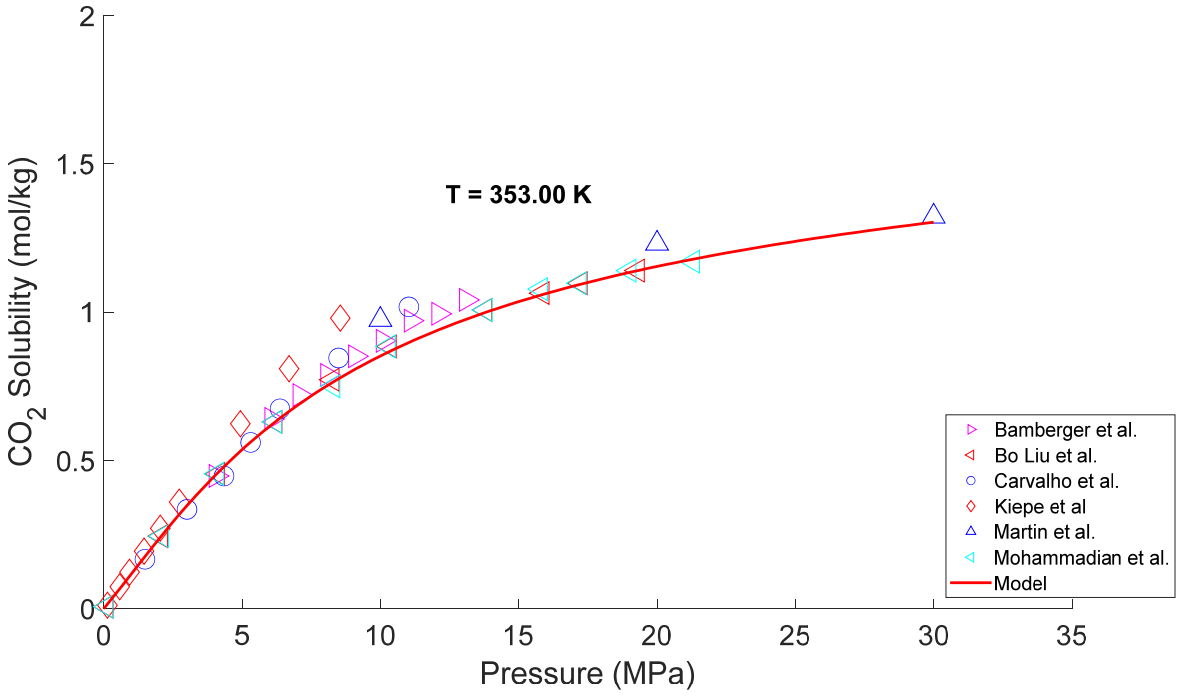

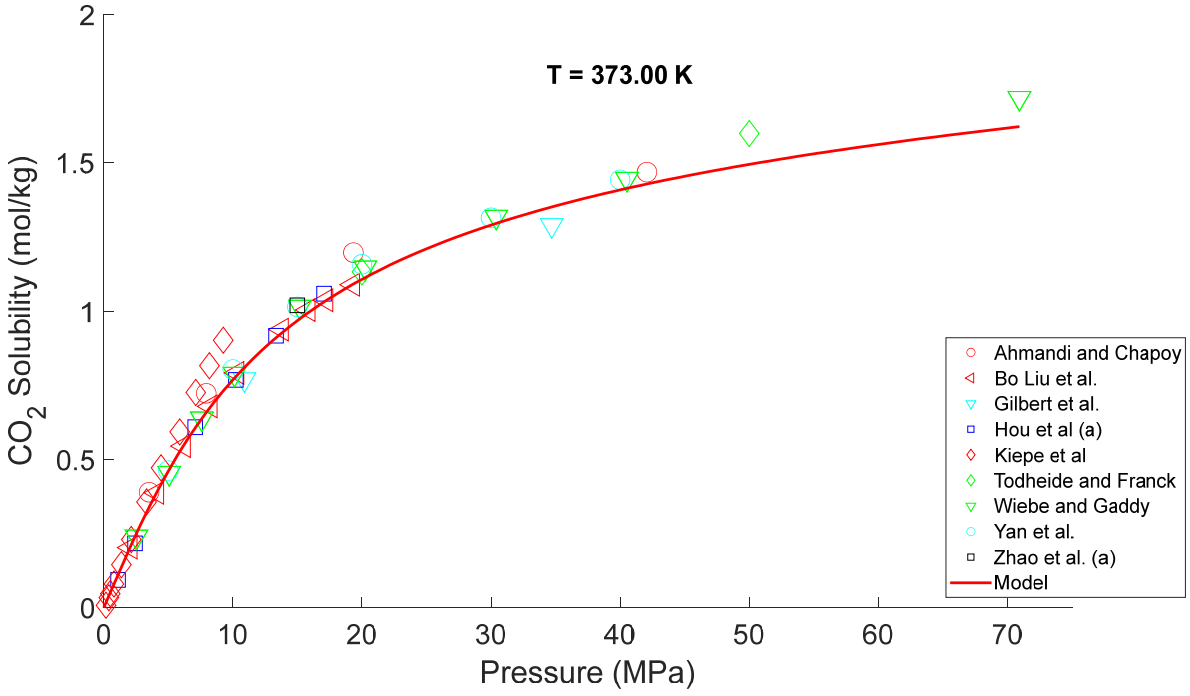

Figure 5. *Cont.*

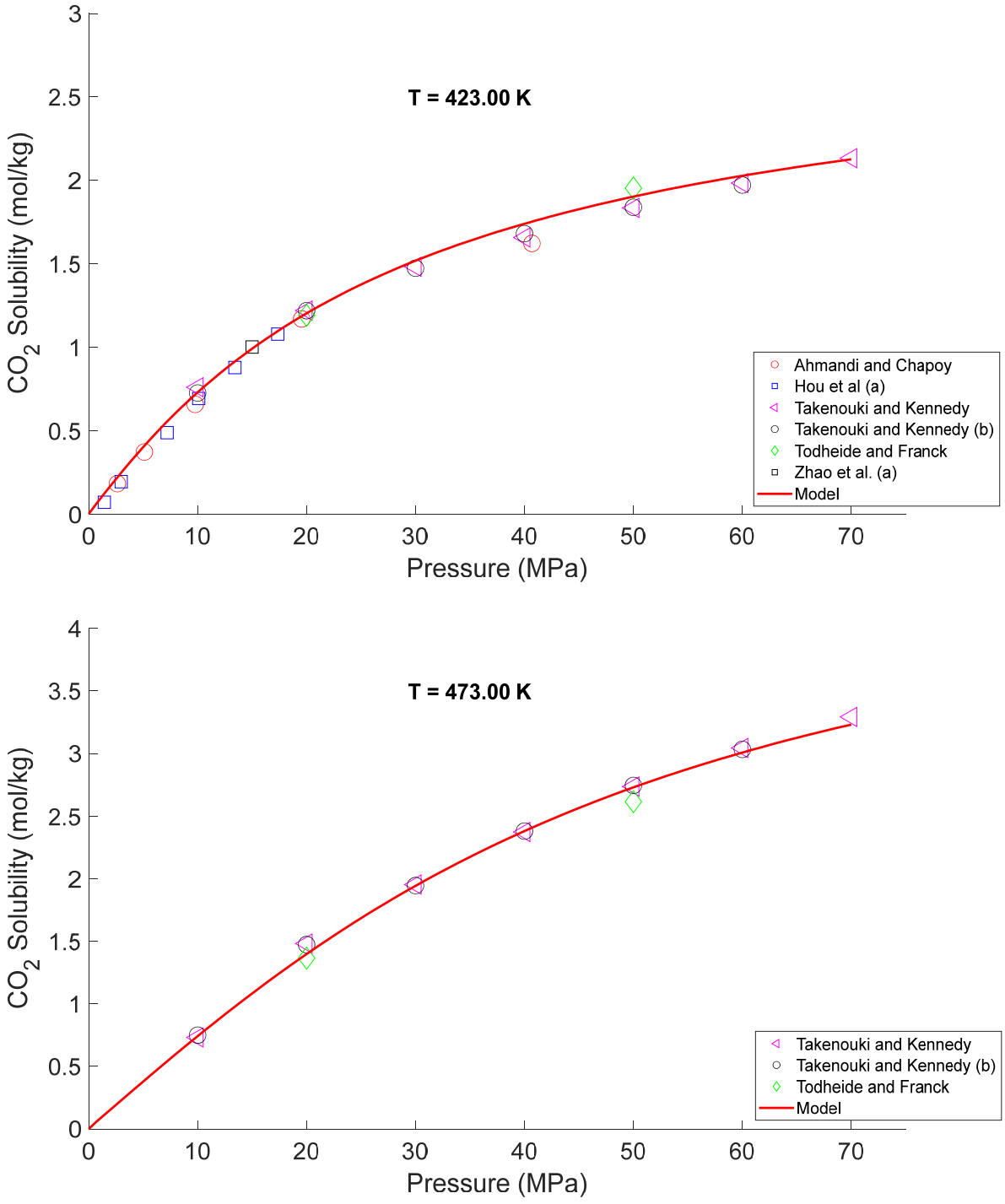

Figure 5. *Cont.*

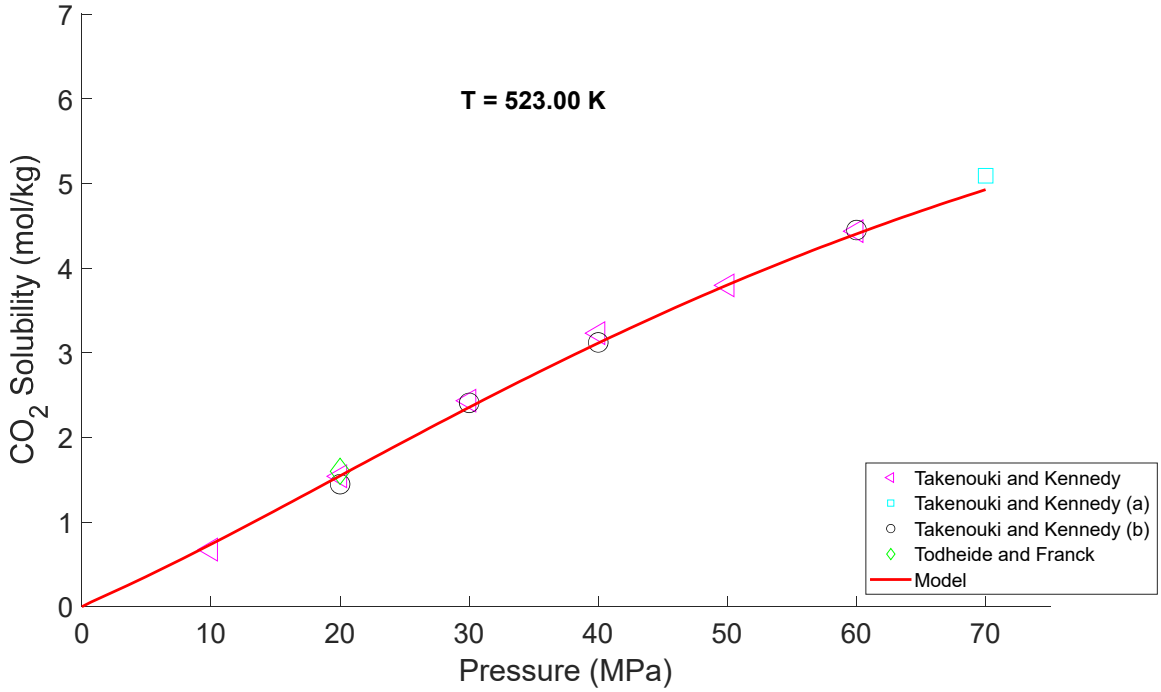

Figure 5. Predicted CO_2 solubility versus experimentally measured data of CO_2 solubility in water at 288 K Refs. [83,84,86,94,96,129], 298 K Refs. [83,84,86,91,92,94,96,97,107,115,125,129,131], 313 K Refs. [88,92–94,102,103,109,131], 323 K Refs. [80,84,85,87,88,91–94,97,102,105,107,113,115,125,129,131, 133,134,136], 353 K Refs. [87,91,93,109,112,114], 373 K Refs. [80,84,91,100,107,109,131,134,136], 423 K Refs. [81,82,84,107,136], 473 K Refs. [80–82], and 523 K Refs. [80–82]. The experimental data are adapted from references shown in the plots.

In Figure 6, the 3D response surface highlights the non–linear relationship between temperature, pressure, and CO_2 solubility. Notably, the surface plot also serves as a phase diagram. The plot demonstrates the obvious effect of pressure on solubility, with solubility increasing steeply at lower temperatures. This behavior aligns with the work of Duan and Sun [52], who reported similar trends in CO_2 solubility in pure water. There exists a high CO_2 solubility region around pressure greater than 5 MPa and temperature less than 300 °K. This high–value region corresponds to the liquid phase of the non–supercritical region based on the temperature and pressure condition of the CO_2 phase diagram. Wiebe and Gaddy [79] conducted early experiments that demonstrated the inverse relationship between temperature and CO_2 solubility. This inverse relationship has been supported by more recent studies, such as those by Sander [215], who reviewed gas solubility data and confirmed that colder temperatures enhance, as seen in Figure 6, solubility due to reduced kinetic energy and enhanced molecular interactions. The surface also suggests that at higher temperatures, the effect of pressure on solubility diminishes slightly, a phenomenon also observed in previous studies by Spycher et al. [49]. Carroll et al. [216] discussed how the exothermic nature of dissolution results in greater solubility at lower temperatures. This is because the lower kinetic energy of molecules in cold water allows for more CO_2 to be absorbed before temperature changes shift the equilibrium.

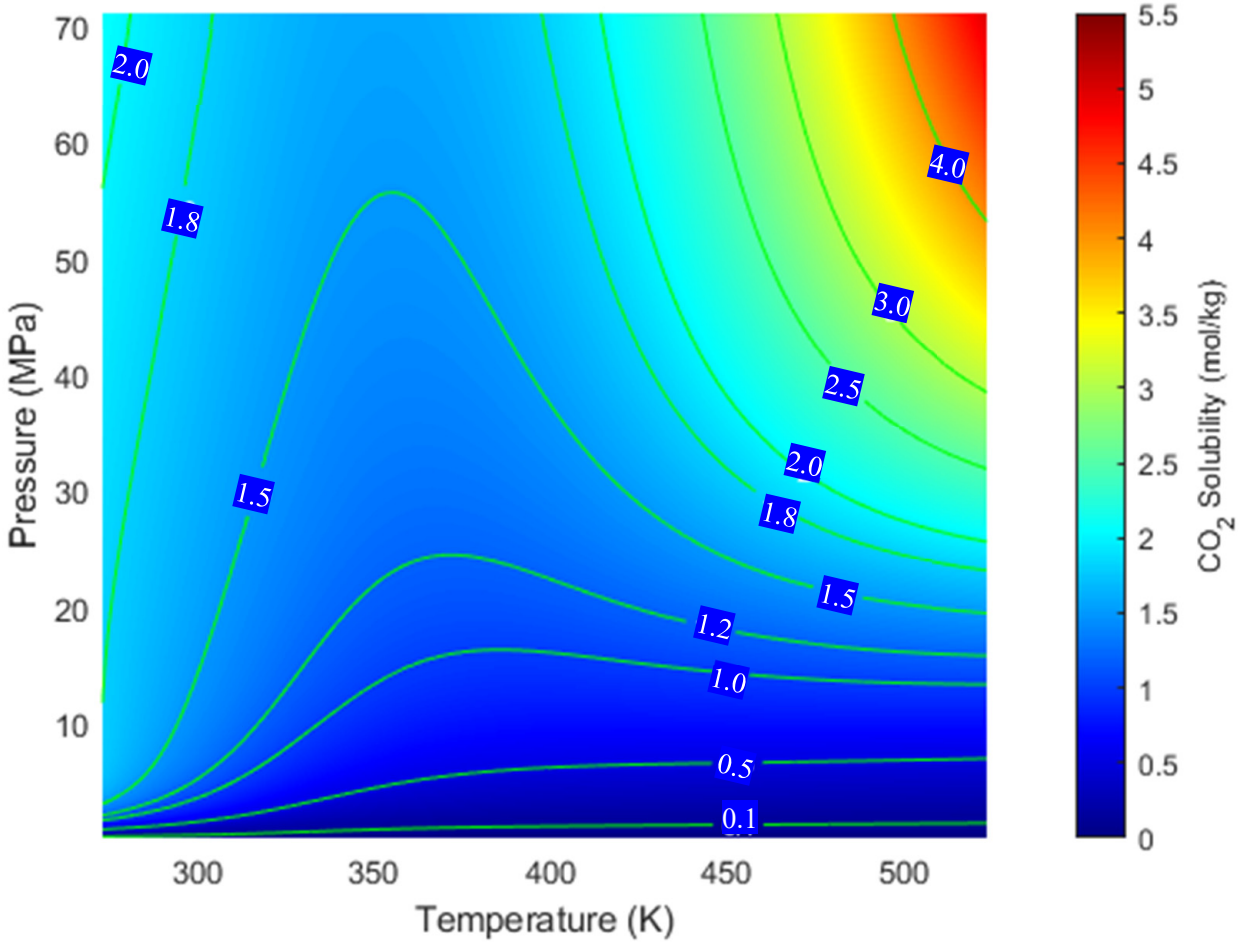

Figure 6. Phase diagram (3D response surface) of CO_2 solubility in water (CO_2–H_2O) system.

4.1.2. CO_2–Water–Salts

The predictive capability of the developed model to predict CO_2 solubility in water (CO_2–H_2O– salt systems) as a function of temperature, pressure, and ionic strength. The developed model strongly agrees with experimental data across various isotherms presented in the following subsections. The subsections present the isotherm curves of mixed salts (Na^+, K^+, Ca^{2+}, Mg^{2+}, Cl^-, HCO_3^-, SO_4^{2-}), monovalent salt (KCl), monovalent salt (NaCl), monovalent salts (NaCl, $NaHCO_3$, and Na_2SO_4) and divalent salts ($CaCl_2$ and $MgCl_2$) system respectively. The isotherm curves presented the predictions of the developed model against experimental data at minimum and maximum ionic strength values for the various systems.

The developed models capture the general trend of increasing CO_2 solubility with rising pressure and the saturation behavior at higher pressures, consistent with observations in the Duan et al. [53]. Similarly, the developed models follow the inverse relationship between temperature and CO_2 solubility. The three–dimensional (3D) surface response was used to illustrate the impact of salinity variation on the solubility of CO_2 in water. The 3D plots depicted in the sections are presented as a function of two factors. In contrast, the third factor was kept at three distinct salinities corresponding to different ionic strength levels. The amount of dissolved CO_2 in water is depicted as a function of the aqueous systems' pressure (MPa) and temperature (K).

Mixed Salts

Mixed salt systems are the commonly encountered salinity in geological engineering applications. The CO_2 solubility in the aqueous phase of mixed salt systems is analyzed in Figures 7–10. The CO_2 solubility is generally less than 1.5 mol/kg at low ionic strength value, with a good agreement between published experimental and model data. Compared to pressure, CO_2 solubility is less sensitive to temperature in mixed salt systems. As shown in Figure 7, CO_2 solubility decreases from about 1.1 mol/kg to 0.8 mol/kg when the temperature increases from 308.15 °K 328.15 °K at 10 MPa. The CO_2 solubility increases gradually as pressure increases, but the variation rate decreases. This same trend of an inverse relationship between temperature and CO_2 solubility was observed in Figures 8–10 with ionic strengths of 1.80, 2.743 and 6.0 mol/kg, respectively. Furthermore, Figure 11 illustrates the salting–out effect on a 3D response surface plot. This effect results from the interaction between the CO_2 molecules, water, and ions, responsible for decreased CO_2 solubility in a saline system as salinity increases.

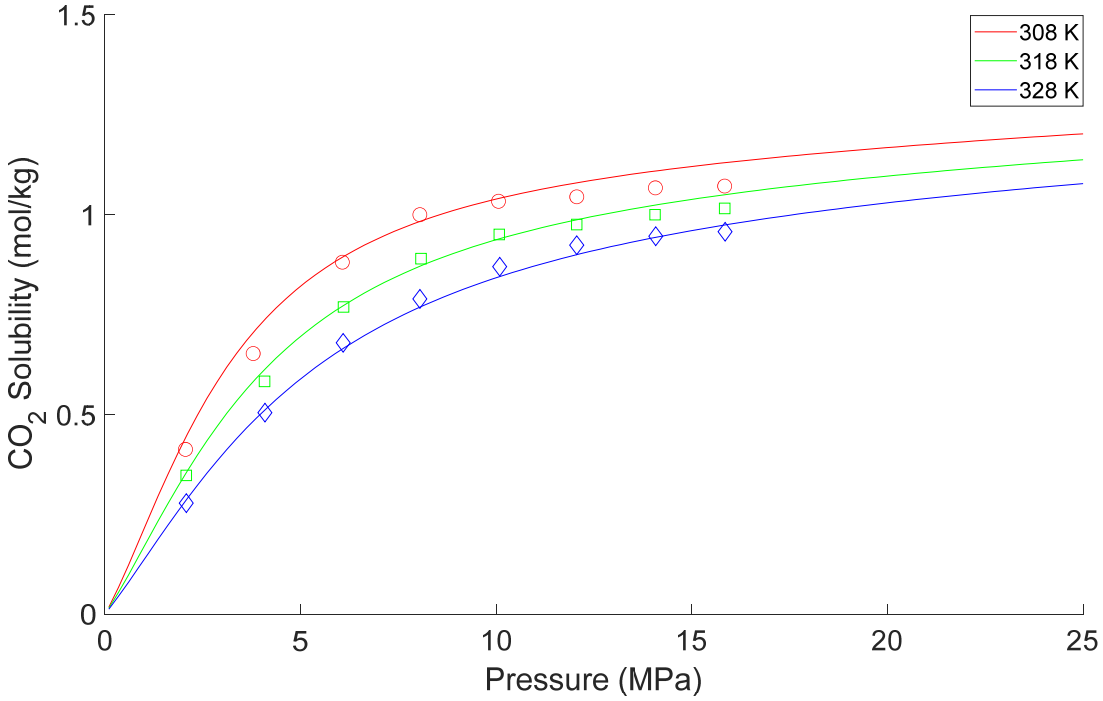

Figure 7. Predicted CO_2 solubility versus experimentally measured data of CO_2 solubility in a mixed salt solution with an ionic strength of 0.9596 mol/kg. The experimental data are adopted from Y. Liu et al. [133]. The symbols represent experimental measurements: circles (308 K), squares (318 K), and diamonds (328 K). The solid lines correspond to the model predictions for each temperature: red for 308 K, green for 318 K, and blue for 328 K.

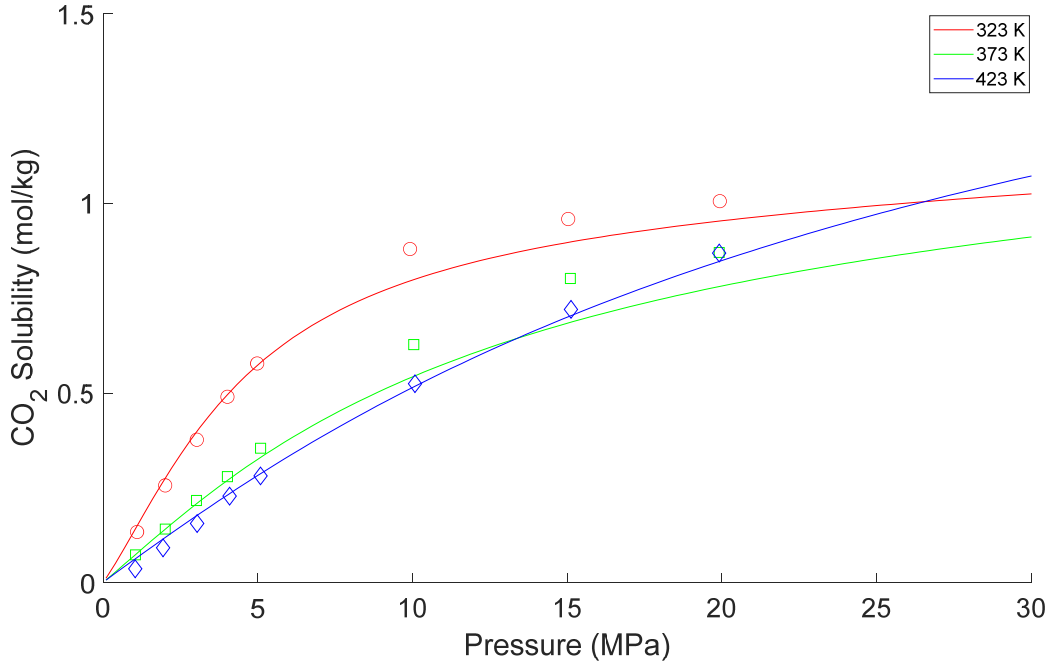

Figure 8. Predicted CO_2 solubility versus experimentally measured data of CO_2 solubility in a mixed salt solution with an ionic strength of 1.80 mol/kg. The experimental data are adopted from Poulain et al. [118]. The symbols represent experimental measurements: circles (323 K), squares (373 K), and diamonds (423 K). The solid lines correspond to the model predictions for each temperature: red for 323 K, green for 373 K, and blue for 423 K.

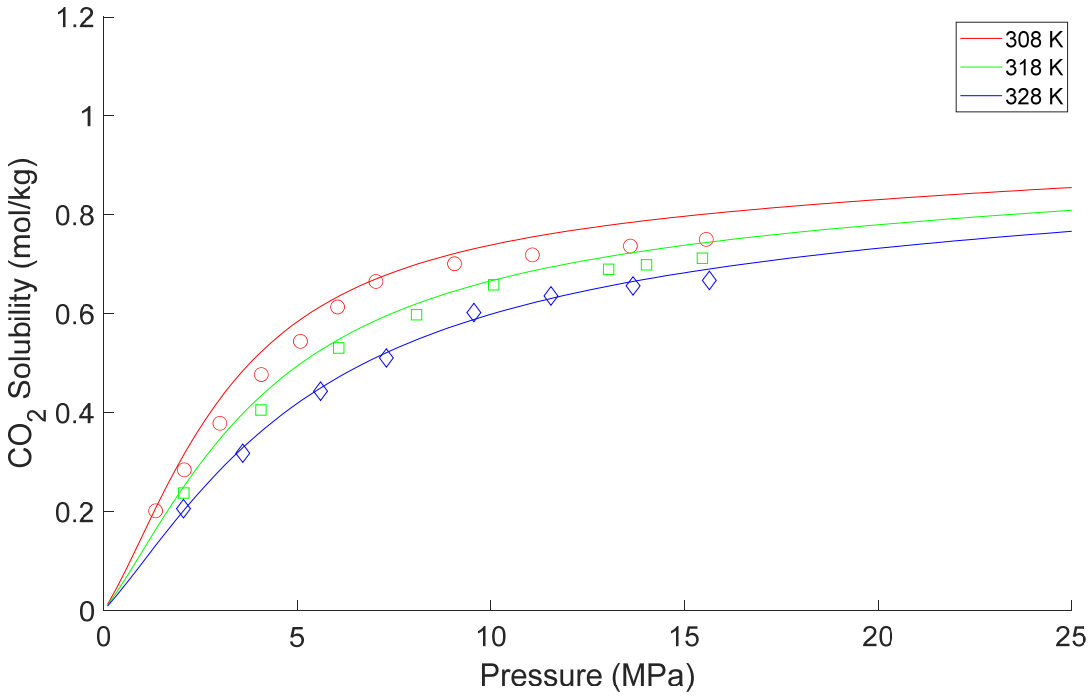

Figure 9. Predicted CO_2 solubility versus experimentally measured data of CO_2 solubility in a mixed salt solution with an ionic strength of 2.743 mol/kg. The experimental data are adopted from Y. Liu et al. [133]. The symbols represent experimental measurements: circles (308 K), squares (318 K), and diamonds (328 K). The solid lines correspond to the model predictions for each temperature: red for 308 K, green for 318 K, and blue for 328 K.

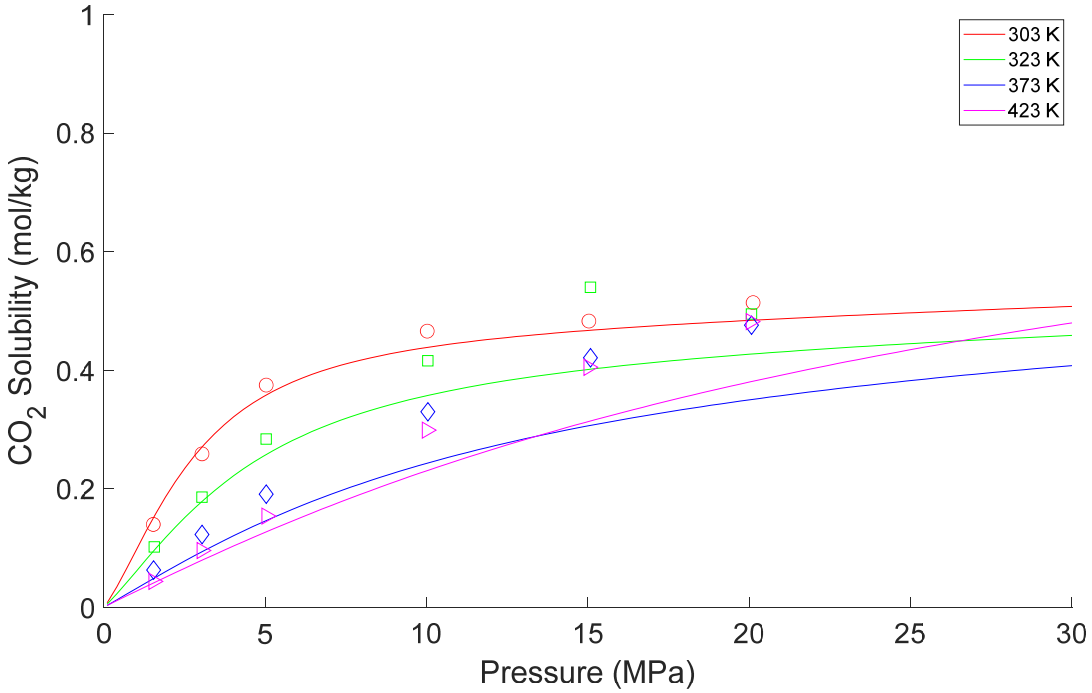

Figure 10. Predicted CO_2 solubility versus experimentally measured data of CO_2 solubility in a mixed salt solution with an ionic strength of 6.0 mol/kg. The experimental data are adopted from Dos Santos al. [98]. The symbols represent experimental measurements at different temperatures: circles for 303 K, squares for 323 K, diamonds for 373 K, and triangles for 423 K. The lines correspond to the model predictions at each temperature: red for 303 K, green for 323 K, blue for 373 K, and magenta for 423 K.

Finally, as seen in Figure 5 through to Figure 11, the developed model's ability to accurately predict CO_2 solubility under various conditions validates its application for sequestration and enhanced oil recovery (EOR) scenarios, where such solubility data is crucial. The consistency of the model with empirical data supports its robustness and reliability for simulating behavior in subsurface environments, which is essential for predicting the performance injection in geological formations. For brevity, details of the CO_2 solubility validation results for the singles salts are presented in the Supplementary Material.

4.2. Validation of the Developed H_2 Solubility Correlations

Here, we present the outcome of the developed correlations for H_2 solubility in water and saline systems composed of NaCl and seawater. The performance of developed correlations is validated against experimentally measured data and presented as isotherms curves and response surface plots.

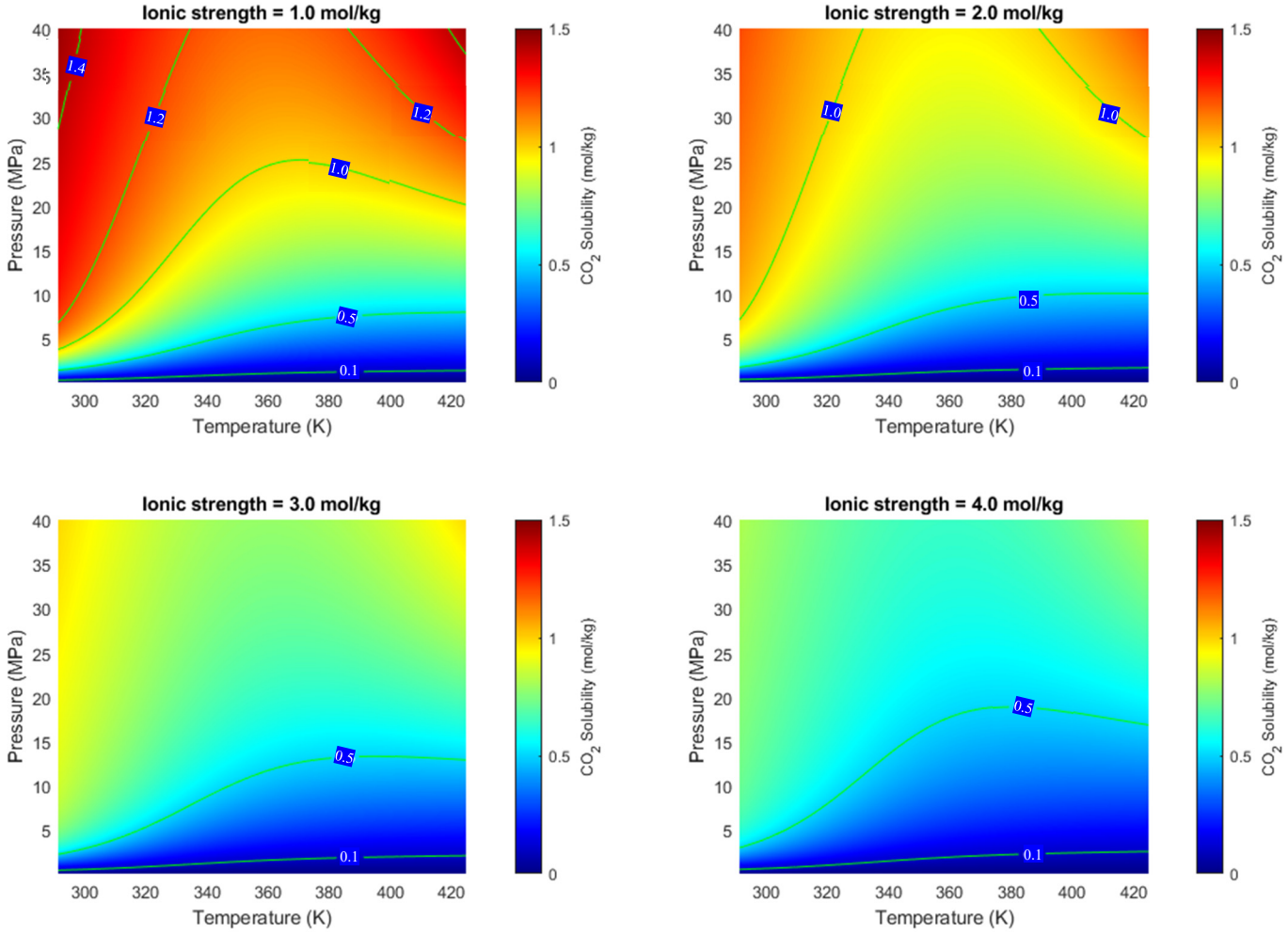

Figure 11. 3D response surfaces of CO_2 solubility (Mixed salt) system at different salinities in terms of ionic strength.

4.2.1. H_2–H_2O

Figure 12 shows the isotherms of H_2 solubility at varying pressures. The model exhibits excellent prediction performance of the experimentally measured data from low and higher temperatures. The developed model shows strong agreement with experimentally measured data across various isotherms. The model captures the typical relationship of increasing H_2 solubility with rising pressure and the saturation behavior at higher pressures, as seen in Figure 12, which is consistent with observations from Zhu et al. [54]. Further, the developed correlation is reliable for modeling the quadratic relationship between temperature and H_2 solubility. As observed in Figure 12, at lower temperatures (273.15 K), H_2 solubility is higher compared to medium temperatures (323.15 K and 373.15 K) at equivalent pressures. However, at 323.15 K, the solubility is lower than at 373.15 K, affirming the quadratic relationship between H_2 solubility and temperature. Thus, H_2 solubility initially decreases as the temperature rises from low to medium levels, then begins to increase as the temperature shifts from medium to high values. According to Lopez–Lazaro [44], the Henry characteristic curve peaks at a temperature of approximately 330 K, which is about 57 °C. This means that hydrogen dissolution is lowest at this temperature. This outcome generally explains how small molecule dissolves in pure water. Also, the temperature at which the minimal solubility occurs depends on the presence and properties of the solute. This pattern has also been noted in the research by Zhu et al. [54]

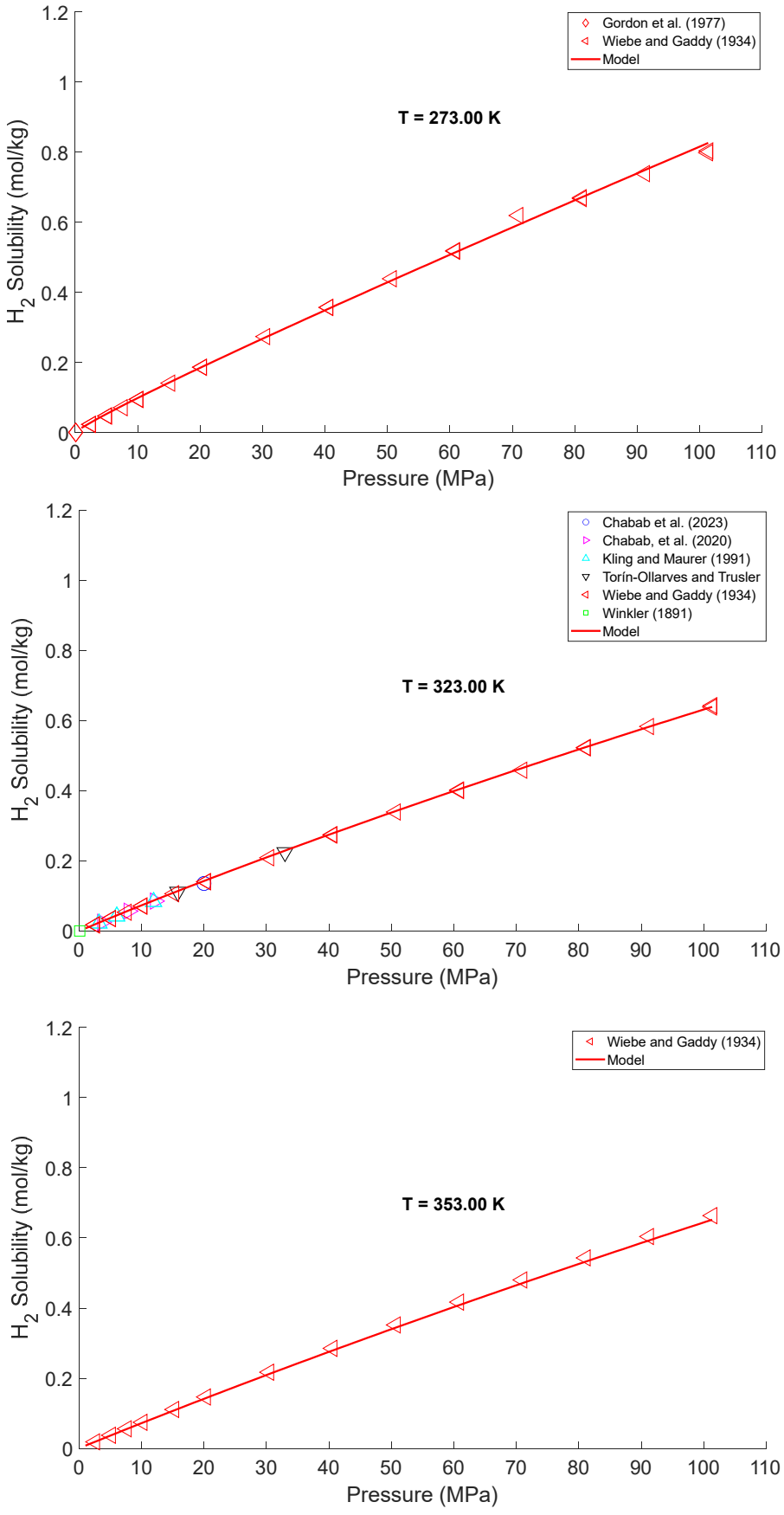

Figure 12. *Cont*.

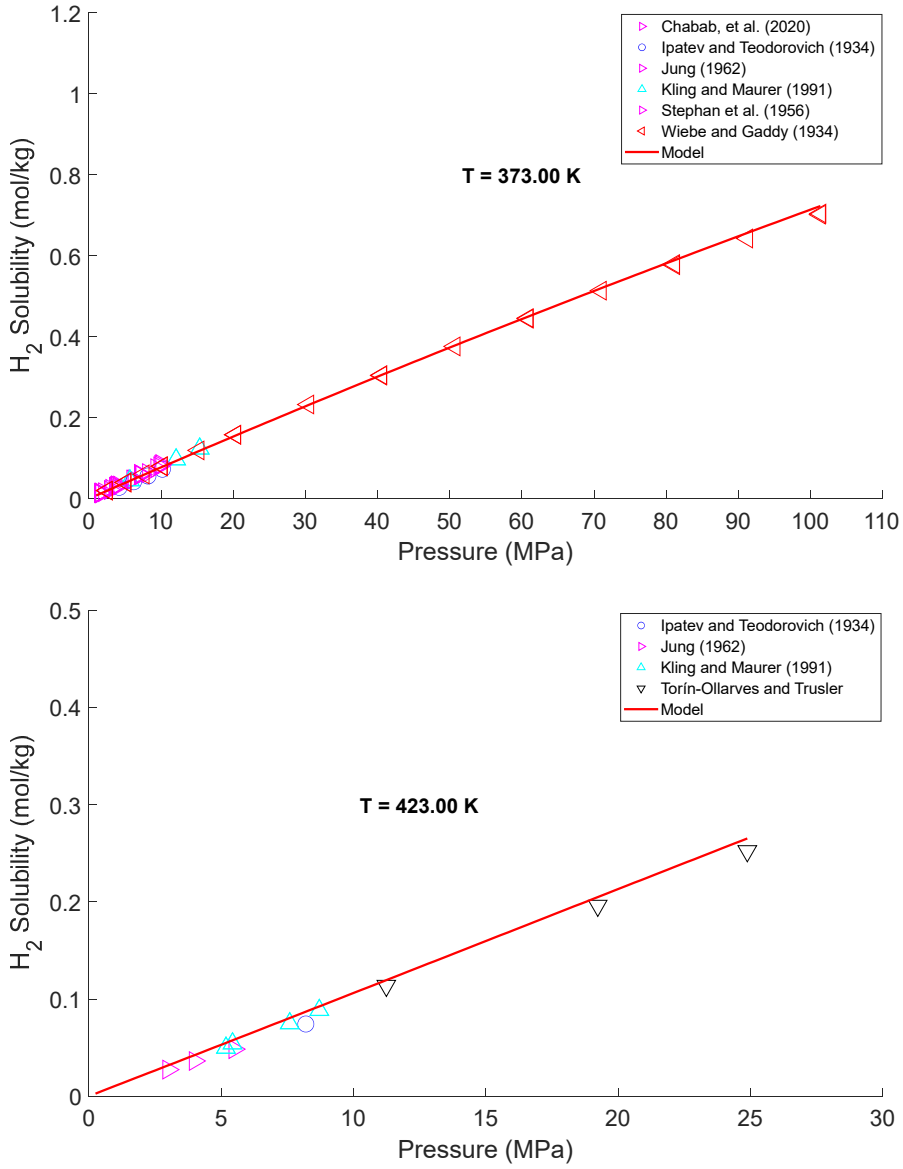

Figure 12. Predicted H_2 solubility versus experimentally measured data of H_2 solubility in water at 273 K Refs. [154,180], 323 K Refs. [59,154,157,160,171,188], 353 K Ref. [154], 373 K Refs. [59,154,167, 171,178,188], and 423 K Refs. [157,167,178,188]. The experimental data are adapted from references shown in the plots.

Figure 13 shows the 3D response surface that highlights the non–linear relationship between temperature, pressure, and H_2 solubility. Notably, the surface plot demonstrates the effects of pressure and temperature on solubility beyond the physical condition of available experimental data. There exists a high H_2 solubility region around pressure greater than 50 MPa and temperature less than 500 °K. This high–value region corresponds to the fluid phase region based on the temperature and pressure condition of the H_2 phase diagram. For instance, the 3D response surface plot reveals high H_2 solubility values up to 5 mol/kg at high temperature and pressure regions. The solubility results of this high pressure and temperature region are essential to natural hydrogen production processes. This region requires experimentally measured data to validate the prediction of the developed models.

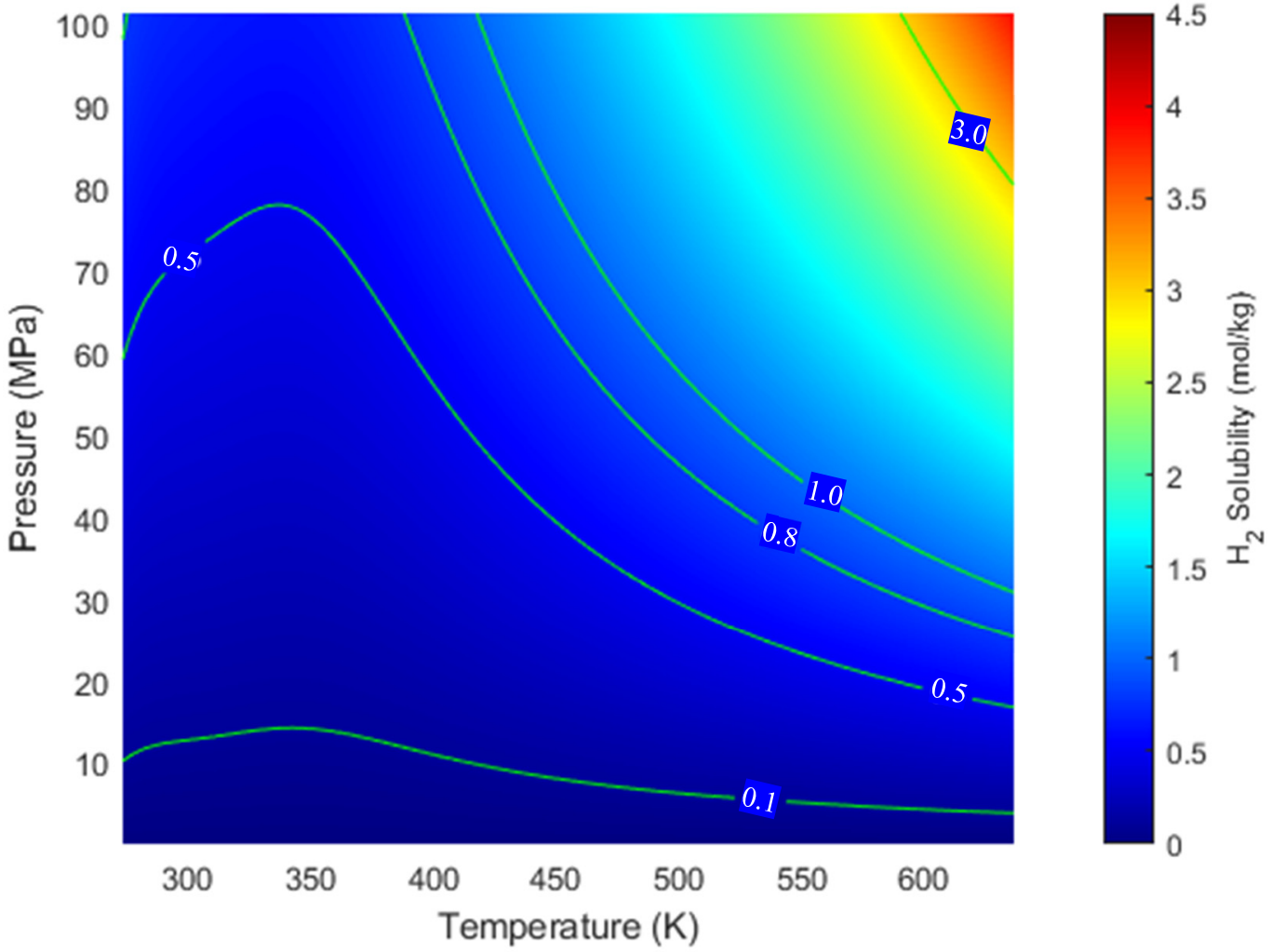

Figure 13. Phase diagram (3D response surface) of H_2 solubility (H_2–H_2O) system.

4.2.2. H_2 + H_2O + Salts (NaCl)

The predictive capability of the developed model is to predict H_2 solubility in water (H_2–H_2O– salt systems) as a function of temperature, pressure, and ionic strength. The developed model shows strong agreement with experimental data across various isotherms, as shown in Figures 14–16. Figures 14–16 represents the isotherm curves of the salt (NaCl) system at ionic strengths of 1.0, 2.0, and 5.0 mol/kg. The isotherm curves presented show the predictions of the developed model against experimental data at the minimum and maximum ionic strength values for the studied system. The developed models capture the general trend of decreasing H_2 solubility in aqueous solutions, which is consistent with observations by Zhu et al. [54]. Similarly, the developed models also follow the inverse relationship between temperature and H_2 solubility.

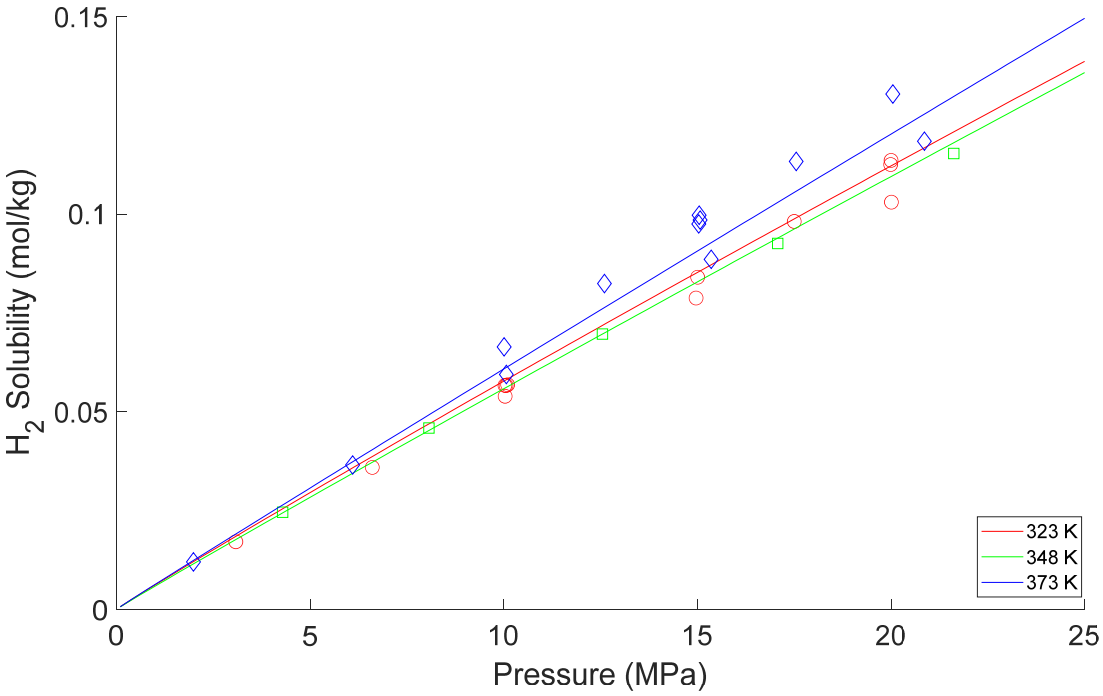

Figure 14. Predicted H_2 solubility versus experimentally measured data of H_2 solubility in a NaCl solution with an ionic strength of 1.0 mol/kg. The experimental data are adapted from Chabab et al. [59] and Chabab et al. [152]. The symbols represent experimental measurements: circles (323 K), squares (348 K), and diamonds (373 K). The solid lines correspond to the model predictions for each temperature: red for 323 K, green for 348 K, and blue for 373 K.

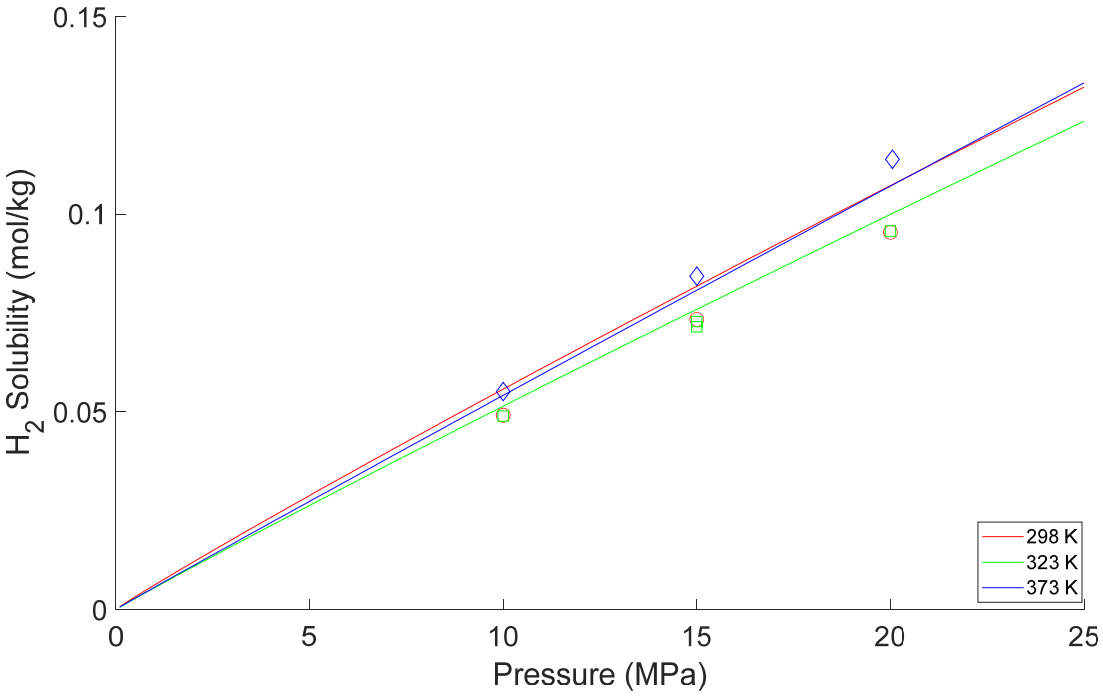

Figure 15. Predicted H_2 solubility versus experimentally measured data of H_2 solubility in a NaCl solution with an ionic strength of 2.0 mol/kg. The experimental data are adapted from Chabab et al. [59]. The symbols represent experimental measurements: circles (298 K), squares (323 K), and diamonds (373 K). The solid lines correspond to the model predictions for each temperature: red for 298 K, green for 323 K, and blue for 373 K.

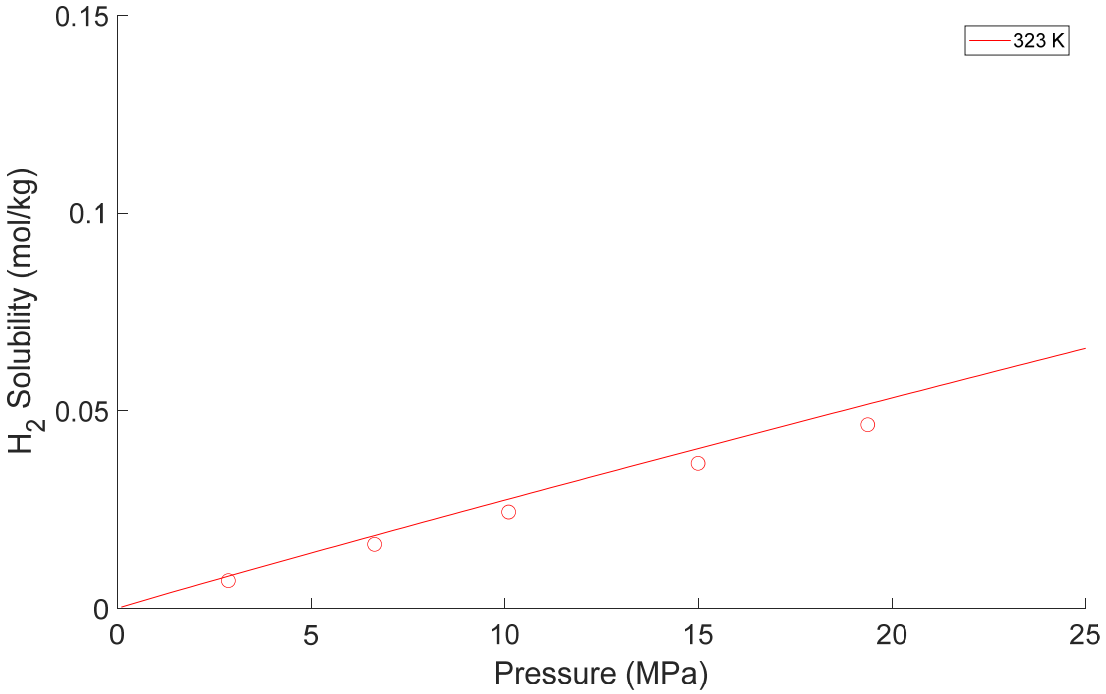

Figure 16. Predicted H_2 solubility versus experimentally measured data of H_2 solubility in a NaCl solution with an ionic strength of 5.0 mol/kg. The experimental data are adapted from Chabab et al. [59]. The symbols represent experimental measurements: circles (323 K). The solid lines correspond to the model predictions for each temperature: red for 323 K.

Figure 17 which describes the 3D surface response (phase diagram) was used to illustrate the impact of salinity variation on the solubility of H_2 in water. The plots depicted in the sections are presented as a function of two varying factors, while the third factor was maintained at three distinct salinity ionic strength levels. The amount of dissolved H_2 in water is depicted in Figure 17 as a function of the aqueous systems' pressure (MPa) and temperature (K). The salinity is maintained at a constant level by using these four ionic strength values (1.0, 2.0, 3.0 and 4.0 mol/kg).

The salting–out effect, which is the result of the interaction between the H_2 molecules, water, and ions, is responsible for the decrease in H_2 solubility in a saline system as the salinity increases. The majority of water molecules are surrounded by the cations/anions that dissociate from dissolved salts, and only a small number of water molecules are capable of interacting with H_2 [54,59,152]. Consequently, it is hypothesized that the solubility of H_2 is reduced due to the interaction between saline water and H_2 during H_2 during the injection and production processes. In the same vein, the reference [54], reported that the solubility of H_2 increases linearly with pressure. The H_2 molecules are compelled to sink into the dense water phase and become adsorbed as a result of the increased pressure exerted on them.

Furthermore, in Figure 12 through to Figure 17, the developed model's ability to accurately predict H_2 solubility under various conditions validates its application for underground hydrogen storage and natural hydrogen production scenarios, where such H_2 solubility data is critical. The consistency of the model with empirical data supports its robustness and reliability for simulating behavior in subsurface environments, which is essential for predicting the performance injection in geological formations.

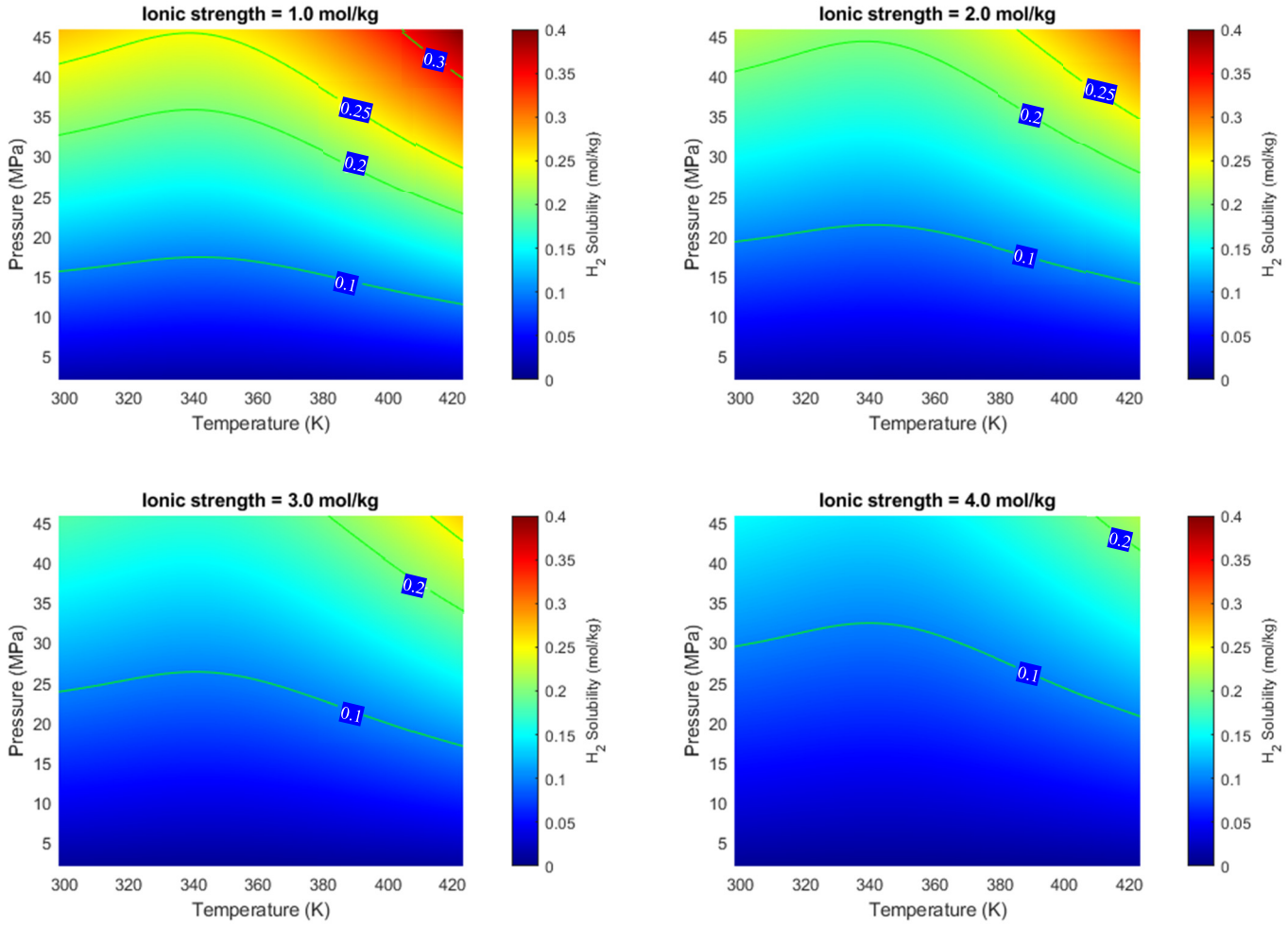

Figure 17. 3D response surfaces of H_2 solubility (NaCl and seawater) system at different salinities in terms of ionic strength.

4.3. Salting–Out Effect

The salting–out effect, which is the result of the interaction between the CO_2 molecules, water, and ions, is responsible for the decrease in CO_2 solubility in a saline system as the salinity increases. The majority of water molecules are surrounded by the cations/anions that dissociate from dissolved salts, and only a small number of water molecules are capable of interacting with CO_2 [49,53]. Consequently, it is hypothesized that the solubility of CO_2 is reduced because of the interaction between saline water and CO_2 during the injection procedure. In the same vein, Duan et al. [53] reported that the solubility of CO_2 increases linearly with pressure. The CO_2 molecules are compelled to sink into the dense water phase and become adsorbed due to increased pressure exerted on them. This increase in solubility continues until a pressure point is reached where the solubility value plateaus.

Kaur et al. [217] thermodynamically studied the solubility of CO_2 in different brine systems and reported the salting–out effect of different electrolyte solutions expressed in terms of their ionic strength. Figure 18 shows the salting–out effect of various salts performed in this study. The decreasing trend of CO_2 solubility observed follows the order $NaHCO_3 > KCl > CaCl_2 \sim MgCl_2 > NaCl > Na_2SO_4$, and it is consistent with those reported by Zhao et al. [135] on the basis of ionic strength.

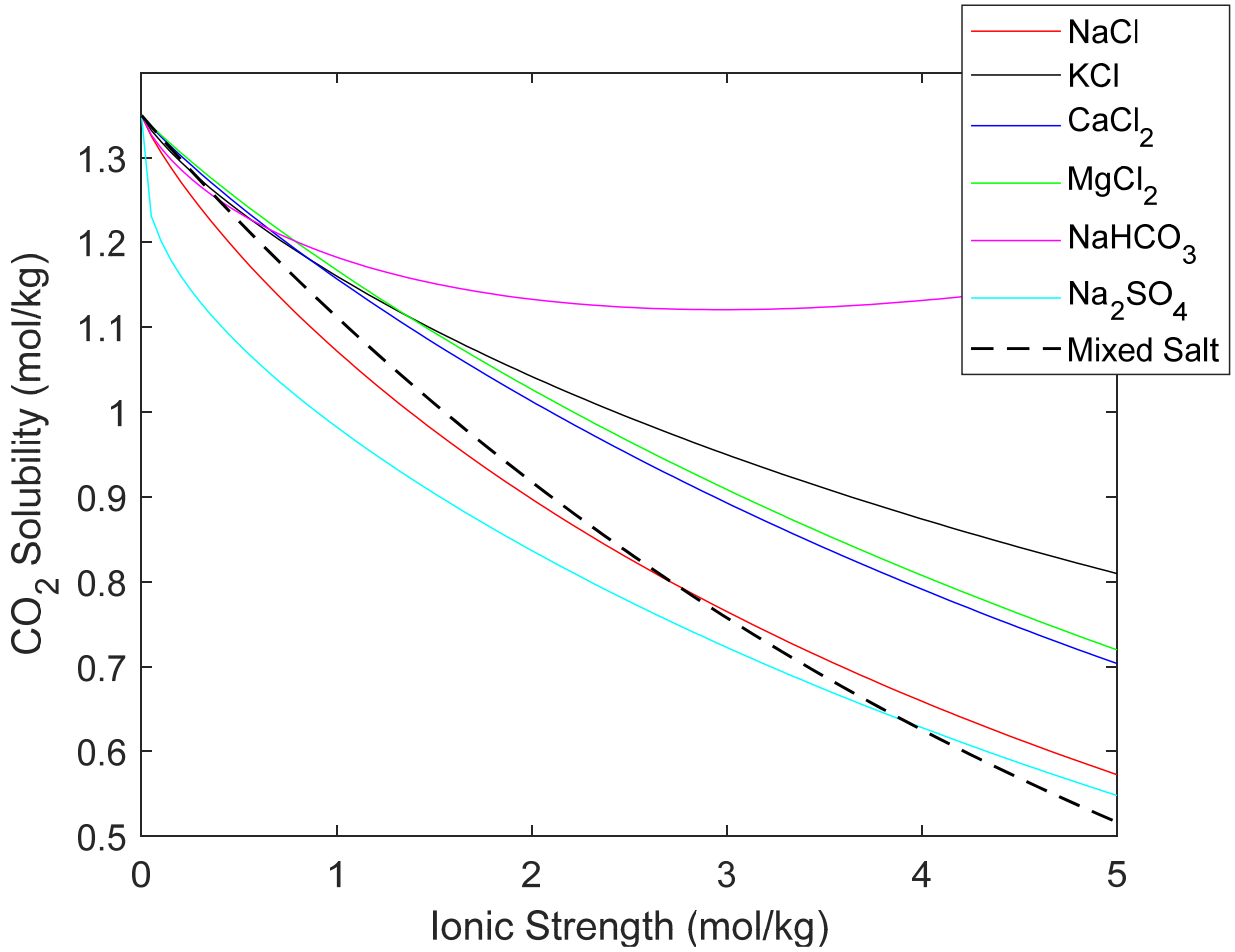

Figure 18. Salting out the effect of the different salts at 20MPa and 323.15K.

Similarly for hydrogen gas solubility in water, Setschenow's constant [18] or the percentage reduction in solubility, $SO = 100\left(\frac{mH_2{}^{water} - mH_2{}^{brine}}{mH_2{}^{water}}\right)$ under the same thermodynamic factors of temperature, pressure, and salinity [110] are usually used to determine the salting–out (SO) impact on gas solubility for hydrogen. In this work, we employed the SO method to quantify the SO impact on the solubility of H_2 in NaCl solution.

Figure 19 shows the salting–out influence of H_2 on the NaCl solution modeled in the present study. The calculated SO values for H_2 solubility in NaCl brine from this work are shown in Table 5, and the comparison is made with three other published studies. Notably, with the exception of Torín–Ollarves and Trusler's [157] findings, the results of this study, and two previous research studies [59,152] demonstrate comparable salting–out behavior for H_2. Despite being carried out at low pressures (because pressure only little influences the salting–out effect), the results are consistent with previous work on other gases using Setschenow's constant [218]. Though solubility is affected by a number of parameters [219], the variance in salting–out behavior is most likely caused by molecule size variations, a trend seen in noble gases (Ballentine et al. [18]). Thus, molecular simulations could offer valuable insight into the distinctive behavior of hydrogen in aqueous solutions in comparison to other gases.

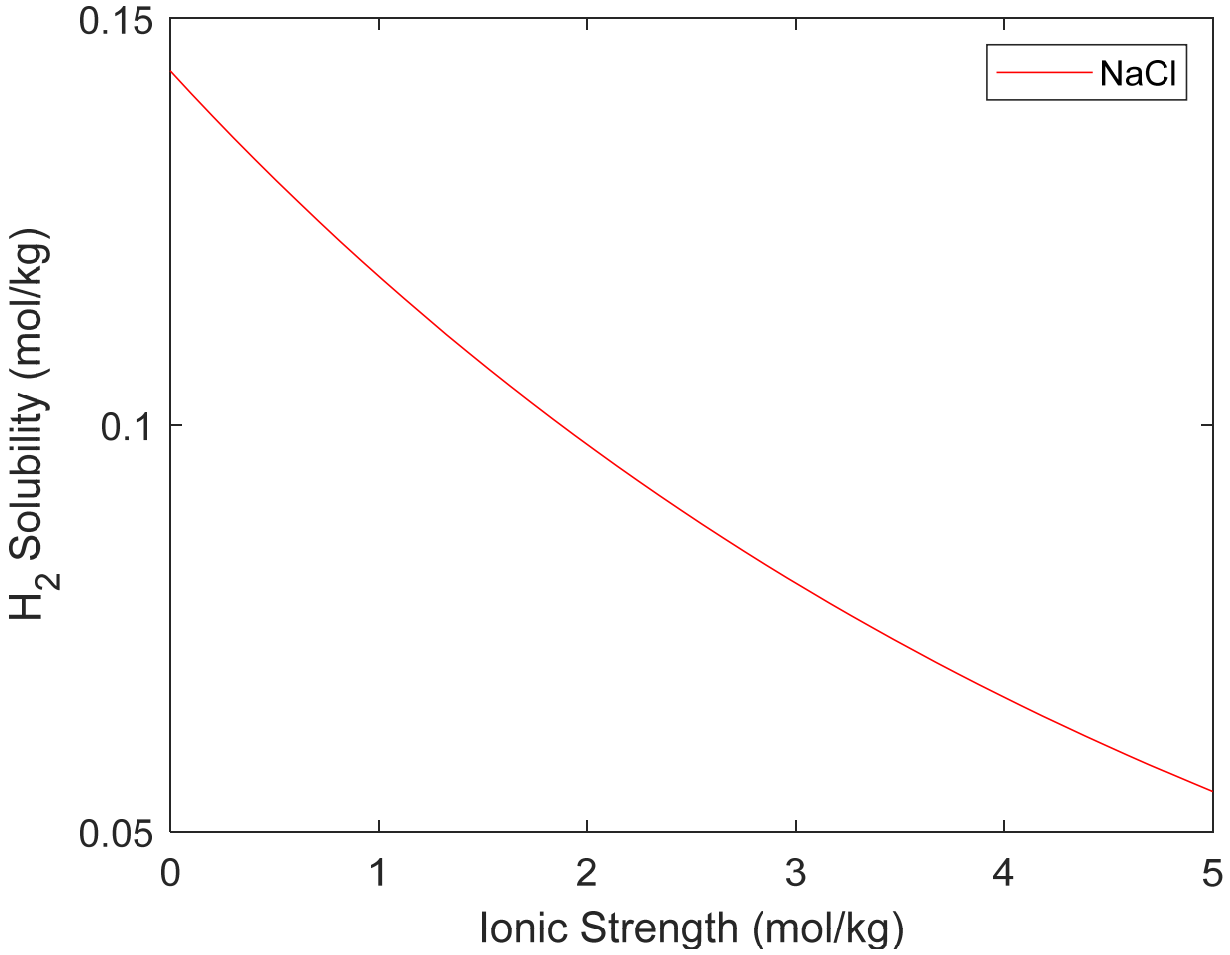

Figure 19. Salting–out effect on the solubility of H_2 in NaCl brine at 20 MPa and 323.15 K.

Table 5. The reduction in solubility due to H_2 gas in NaCl brine (Salting–out effect).

	NaCl Molality (mol/kg)	
SO (%) at 323.15 K	**1**	**4**
Chabab et al. [59]	24.28	60.09
Torín–Ollarves and Trusler r [157]	13.10	42.98
Chabab et al. [152]	16.23	50.70
This study	17.60	53.67

4.4. Evaluation of Developed Solubility Models

The following statistical evaluation metrics were used to assess the performance of the developed models: coefficient of correlation (R^2), average percent deviation (APE), and average absolute percent deviation (AAPE). The mathematical expressions for these criteria are provided in Equations (15)–(17).

$$R^2 = 1 - \frac{\sum_{i=0}^{n}\left(X_{i,\,exp} - X_{i,\,pred}\right)^2}{\sum_{i=0}^{n}\left(X_{i,\,exp} - \overline{X}\right)^2} \tag{15}$$

$$APE = \frac{1}{n}\sum_{i=0}^{n}\left(\frac{X_{i,\,exp} - X_{i,\,pred}}{X_{i,\,exp}} * 100\right) \tag{16}$$

$$AAPE = \frac{1}{n}\sum_{i=0}^{n}\left|\frac{X_{i,\,exp} - X_{i,\,pred}}{X_{i,\,exp}} * 100\right| \quad (17)$$

In these equations, $X_{i,exp}$ represent experimentally measured solubility data, $X_{i,pred}$ refers to the solubility values predicted by the model and $\overline{X}$, denotes the average value of the experimentally obtained solubility dataset. The predictability of the developed correlations was evaluated using statistical analyses. The evaluation of the developed empirical correlations for CO_2 and H_2 solubilities is provided in Table 6.

Table 6. Summary of the performance of developed empirical correlations against CO_2 and H_2 solubility experimental data.

Correlation	Systems	Parameter Ranges	Correlations Performance Metrics			
			No. of Data Points	R^2	APE (%)	AAPE (%)
CO_2–Water	—		926	0.993	2.34	7.62
CO_2–Water–Salt	Mixed Salts (K^+, Na^+, Ca^{2+}, Mg^{2+})		391	0.971	−0.7585	8.1914
	KCl		260	0.958	−4.89	12.04
	NaCl		766	0.983	−3.87	10.01
	Na_2SO_4		226	0.945	0.46	9.13
	$NaHCO_3$		75	0.992	−5.15	8.52
	$CaCl_2$		355	0.989	1.81	6.91
	$MgCl_2$		223	0.988	−0.49	6.81
H_2–Water	—		360	0.999	−0.90	4.03
H_2–Water– Salt	NaCl		78	0.965	−4.94	9.91

Table 6 shows the R^2, APE, and AAPE metrics for each developed CO_2 solubility correlation. Overall, the correlation for the CO_2–H_2O system is the most reliable, closely followed by the correlation for the CO_2–H_2O–divalent salt system. However, during the development of all CO_2 correlations exhibited good prediction results ($R^2 > 0.945$), which means that the proposed models can explain 94.5% of the variability in solubility of CO_2 (mol/kg). The correlation for the CO_2–H_2O system presents the performance compared with experimental data ($R^2 = 0.993$ and AAPE = 7.62). The relative closeness of the R^2 to 1 and low of the AAPE value show that predictions of the developed correlations are closely fitted to the true measured values. Therefore, it is an indication that the mathematical models are good enough to describe the CO_2 experimental measured data.

Similarly, for H_2 solubility data, Table 6 shows the statistical evaluation metrics for each developed H_2 solubility correlation. Overall, the correlation for the H_2–H_2O system is the most reliable, closely followed by the correlation for the H_2–H_2O–salts (NaCl) system. However, the overall performance of the correlations during the development of the H_2 correlations achieved good prediction results ($R^2 > 0.965$). which means that the proposed models can explain 96.4% of the variability in solubility of H_2 (mol/kg). The H_2–H_2O system model performs best ($R^2 = 0.999$ and AAPE = 4.03). The relative closeness of the R^2 to 1 and low of the AAPE value show that the predictions of the developed correlations are closely fitted to the experimental values. Therefore, it is an indication that the mathematical models are good enough to describe the H_2 experimental measured data.

5. Conclusions and Recommendations

This paper presents current progress of various techniques for predicting CO_2 solubility and H_2 solubility and experimental databank of CO_2 and H_2 solubility data. The compiled data was used to develop novel simple, non–iterative and reliable models for predicting the solubility factor (mol/kg) in CO_2 and H_2 in pure water and different salt systems. The developed models are a function of pressure, temperature, and salinity in terms of ionic strength. The development and validation of developed CO_2 solubility

and H_2 solubility models were conducted using the collected experimental databank from previous studies. The major findings can be summarized as follows:

1. Available literature data show that there is sufficient data to evaluate CO_2 solubility in low to medium–pressure regions. However, for CO_2 storage applications in high–pressure and high–temperature regions such as those in deep saline aquifers or gas reservoirs, there is need for more experimental data, especially for mixed salt systems that represent real formation brines.
2. For the hydrogen system, there is significant lack of experimental data at higher temperatures (above 400 K) and higher pressures (above 40 MPa). To date, experimental data for mixed salt systems that represent natural formation brine is lacking. These high–temperature and high–pressure region data are critical for understanding H_2 solubility under extreme conditions like those encountered in natural hydrogen production. The limited data in these regions suggests that more experimental studies are needed to understand H_2 solubility under such conditions.
3. Reliable and quick empirical models have been developed to accurately predict the solubility of CO in pure water and various salt systems. The pressure range is between 0.1 and 71 MPa, and the temperature range is between 273.15 and 523.15 K. The CO_2 solubility model performs excellently, with an absolute mean error of 7.26 and 8.8% for the pure water and salt systems, respectively, when compared with experimentally measured data.
4. Furthermore, the developed simple models can accurately predict the solubility of H_2 in pure water and NaCl salt systems. The pressure range is between 0.1 and 101.3 MPa, and the temperature range is between 273.15 and 636.1 K. Comparison with experimental data shows that the H_2 solubility model performs excellently, with an absolute mean error of 4.03 and 9.1% for the pure water and NaCl salt systems, respectively.
5. The salting–out characteristics of various salt systems on CO_2 solubility was accurately captured. Decreasing trend of CO_2 solubility observed based on ionic strength follows the order $NaHCO_3$ > KCl > $CaCl_2$ ∼ $MgCl_2$ > NaCl > Na_2SO_4, and it is consistent with those reported by Zhao et al. [135]. Similarly, the SO characteristics of H_2 gas in NaCl brine are consistent with previous studies by Chabab et al. [152].

It is worth noting that correlations presented here update the CO_2 and H_2 solubility equations presented in the literature and could have a practical application in estimating CO_2 and H_2 solubility in water and saline systems for CO_2–EOR, geologic carbon storage, underground hydrogen storage, and natural hydrogen production processes. However, they may have a limitation: Firstly, these correlations were developed with experimentally measured CO_2 and H_2 solubility data with limited parameter ranges; therefore, these equations can only be used to estimate the CO_2 and H_2 solubility with physical condition ranges presented in Tables 1 and 2. The application of the developed correlations to calculate CO_2 and H_2 solubility with physical conditions outside these ranges could be associated with the risk of estimations that might be less accurate. Secondly, more experimental data is required to complement the lack of sufficient data, especially the H_2 solubility data at high temperatures, to understand the solubility behavior that occurs in natural hydrogen production. Finally, a comparative study of the performance of equations of state (EoS), empirical correlations, molecular dynamics simulations, and machine learning methods in predicting CO_2 and H_2 solubility is recommended for future studies.

Supplementary Materials: The following supporting information can be downloaded at: https://www.mdpi.com/article/10.3390/en17225723/s1. Figure S1. Predicted CO_2 solubility versus experimentally measured data of CO_2 solubility with ionic strength of 1 mol/kg (KCl solution). The experimental data are adopted from Kiepe et al. [109]; Figure S2. Predicted CO_2 solubility versus experimentally measured data of CO_2 solubility with ionic strength of 1.942 mol/kg (KCl solution). The experimental data are adopted from Kamps et al. [108]; Figure S3. Predicted CO_2 solubility versus experimentally measured data of CO_2 solubility with ionic strength of 2.50 mol/kg (KCl

solution). The experimental data are adopted from Hou et al. [46] and Kiepe et al. [109]; Figure S4. Predicted CO_2 solubility versus experimentally measured data of CO_2 solubility with ionic strength of 4.0 mol/kg (KCl solution). The experimental data are adopted from Hou et al. [46], Kiepe et al. [109], Koschel et al. [110] and Zhao et al. [135]; Figure S5. 3D response surfaces of CO_2 solubility (KCl) system at different salinities in terms of ionic strength; Figure S6. Predicted CO_2 solubility versus experimentally measured data of CO_2 solubility with ionic strength of 1 mol/kg (NaCl solution). The experimental data are adopted from Carvalho et al. [93], Guo et al. [101], Koschel et al. [110], Messabeb et al. [113], Yan et al. [134] and Zhao et al. [136]; Figure S7. Predicted CO_2 solubility versus experimentally measured data of CO_2 solubility with ionic strength of 6 mol/kg (NaCl solution). The experimental data are adopted from Dos Santos et al., Messabeb et al. [113] and Zhao et al. [136]; Figure S8. 3D response surfaces of CO_2 solubility (NaCl salt) system at different salinities in terms of ionic strength; Figure S9. Predicted CO_2 solubility versus experimentally measured data of CO_2 solubility with ionic strength of 0.747 mol/kg (Na_2SO_4 solution). The experimental data are adopted from Bermejo et al. [90]; Figure S10. Predicted CO_2 solubility versus experimentally measured data of CO_2 solubility with ionic strength of 3.0 mol/kg (Na_2SO_4 solution). The experimental data are adopted from Bermejo et al. [90], Rumpf and Maurer [122] and Zhao et al. [135]; Figure S11. 3D response surfaces of CO_2 solubility (Na_2SO_4) system at different salinities in terms of ionic strength; Figure S 12. Predicted CO_2 solubility versus experimentally measured data of CO_2 solubility with ionic strength of 0.05 mol/kg ($NaHCO_3$ solution). The experimental data are adapted from Han et al. [102]; Figure S13. Predicted CO_2 solubility versus experimentally measured data of CO_2 solubility with ionic strength of 0.5 mol/kg ($NaHCO_3$ solution). The experimental data are adapted from Han et al. [102]; Figure S14. Predicted CO_2 solubility versus experimentally measured data of CO_2 solubility with ionic strength of 1 mol/kg ($NaHCO_3$ solution). The experimental data are adapted from Han et al. [102]; Figure S15. 3D response surfaces of CO_2 solubility ($NaHCO_3$) system at different salinities in terms of ionic strength; Figure S16. Predicted CO_2 solubility versus experimentally measured data of CO_2 solubility with ionic strength of 3.04 mol/kg ($CaCl_2$ solution). The experimental data are adapted from Prutton and Savage [119]; Figure S17. Predicted CO_2 solubility versus experimentally measured data of CO_2 solubility with ionic strength of 11.7 mol/kg ($CaCl_2$ solution). The experimental data are adapted from Prutton and Savage [119]; Figure S18. 3D response surfaces of CO_2 solubility ($CaCl_2$) system at different salinities in terms of ionic strength; Figure S19. Predicted CO_2 solubility versus experimentally measured data of CO_2 solubility with ionic strength of 0.48 mol/kg ($MgCl_2$ solution). The experimental data are adapted from Bo Liu et al. [91]; Figure S20. Predicted CO_2 solubility versus experimentally measured data of CO_2 solubility with ionic strength of 3.0 mol/kg ($MgCl_2$ solution). The experimental data are adapted from Zhao et al. [135];, Koschel et al. [110] and Dos Santos et al. [98]; Figure S21. Predicted CO_2 solubility versus experimentally measured data of CO_2 solubility with ionic strength of 15.0 mol/kg ($MgCl_2$ solution). The experimental data are adapted from Tong et al. [128]; Figure S22. 3D response surfaces of CO_2 solubility ($MgCl_2$) system at different salinities in terms of ionic strength.

Author Contributions: Conceptualization, project administration, supervision, Methodology, review of various drafts, R.G.B. Literature search, methodology, data analysis, visualization and writing (original draft and applying revisions of various drafts), P.O.L., D.K.D. and G.G.; data curation, formal analysis, visualization and software, P.O.L.; supervision, validation, writing (review and editing), J.S.T., X.L., M.M.A. and M.R. All authors have read and agreed to the published version of the manuscript.

Funding: This research received support from funding. We wish to acknowledge the Don W. Green Professorship funding at the University of Kansas, Lawrence, USA, that supported the graduate students working on this project. We would also like to acknowledge the Tertiary Oil Recovery Program (TORP) for partially funding this work.

Acknowledgments: We appreciate MathWorks for a license for their use of software (MATLAB R2024a).

Conflicts of Interest: The authors declare no conflicts of interest.

References

1. Nagireddi, S.; Agarwal, J.R.; Vedapuri, D. Carbon Dioxide Capture, Utilization, and Sequestration: Current Status, Challenges, and Future Prospects for Global Decarbonization. *ACS Eng. Au* **2024**, *4*, 22–48. [CrossRef]
2. Intergovernmental Panel on Climate Change (IPCC). *Global Warming of 1.5 °C: Summary for Policymakers*; IPCC: Geneva, Switzerland, 2018.
3. IEA. *World Energy Outlook*; IEA: Paris, France, 2023; Available online: https://www.iea.org/reports/world-energy-outlook-2023 (accessed on 18 May 2024).
4. Izadpanahi, A.; Blunt, M.J.; Kumar, N.; Ali, M.; Gaeta Tassinari, C.C.; Sampaio, M.A. A Review of Carbon Storage in Saline Aquifers: Mechanisms, Prerequisites, and Key Considerations. *Fuel* **2024**, *369*, 131744. [CrossRef]
5. Longe, P.; Molomjav, S.; Barati, R.; Tsau, J.-S.; Musgrove, S.; Villalobos, J.; D'Erasmo, J.; Alhajeri, M.M. Field-Scale Simulations of Water-Alternating-Gas Injection in Morrowan Fluvial Sandstones of Stewart Field, Kansas, Using Captured CO^2 from an Ethanol Plant. In Proceedings of the International Petroleum Technology Conference, Dhahran, Saudi Arabia, 12–14 February 2024; p. D031S098R007.
6. Raza, A.; Gholami, R.; Rezaee, R.; Bing, C.H.; Nagarajan, R.; Hamid, M.A. Assessment of CO 2 Residual Trapping in Depleted Reservoirs Used for Geosequestration. *J. Nat. Gas Sci. Eng.* **2017**, *43*, 137–155. [CrossRef]
7. Longe, P.; Tsau, J.-S.; Musgrove, S.; Villalobos, J.; D'Erasmo, J.; Alhajeri, M.M.; Barati, R. An Overview of Stewart Field Unit Project: A Field Case Study of CO_2 Capture, Utilization, and Storage. In Proceedings of the SPE Energy Transition Symposium, Houston, TX, USA, 12–14 August 2024; p. D011S003R002.
8. Jiang, L.; Chen, Z.; Farouq Ali, S.M.; Zhang, J.; Chen, Y.; Chen, S. Storing Carbon Dioxide in Deep Unmineable Coal Seams for Centuries Following Underground Coal Gasification. *J. Clean. Prod.* **2022**, *378*, 134565. [CrossRef]
9. Al-Khdheeawi, E.A.; Mahdi, D.S.; Ali, M.; Fauziah, C.A.; Barifcani, A. Impact of Caprock Type on Geochemical Reactivity and Mineral Trapping Efficiency of CO_2. In Proceedings of the Offshore Technology Conference Asia, Kuala Lumpur, Malaysia, 2–6 November 2020; p. D012S001R060.
10. Krevor, S.; Blunt, M.J.; Benson, S.M.; Pentland, C.H.; Reynolds, C.; Al-Menhali, A.; Niu, B. Capillary Trapping for Geologic Carbon Dioxide Storage—From Pore Scale Physics to Field Scale Implications. *Int. J. Greenh. Gas Control* **2015**, *40*, 221–237. [CrossRef]
11. *IPCC Special Report on Carbon Dioxide Capture and Storage*; Metz, B., Intergovernmental Panel on Climate, Change, Eds.; Cambridge University Press: Cambridge, UK, 2005; ISBN 978-0-521-68551-1.
12. Massarweh, O.; Abushaikha, A.S. CO_2 Sequestration in Subsurface Geological Formations: A Review of Trapping Mechanisms and Monitoring Techniques. *Earth-Sci. Rev.* **2024**, *253*, 104793. [CrossRef]
13. Gyamfi, G.; Danso, D.K.; Li, X. Practical Models for Computing CO2 Solubility in Brines with Complex Ions for Carbon Geo-Sequestration Applications. In Proceedings of the SPE/AAPG/SEG Unconventional Resources Technology Conference, Houston, TX, USA, 13–15 August 2024; p. D011S005R002.
14. Meng, S.; Liu, C.; Liu, Y.; Rui, Z.; Liu, H.; Jin, X.; Tao, J. CO_2 Utilization and Sequestration in Organic-Rich Shale from the Nanoscale Perspective. *Appl. Energy* **2024**, *361*, 122907. [CrossRef]
15. Meng, S.; Fu, Q.; Tao, J.; Liang, L.; Xu, J. Predicting CO2-EOR and Storage in Low-Permeability Reservoirs with Deep Learning-Based Surrogate Flow Models. *Geoenergy Sci. Eng.* **2024**, *233*, 212467. [CrossRef]
16. Tang, J.; Zhang, M.; Guo, X.; Geng, J.; Li, Y. Investigation of Creep and Transport Mechanisms of CO2 Fracturing within Natural Gas Hydrates. *Energy* **2024**, *300*, 131214. [CrossRef]
17. Pi, Y.; Liu, J.; Liu, L.; Guo, X.; Li, C.; Li, Z. The Effect of Formation Water Salinity on the Minimum Miscibility Pressure of CO2-Crude Oil for Y Oilfield. *Front. Earth Sci.* **2021**, *9*, 711695. [CrossRef]
18. Ballentine, C.J.; Burgess, R.; Marty, B. Tracing Fluid Origin, Transport and Interaction in the Crust. *Rev Miner. Geochem* **2002**, *47*, 539–614. [CrossRef]
19. Sun, X.; Li, H.; He, H.; Fu, W.; Wang, Z.; Gao, Y.; Sun, B. Experiments and Modeling of CO2 Solubility in Water-Based and Oil-Based Drilling Fluids. *J. Pet. Sci. Eng.* **2022**, *212*, 110336. [CrossRef]
20. Olawale, S.B.; Longe, P.; Ofesi, S.F. Evaluating the Effect of Drill String Rotation and Change in Drilling Fluid Viscosity on Hole Cleaning. *J. Pet. Explor. Prod. Technol.* **2021**, *11*, 2981–2989. [CrossRef]
21. Sun, B.; Sun, X.; Wang, Z.; Chen, Y. Effects of Phase Transition on Gas Kick Migration in Deepwater Horizontal Drilling. *J. Nat. Gas Sci. Eng.* **2017**, *46*, 710–729. [CrossRef]
22. Iglauer, S. Optimum Geological Storage Depths for Structural H2 Geo-Storage. *J. Pet. Sci. Eng.* **2022**, *212*, 109498. [CrossRef]
23. Iglauer, S.; Al-Yaseri, A.Z.; Rezaee, R.; Lebedev, M. CO_2 Wettability of Caprocks: Implications for Structural Storage Capacity and Containment Security. *Geophys. Res. Lett.* **2015**, *42*, 9279–9284. [CrossRef]
24. Raza, A.; Rezaee, R.; Gholami, R.; Rasouli, V.; Bing, C.H.; Nagarajan, R.; Hamid, M.A. Injectivity and Quantification of Capillary Trapping for CO 2 Storage: A Review of Influencing Parameters. *J. Nat. Gas Sci. Eng.* **2015**, *26*, 510–517. [CrossRef]
25. Iglauer, S. *Dissolution Trapping of Carbon Dioxide in Reservoir Formation Brine-a Carbon Storage Mechanism*; INTECH Open Access Publisher: London, UK, 2011.
26. Awan, F.U.R.; Arif, M.; Iglauer, S.; Keshavarz, A. Coal Fines Migration: A Holistic Review of Influencing Factors. *Adv. Colloid Interface Sci.* **2022**, *301*, 102595. [CrossRef]
27. Arif, M.; Rasool Abid, H.; Keshavarz, A.; Jones, F.; Iglauer, S. Hydrogen Storage Potential of Coals as a Function of Pressure, Temperature, and Rank. *J. Colloid Interface Sci.* **2022**, *620*, 86–93. [CrossRef]

28. Zhou, J.; Xie, S.; Jiang, Y.; Xian, X.; Liu, Q.; Lu, Z.; Lyu, Q. Influence of Supercritical CO_2 Exposure on CH_4 and CO_2 Adsorption Behaviors of Shale: Implications for CO_2 Sequestration. *Energy Fuels* **2018**, *32*, 6073–6089. [CrossRef]
29. Hashemi, L.; Blunt, M.; Hajibeygi, H. Pore-Scale Modelling and Sensitivity Analyses of Hydrogen-Brine Multiphase Flow in Geological Porous Media. *Sci. Rep.* **2021**, *11*, 8348. [CrossRef] [PubMed]
30. Muhammed, N.S.; Haq, B.; Al Shehri, D.; Al-Ahmed, A.; Rahman, M.M.; Zaman, E. A Review on Underground Hydrogen Storage: Insight into Geological Sites, Influencing Factors and Future Outlook. *Energy Rep.* **2022**, *8*, 461–499. [CrossRef]
31. Matos, C.R.; Carneiro, J.F.; Silva, P.P. Overview of Large-Scale Underground Energy Storage Technologies for Integration of Renewable Energies and Criteria for Reservoir Identification. *J. Energy Storage* **2019**, *21*, 241–258. [CrossRef]
32. Epelle, E.I.; Obande, W.; Udourioh, G.A.; Afolabi, I.C.; Desongu, K.S.; Orivri, U.; Gunes, B.; Okolie, J.A. Perspectives and Prospects of Underground Hydrogen Storage and Natural Hydrogen. *Sustain. Energy Fuels* **2022**, *6*, 3324–3343. [CrossRef]
33. Raza, A.; Arif, M.; Glatz, G.; Mahmoud, M.; Al Kobaisi, M.; Alafnan, S.; Iglauer, S. A Holistic Overview of Underground Hydrogen Storage: Influencing Factors, Current Understanding, and Outlook. *Fuel* **2022**, *330*, 125636. [CrossRef]
34. Ramesh Kumar, K.; Honorio, H.; Chandra, D.; Lesueur, M.; Hajibeygi, H. Comprehensive Review of Geomechanics of Underground Hydrogen Storage in Depleted Reservoirs and Salt Caverns. *J. Energy Storage* **2023**, *73*, 108912. [CrossRef]
35. Panfilov, M. Underground and Pipeline Hydrogen Storage. In *Compendium of Hydrogen Energy*; Elsevier: Amsterdam, The Netherlands, 2016; pp. 91–115. ISBN 978-1-78242-362-1.
36. Zgonnik, V. The Occurrence and Geoscience of Natural Hydrogen: A Comprehensive Review. *Earth-Sci. Rev.* **2020**, *203*, 103140. [CrossRef]
37. Huang, R.; Sun, W.; Ding, X.; Zhao, Y.; Song, M. Effect of Pressure on the Kinetics of Peridotite Serpentinization. *Phys. Chem. Miner.* **2020**, *47*, 33. [CrossRef]
38. Lamadrid, H.M.; Zajacz, Z.; Klein, F.; Bodnar, R.J. Synthetic Fluid Inclusions XXIII. Effect of Temperature and Fluid Composition on Rates of Serpentinization of Olivine. *Geochim. Cosmochim. Acta* **2021**, *292*, 285–308. [CrossRef]
39. Lollar, B.S.; Onstott, T.C.; Lacrampe-Couloume, G.; Ballentine, C.J. The Contribution of the Precambrian Continental Lithosphere to Global H_2 Production. *Nature* **2014**, *516*, 379–382. [CrossRef]
40. Bazarkina, E.F.; Chou, I.-M.; Goncharov, A.F.; Akinfiev, N.N. The Behavior of H2 in Aqueous Fluids under High Temperature and Pressure. *Elements* **2020**, *16*, 33–38. [CrossRef]
41. Rahbari, A.; Brenkman, J.; Hens, R.; Ramdin, M.; Van Den Broeke, L.J.P.; Schoon, R.; Henkes, R.; Moultos, O.A.; Vlugt, T.J.H. Solubility of Water in Hydrogen at High Pressures: A Molecular Simulation Study. *J. Chem. Eng. Data* **2019**, *64*, 4103–4115. [CrossRef]
42. Ratnakar, R.R.; Dindoruk, B.; Harvey, A. Thermodynamic Modeling of Hydrogen-Water System for High-Pressure Storage and Mobility Applications. *J. Nat. Gas Sci. Eng.* **2020**, *81*, 103463. [CrossRef]
43. Li, D.; Beyer, C.; Bauer, S. A Unified Phase Equilibrium Model for Hydrogen Solubility and Solution Density. *Int. J. Hydrogen Energy* **2018**, *43*, 512–529. [CrossRef]
44. Lopez-Lazaro, C.; Bachaud, P.; Moretti, I.; Ferrando, N. Predicting the Phase Behavior of Hydrogen in NaCl Brines by Molecular Simulation for Geological Applications. *BSGF-Earth Sci. Bull.* **2019**, *190*, 7. [CrossRef]
45. Sun, R.; Lai, S.; Dubessy, J. Calculations of Vapor–Liquid Equilibria of the H_2O-N_2 and H_2O-H_2 Systems with Improved SAFT-LJ EOS. *Fluid Phase Equilibria* **2015**, *390*, 23–33. [CrossRef]
46. Hou, S.-X.; Maitland, G.C.; Trusler, J.P.M. Phase Equilibria of (CO_2 + H_2O + NaCl) and (CO_2 + H_2O + KCl): Measurements and Modeling. *J. Supercrit. Fluids* **2013**, *78*, 78–88. [CrossRef]
47. Bahadori, A.; Mokhatab, S. New Correlations Predict Aqueous Solubility and Density of Carbon Dioxide. *Int. J. Greenh. Gas Control* **2009**, *3*, 474–480. [CrossRef]
48. Li, Y.; Nghiem, L.X. Phase Equilibria of Oil, Gas and Water/Brine Mixtures from a Cubic Equation of State and Henry's Law. *Can. J. Chem. Eng.* **1986**, *64*, 486–496. [CrossRef]
49. Spycher, N.; Pruess, K.; Ennis-King, J. CO_2-H_2O Mixtures in the Geological Sequestration of CO2. I. Assessment and Calculation of Mutual Solubilities from 12 to 100 °C and up to 600 Bar. *Geochim. Cosmochim. Acta* **2003**, *67*, 3015–3031. [CrossRef]
50. Spycher, N.; Pruess, K. A Phase-Partitioning Model for CO_2–Brine Mixtures at Elevated Temperatures and Pressures: Application to CO2-Enhanced Geothermal Systems. *Transp. Porous Media* **2010**, *82*, 173–196. [CrossRef]
51. Yan, Y.; Chen, C.-C. Thermodynamic Modeling of CO_2 Solubility in Aqueous Solutions of NaCl and Na_2SO_4. *J. Supercrit. Fluids* **2010**, *55*, 623–634. [CrossRef]
52. Duan, Z.; Sun, R. An Improved Model Calculating CO2 Solubility in Pure Water and Aqueous NaCl Solutions from 273 to 533 K and from 0 to 2000 Bar. *Chem. Geol.* **2003**, *193*, 257–271. [CrossRef]
53. Duan, Z.; Sun, R.; Zhu, C.; Chou, I.-M. An Improved Model for the Calculation of CO_2 Solubility in Aqueous Solutions Containing Na^+, K^+, Ca^{2+}, Mg^{2+}, Cl^-, and SO_4^{2-}. *Mar. Chem.* **2006**, *98*, 131–139. [CrossRef]
54. Zhu, Z.; Cao, Y.; Zheng, Z.; Chen, D. An Accurate Model for Estimating H_2 Solubility in Pure Water and Aqueous NaCl Solutions. *Energies* **2022**, *15*, 5021. [CrossRef]
55. Darwish, N.A.; Hilal, N. A Simple Model for the Prediction of CO_2 Solubility in H_2O–NaCl System at Geological Sequestration Conditions. *Desalination* **2010**, *260*, 114–118. [CrossRef]
56. Barta, L.; Bradley, D.J. Extension of the Specific Interaction Model to Include Gas Solubilities in High Temperature Brines. *Geochim. Cosmochim. Acta* **1985**, *49*, 195–203. [CrossRef]

57. Sun, X.; Wang, Z.; Li, H.; He, H.; Sun, B. A Simple Model for the Prediction of Mutual Solubility in CO_2-Brine System at Geological Conditions. *Desalination* **2021**, *504*, 114972. [CrossRef]
58. Enick, R.M.; Klara, S.M. CO_2 Solubility in Water and Brine Under Reservoir Conditions. *Chem. Eng. Commun.* **1990**, *90*, 23–33. [CrossRef]
59. Chabab, S.; Théveneau, P.; Coquelet, C.; Corvisier, J.; Paricaud, P. Measurements and Predictive Models of High-Pressure H_2 Solubility in Brine (H_2O+NaCl) for Underground Hydrogen Storage Application. *Int. J. Hydrogen Energy* **2020**, *45*, 32206–32220. [CrossRef]
60. Kerkache, H.; Hoang, H.; Cézac, P.; Galliéro, G.; Chabab, S. The Solubility of H_2 in NaCl Brine at High Pressures and High Temperatures: Molecular Simulation Study and Thermodynamic Modeling. *J. Mol. Liq.* **2024**, *400*, 124497. [CrossRef]
61. Van Rooijen, W.A.; Habibi, P.; Xu, K.; Dey, P.; Vlugt, T.J.H.; Hajibeygi, H.; Moultos, O.A. Interfacial Tensions, Solubilities, and Transport Properties of the H_2/H_2O/NaCl System: A Molecular Simulation Study. *J. Chem. Eng. Data* **2024**, *69*, 307–319. [CrossRef]
62. Liu, Y.; Lafitte, T.; Panagiotopoulos, A.Z.; Debenedetti, P.G. Simulations of Vapor–Liquid Phase Equilibrium and Interfacial Tension in the CO_2–H_2O–NaCl System. *AIChE J.* **2013**, *59*, 3514–3522. [CrossRef]
63. Liu, Y.; Panagiotopoulos, A.Z.; Debenedetti, P.G. Monte Carlo Simulations of High-Pressure Phase Equilibria of CO_2–H_2O Mixtures. *J. Phys. Chem. B* **2011**, *115*, 6629–6635. [CrossRef] [PubMed]
64. Vorholz, J.; Harismiadis, V.I.; Rumpf, B.; Panagiotopoulos, A.Z.; Maurer, G. Vapor+liquid Equilibrium of Water, Carbon Dioxide, and the Binary System, Water+carbon Dioxide, from Molecular Simulation. *Fluid Phase Equilibria* **2000**, *170*, 203–234. [CrossRef]
65. Hosseinzadeh Dehaghani, Y.; Assareh, M.; Feyzi, F. Simultaneous Prediction of Equilibrium, Interfacial, and Transport Properties of CO_2-Brine Systems Using Molecular Dynamics Simulation: Applications to CO_2 Storage. *Ind. Eng. Chem. Res.* **2022**, *61*, 15390–15406. [CrossRef]
66. Zhu, Y.; Wang, H.; Vano, K. Applying the Wavelet Neural Network to Estimate Hydrogen Dissolution in Underground Sodium Chloride Solutions. *Int. J. Hydrogen Energy* **2022**, *47*, 22720–22730. [CrossRef]
67. Menad, N.A.; Hemmati-Sarapardeh, A.; Varamesh, A.; Shamshirband, S. Predicting Solubility of CO2 in Brine by Advanced Machine Learning Systems: Application to Carbon Capture and Sequestration. *J. CO2 Util.* **2019**, *33*, 83–95. [CrossRef]
68. Mohammadian, E.; Hadavimoghaddam, F.; Kheirollahi, M.; Jafari, M.; Chenlu, X.; Liu, B. Probing Solubility and pH of CO_2 in Aqueous Solutions: Implications for CO_2 Injection into Oceans. *J. CO2 Util.* **2023**, *71*, 102463. [CrossRef]
69. Jeon, P.R.; Lee, C.-H. Artificial Neural Network Modelling for Solubility of Carbon Dioxide in Various Aqueous Solutions from Pure Water to Brine. *J. CO2 Util.* **2021**, *47*, 101500. [CrossRef]
70. Mahmoudzadeh, A.; Amiri-Ramsheh, B.; Atashrouz, S.; Abedi, A.; Abuswer, M.A.; Ostadhassan, M.; Mohaddespour, A.; Hemmati-Sarapardeh, A. Modeling CO_2 Solubility in Water Using Gradient Boosting and Light Gradient Boosting Machine. *Sci. Rep.* **2024**, *14*, 13511. [CrossRef] [PubMed]
71. Lv, Q.; Zhou, T.; Zheng, H.; Amiri-Ramsheh, B.; Hadavimoghaddam, F.; Hemmati-Sarapardeh, A.; Li, X.; Li, L. Modeling Hydrogen Solubility in Water: Comparison of Adaptive Boosting Support Vector Regression, Gene Expression Programming, and Cubic Equations of State. *Int. J. Hydrogen Energy* **2024**, *57*, 637–650. [CrossRef]
72. Vo Thanh, H.; Zhang, H.; Dai, Z.; Zhang, T.; Tangparitkul, S.; Min, B. Data-Driven Machine Learning Models for the Prediction of Hydrogen Solubility in Aqueous Systems of Varying Salinity: Implications for Underground Hydrogen Storage. *Int. J. Hydrogen Energy* **2024**, *55*, 1422–1433. [CrossRef]
73. Oxburgh, E.R. (W.S.) Fyfe, (N.J.) Price and (A.B.) Thompson Fluids in the Earth's Crust (Developments in Geochemistry, I). Amsterdam, Oxford, and New York (Elsevier) 1978 Xviii + 383 Pp., 225 Figs., 1 Coloured Pl. Price Dfl 125.00 ($49.75). *Mineral. Mag.* **1980**, *43*, 827. [CrossRef]
74. Pytkowicz, R.M. Riley, J. P., and G. Skirrow [Eds.]. 1975. Chemical Oceanography, v. 1. 2nd Ed. Academic Press, New York and London, Xx + 606 p. $49.00. £18.50. *Limnol. Oceanogr.* **1976**, *21*, 345–347. [CrossRef]
75. Elderfield, H. S. S. Butcher, R. J. Charlson, G. H. Orians & G. V. Wolfe (Eds) 1992. Global Biogeochemical Cycles. Xvi + 379 Pp. London, San Diego, New York, Boston, Sydney, Tokyo, Toronto: Academic Press (Harcourt Brace Jovanovich). Price £24.95, US $59.00 (paperback). ISBN 0 12 147686 3. *Geol. Mag.* **1993**, *130*, 408. [CrossRef]
76. Millero, F.J. Thermodynamics of the Carbon Dioxide System in the Oceans. *Geochim. Cosmochim. Acta* **1995**, *59*, 661–677. [CrossRef]
77. Friedmann, S.J. NETL Carbon Storage Atlas—Fifth Edition—ATLAS-V-2015.Pdf—EDX. Available online: https://edx.netl.doe.gov/dataset/netl-carbon-storage-atlas-fifth-edition/resource/4f44abdf-0976-4251-8838-457c60e638ba (accessed on 21 August 2024).
78. Sun, Z.; Li, H. Phase Behavior Modeling for Carbon Dioxide/Brine Mixtures Using PR EOS and Huron-Vidal Mixing Rule. In Proceedings of the ASME 2022 41st International Conference on Ocean, Offshore and Arctic Engineering; American Society of Mechanical Engineers, Hamburg, Germany, 5–10 June 2022; Volume 10, p. V010T11A002.
79. Wiebe, R.; Gaddy, V.L. The Solubility of Carbon Dioxide in Water at Various Temperatures from 12 to 40° and at Pressures to 500 Atmospheres. Critical Phenomena*. *J. Am. Chem. Soc.* **1940**, *62*, 815–817. [CrossRef]
80. Tödheide, K.; Franck, E. The Two-Phase Region and the Critical Curve in the Carbon Dioxide-Water System up to Pressures of 3500 Bar. *J. Phys. Chem.* **1963**, *37*, 387–401.
81. Takenouchi, S.; Kennedy, G.C. The Solubility of Carbon Dioxide in Nacl Solutions at High Temperatures and Pressures. *Am. J. Sci.* **1965**, *263*, 445–454. [CrossRef]

82. Takenouchi, S.; Kennedy, G.C. The Binary System H_2O-CO_2 at High Temperatures and Pressures. *Am. J. Sci.* **1964**, *262*, 1055–1074. [CrossRef]
83. King, M.B.; Mubarak, A.; Kim, J.D.; Bott, T.R. The Mutual Solubilities of Water with Supercritical and Liquid Carbon Dioxides. *J. Supercrit. Fluids* **1992**, *5*, 296–302. [CrossRef]
84. Ahmadi, P.; Chapoy, A. CO_2 Solubility in Formation Water under Sequestration Conditions. *Fluid Phase Equilibria* **2018**, *463*, 80–90. [CrossRef]
85. Al Ghafri, S.Z.; Forte, E.; Galindo, A.; Maitland, G.C.; Trusler, J.P.M. Experimental and Modeling Study of the Phase Behavior of (Heptane + Carbon Dioxide + Water) Mixtures. *J. Chem. Eng. Data* **2015**, *60*, 3670–3681. [CrossRef]
86. Anderson, G.K. Solubility of Carbon Dioxide in Water under Incipient Clathrate Formation Conditions. *J. Chem. Eng. Data* **2002**, *47*, 219–222. [CrossRef]
87. Bamberger, A.; Sieder, G.; Maurer, G. High-Pressure (Vapor + liquid) Equilibrium in Binary Mixtures of (Carbon Dioxide + water or Acetic Acid) at Temperatures from 313 to 353 K. *J. Supercrit. Fluids* **2000**, *17*, 97–110. [CrossRef]
88. Bando, S.; Takemura, F.; Nishio, M.; Hihara, E.; Akai, M. Solubility of CO_2 in Aqueous Solutions of NaCl at (30 to 60) °C and (10 to 20) MPa. *J. Chem. Eng. Data* **2003**, *48*, 576–579. [CrossRef]
89. Bastami, A.; Allahgholi, M.; Pourafshary, P. Experimental and Modelling Study of the Solubility of CO_2 in Various CaCl2 Solutions at Different Temperatures and Pressures. *Pet. Sci.* **2014**, *11*, 569–577. [CrossRef]
90. Bermejo, M.D.; Martín, A.; Florusse, L.J.; Peters, C.J.; Cocero, M.J. The Influence of Na_2SO4 on the CO_2 Solubility in Water at High Pressure. *Fluid Phase Equilibria* **2005**, *238*, 220–228. [CrossRef]
91. Liu, B.; Mahmood, B.S.; Mohammadian, E.; Khaksar Manshad, A.; Rosli, N.R.; Ostadhassan, M. Measurement of Solubility of CO_2 in NaCl, $CaCl_2$, $MgCl_2$ and $MgCl_2$ + $CaCl_2$ Brines at Temperatures from 298 to 373 K and Pressures up to 20 MPa Using the Potentiometric Titration Method. *Energies* **2021**, *14*, 7222. [CrossRef]
92. Siqueira Campos, C.E.P.; Villardi, H.G.D.; Pessoa, F.L.P.; Uller, A.M.C. Solubility of Carbon Dioxide in Water and Hexadecane: Experimental Measurement and Thermodynamic Modeling. *J. Chem. Eng. Data* **2009**, *54*, 2881–2886. [CrossRef]
93. Carvalho, P.J.; Pereira, L.M.C.; Gonçalves, N.P.F.; Queimada, A.J.; Coutinho, J.A.P. Carbon Dioxide Solubility in Aqueous Solutions of NaCl: Measurements and Modeling with Electrolyte Equations of State. *Fluid Phase Equilibria* **2015**, *388*, 100–106. [CrossRef]
94. Chapoy, A.; Mohammadi, A.H.; Chareton, A.; Tohidi, B.; Richon, D. Measurement and Modeling of Gas Solubility and Literature Review of the Properties for the Carbon Dioxide−Water System. *Ind. Eng. Chem. Res.* **2004**, *43*, 1794–1802. [CrossRef]
95. Corti, H.R.; Krenzer, M.E.; De Pablo, J.J.; Prausnitz, J.M. Effect of a Dissolved Gas on the Solubility of an Electrolyte in Aqueous Solution. *Ind. Eng. Chem. Res.* **1990**, *29*, 1043–1050. [CrossRef]
96. Dalmolin, I.; Skovroinski, E.; Biasi, A.; Corazza, M.L.; Dariva, C.; Oliveira, J.V. Solubility of Carbon Dioxide in Binary and Ternary Mixtures with Ethanol and Water. *Fluid Phase Equilibria* **2006**, *245*, 193–200. [CrossRef]
97. Dell'Era, C.; Uusi-Kyyny, P.; Pokki, J.-P.; Pakkanen, M.; Alopaeus, V. Solubility of Carbon Dioxide in Aqueous Solutions of Diisopropanolamine and Methyldiethanolamine. *Fluid Phase Equilibria* **2010**, *293*, 101–109. [CrossRef]
98. dos Santos, P.F.; André, L.; Ducousso, M.; Contamine, F.; Cézac, P. Experimental Measurements of CO_2 Solubility in Aqueous MgCl2 Solution at Temperature between 323.15 and 423.15 K and Pressure up to 20 MPa. *J. Chem. Eng. Data* **2021**, *66*, 4166–4173. [CrossRef]
99. Ellis, A.J.; Golding, R.M. The Solubility of Carbon Dioxide above 100 Degrees C in Water and in Sodium Chloride Solutions. *Am. J. Sci.* **1963**, *261*, 47–60. [CrossRef]
100. Gilbert, K.; Bennett, P.C.; Wolfe, W.; Zhang, T.; Romanak, K.D. CO_2 Solubility in Aqueous Solutions Containing Na^+, Ca^{2+}, Cl^-, SO_4^{2-} and HCO_3^-: The Effects of Electrostricted Water and Ion Hydration Thermodynamics. *Appl. Geochem.* **2016**, *67*, 59–67. [CrossRef]
101. Guo, H.; Huang, Y.; Chen, Y.; Zhou, Q. Quantitative Raman Spectroscopic Measurements of CO_2 Solubility in NaCl Solution from (273.15 to 473.15) K at p = (10.0, 20.0, 30.0, and 40.0) MPa. *J. Chem. Eng. Data* **2016**, *61*, 466–474. [CrossRef]
102. Han, X.; Yu, Z.; Qu, J.; Qi, T.; Guo, W.; Zhang, G. Measurement and Correlation of Solubility Data for CO_2 in $NaHCO_3$ Aqueous Solution. *J. Chem. Eng. Data* **2011**, *56*, 1213–1219. [CrossRef]
103. Han, J.M.; Shin, H.Y.; Min, B.-M.; Han, K.-H.; Cho, A. Measurement and Correlation of High Pressure Phase Behavior of Carbon Dioxide + Water System. *J. Ind. Eng. Chem.* **2009**, *15*, 212–216. [CrossRef]
104. He, S.; Morse, J.W. The Carbonic Acid System and Calcite Solubility in Aqueous Na-K-Ca-Mg-Cl-SO4 Solutions from 0 to 90 °C. *Geochim. Cosmochim. Acta* **1993**, *57*, 3533–3554. [CrossRef]
105. He, H.; Sun, B.; Sun, X.; Wang, Z. Experimental and Theoretical Study on Water Solubility of Carbon Dioxide in Oil and Gas Displacement. *J. Pet. Sci. Eng.* **2021**, *203*, 108685. [CrossRef]
106. Hoballah, R. On the Solubility of Acid and Sour Gases in Water and Brines under Reservoir Conditions. Ph.D. Thesis, Imperial College London, London, UK, 2017.
107. Hou, S.-X.; Maitland, G.C.; Trusler, J.P.M. Measurement and Modeling of the Phase Behavior of the (Carbon Dioxide + Water) Mixture at Temperatures from 298.15 K to 448.15 K. *J. Supercrit. Fluids* **2013**, *73*, 87–96. [CrossRef]
108. Pérez-Salado Kamps, Á.; Meyer, E.; Rumpf, B.; Maurer, G. Solubility of CO_2 in Aqueous Solutions of KCl and in Aqueous Solutions of K_2CO_3. *J. Chem. Eng. Data* **2007**, *52*, 817–832. [CrossRef]

109. Kiepe, J.; Horstmann, S.; Fischer, K.; Gmehling, J. Experimental Determination and Prediction of Gas Solubility Data for CO_2 + H_2O Mixtures Containing NaCl or KCl at Temperatures between 313 and 393 K and Pressures up to 10 MPa. *Ind. Eng. Chem. Res.* **2002**, *41*, 4393–4398. [CrossRef]
110. Koschel, D.; Coxam, J.-Y.; Rodier, L.; Majer, V. Enthalpy and Solubility Data of CO_2 in Water and NaCl(Aq) at Conditions of Interest for Geological Sequestration. *Fluid Phase Equilibria* **2006**, *247*, 107–120. [CrossRef]
111. Malinin, S.; Kurovskaya, N. Investigation of CO_2 Solubility in a Solution of Chlorides at Elevated Temperatures and Pressures of CO_2. *Geokhimiya* **1975**, *4*, 547–551.
112. Martín, Á.; Pham, H.M.; Kilzer, A.; Kareth, S.; Weidner, E. Phase Equilibria of Carbon Dioxide + Poly Ethylene Glycol + Water Mixtures at High Pressure: Measurements and Modelling. *Fluid Phase Equilibria* **2009**, *286*, 162–169. [CrossRef]
113. Messabeb, H.; Contamine, F.; Cézac, P.; Serin, J.P.; Pouget, C.; Gaucher, E.C. Experimental Measurement of CO_2 Solubility in Aqueous CaCl $_2$ Solution at Temperature from 323.15 to 423.15 K and Pressure up to 20 MPa Using the Conductometric Titration. *J. Chem. Eng. Data* **2017**, *62*, 4228–4234. [CrossRef]
114. Mohammadian, E.; Hamidi, H.; Asadullah, M.; Azdarpour, A.; Motamedi, S.; Junin, R. Measurement of CO_2 Solubility in NaCl Brine Solutions at Different Temperatures and Pressures Using the Potentiometric Titration Method. *J. Chem. Eng. Data* **2015**, *60*, 2042–2049. [CrossRef]
115. Muromachi, S.; Shijima, A.; Miyamoto, H.; Ohmura, R. Experimental Measurements of Carbon Dioxide Solubility in Aqueous Tetra-*n*-Butylammonium Bromide Solutions. *J. Chem. Thermodyn.* **2015**, *85*, 94–100. [CrossRef]
116. Nighswander, J.A.; Kalogerakis, N.; Mehrotra, A.K. Solubilities of Carbon Dioxide in Water and 1 Wt. % Sodium Chloride Solution at Pressures up to 10 MPa and Temperatures from 80 to 200.Degree.C. *J. Chem. Eng. Data* **1989**, *34*, 355–360. [CrossRef]
117. Portier, S.; Rochelle, C. Modelling CO_2 Solubility in Pure Water and NaCl-Type Waters from 0 to 300 °C and from 1 to 300 Bar. *Chem. Geol.* **2005**, *217*, 187–199. [CrossRef]
118. Poulain, M.; Messabeb, H.; Lach, A.; Contamine, F.; Cézac, P.; Serin, J.-P.; Dupin, J.-C.; Martinez, H. Experimental Measurements of Carbon Dioxide Solubility in Na–Ca–K–Cl Solutions at High Temperatures and Pressures up to 20 MPa. *J. Chem. Eng. Data* **2019**, *64*, 2497–2503. [CrossRef]
119. Prutton, C.F.; Savage, R.L. The Solubility of Carbon Dioxide in Calcium Chloride-Water Solutions at 75, 100, 120° and High Pressures1. *J. Am. Chem. Soc.* **1945**, *67*, 1550–1554. [CrossRef]
120. Qin, J.; Rosenbauer, R.J.; Duan, Z. Experimental Measurements of Vapor–Liquid Equilibria of the H_2O + CO_2 + CH_4 Ternary System. *J. Chem. Eng. Data* **2008**, *53*, 1246–1249. [CrossRef]
121. Ruffine, L.; Trusler, J.P.M. Phase Behaviour of Mixed-Gas Hydrate Systems Containing Carbon Dioxide. *J. Chem. Thermodyn.* **2010**, *42*, 605–611. [CrossRef]
122. Rumpf, B.; Maurer, G. An Experimental and Theoretical Investigation on the Solubility of Carbon Dioxide in Aqueous Solutions of Strong Electrolytes. *Berichte Bunsenges. Für Phys. Chem.* **1993**, *97*, 85–97. [CrossRef]
123. Rumpf, B.; Nicolaisen, H.; Öcal, C.; Maurer, G. Solubility of Carbon Dioxide in Aqueous Solutions of Sodium Chloride: Experimental Results and Correlation. *J. Solut. Chem.* **1994**, *23*, 431–448. [CrossRef]
124. Sako, T.; Sugeta, T.; Nakazawa, N.; Okubo, T.; Sato, M.; Taguchi, T.; Hiaki, T. Phase Equilibrium Study of Extraction and Concentration of Furfural Produced in Reactor Using Supercritical Carbon Dioxide. *J. Chem. Eng. Jpn.* **1991**, *24*, 449–455. [CrossRef]
125. Serpa, F.S.; Vidal, R.S.; Filho, J.H.B.A.; do Nascimento, J.F.; Ciambelli, J.R.P.; Figueiredo, C.M.S.; Salazar-Banda, G.R.; Santos, A.F.; Fortuny, M.; Franceschi, E.; et al. Solubility of Carbon Dioxide in Ethane-1,2-Diol–Water Mixtures. *J. Chem. Eng. Data* **2013**, *58*, 3464–3469. [CrossRef]
126. Servio, P.; Englezos, P. Effect of Temperature and Pressure on the Solubility of Carbon Dioxide in Water in the Presence of Gas Hydrate. *Fluid Phase Equilibria* **2001**, *190*, 127–134. [CrossRef]
127. Tang, Y.; Bian, X.; Du, Z.; Wang, C. Measurement and Prediction Model of Carbon Dioxide Solubility in Aqueous Solutions Containing Bicarbonate Anion. *Fluid Phase Equilibria* **2015**, *386*, 56–64. [CrossRef]
128. Tong, D.; Trusler, J.P.M.; Vega-Maza, D. Solubility of CO_2 in Aqueous Solutions of $CaCl_2$ or $MgCl_2$ and in a Synthetic Formation Brine at Temperatures up to 423 K and Pressures up to 40 MPa. *J. Chem. Eng. Data* **2013**, *58*, 2116–2124. [CrossRef]
129. Valtz, A.; Chapoy, A.; Coquelet, C.; Paricaud, P.; Richon, D. Vapour–Liquid Equilibria in the Carbon Dioxide–Water System, Measurement and Modelling from 278.2 to 318.2 K. *Fluid Phase Equilibria* **2004**, *226*, 333–344. [CrossRef]
130. Wiebe, R. The Binary System Carbon Dioxide-Water under Pressure. *Chem. Rev.* **1941**, *29*, 475–481. [CrossRef]
131. Wiebe, R.; Gaddy, V. The Solubility in Water of Carbon Dioxide at 50, 75 and 100, at Pressures to 700 Atmospheres. *J. Am. Chem. Soc.* **1939**, *61*, 315–318. [CrossRef]
132. Liu, Y.; Hou, M.; Yang, G.; Han, B. Solubility of CO_2 in Aqueous Solutions of NaCl, KCl, $CaCl_2$ and Their Mixed Salts at Different Temperatures and Pressures. *J. Supercrit. Fluids* **2011**, *56*, 125–129. [CrossRef]
133. Liu, Y.; Hou, M.; Ning, H.; Yang, D.; Yang, G.; Han, B. Phase Equilibria of CO_2 + N_2 + H_2O and N_2 + CO_2 + H_2O + NaCl + KCl + $CaCl_2$ Systems at Different Temperatures and Pressures. *J. Chem. Eng. Data* **2012**, *57*, 1928–1932. [CrossRef]
134. Yan, W.; Huang, S.; Stenby, E.H. Measurement and Modeling of CO_2 Solubility in NaCl Brine and CO_2–Saturated NaCl Brine Density. *Int. J. Greenh. Gas Control* **2011**, *5*, 1460–1477. [CrossRef]
135. Zhao, H.; Dilmore, R.M.; Lvov, S.N. Experimental Studies and Modeling of CO2 Solubility in High Temperature Aqueous CaCl2, MgCl2, Na2SO4, and KCl Solutions. *AIChE J.* **2015**, *61*, 2286–2297. [CrossRef]

136. Zhao, H.; Fedkin, M.V.; Dilmore, R.M.; Lvov, S.N. Carbon Dioxide Solubility in Aqueous Solutions of Sodium Chloride at Geological Conditions: Experimental Results at 323.15, 373.15, and 423.15 K and 150 Bar and Modeling up to 573.15 K and 2000 Bar. *Geochim. Cosmochim. Acta* **2015**, *149*, 165–189. [CrossRef]
137. Peng, D.; Robinson, D. A New Two-Constant Equation of State. *IndEngChem Fundam.* **1976**, *15*, 59–64. [CrossRef]
138. Peng, D.; Robinson, D.B. Two- and Three-Phase Equilibrium Calculations for Coal Gasification and Related Processes. In *Thermodynamics of Aqueous Systems With Industrial Applications*; ACS Symposium Series; American Chemical Society: Washington, DC, USA, 1980; Volume 133, pp. 393–414. ISBN 978-0-8412-0569-7.
139. Søreide, I.; Whitson, C.H. Peng-Robinson Predictions for Hydrocarbons, CO_2, N_2, and H_2 S with Pure Water and NaCI Brine. *Fluid Phase Equilibria* **1992**, *77*, 217–240. [CrossRef]
140. Ji, Z.; Wang, H.; Wang, M.; Lv, W.; Wang, S.; Kou, Z.; He, C.; Wang, L. Experimental and Modeling Study of CO_2 Solubility in Formation Brines at In-Situ Conditions. *J. Clean. Prod.* **2024**, *438*, 140840. [CrossRef]
141. Diamond, L.W.; Akinfiev, N.N. Solubility of CO_2 in Water from −1.5 to 100 °C and from 0.1 to 100 MPa: Evaluation of Literature Data and Thermodynamic Modelling. *Fluid Phase Equilibria* **2003**, *208*, 265–290. [CrossRef]
142. Thompson, A.P.; Aktulga, H.M.; Berger, R.; Bolintineanu, D.S.; Brown, W.M.; Crozier, P.S.; in'T Veld, P.J.; Kohlmeyer, A.; Moore, S.G.; Nguyen, T.D.; et al. LAMMPS—A Flexible Simulation Tool for Particle-Based Materials Modeling at the Atomic, Meso, and Continuum Scales. *Comput. Phys. Commun.* **2022**, *271*, 108171. [CrossRef]
143. Frenkel, D. *Understanding Molecular Simulation: From Algorithms to Applications*; Academic Press: San Diego, CA, USA, 1996; ISBN 978-0-12-267370-2.
144. Orozco, G.A.; Economou, I.G.; Panagiotopoulos, A.Z. Optimization of Intermolecular Potential Parameters for the CO2/H2O Mixture. *J. Phys. Chem. B* **2014**, *118*, 11504–11511. [CrossRef]
145. Lobanova, O.; Mejía, A.; Jackson, G.; Müller, E.A. SAFT-γ Force Field for the Simulation of Molecular Fluids 6: Binary and Ternary Mixtures Comprising Water, Carbon Dioxide, and *n*-Alkanes. *J. Chem. Thermodyn.* **2016**, *93*, 320–336. [CrossRef]
146. Jiang, H.; Economou, I.G.; Panagiotopoulos, A.Z. Phase Equilibria of Water/CO_2 and Water/n-Alkane Mixtures from Polarizable Models. *J. Phys. Chem. B* **2017**, *121*, 1386–1395. [CrossRef] [PubMed]
147. Hulikal Chakrapani, T.; Hajibeygi, H.; Moultos, O.A.; Vlugt, T.J.H. Mutual Diffusivities of Mixtures of Carbon Dioxide and Hydrogen and Their Solubilities in Brine: Insight from Molecular Simulations. *Ind. Eng. Chem. Res.* **2024**, *63*, 10456–10481. [CrossRef] [PubMed]
148. Adam, A.M.; Bahamon, D.; Al Kobaisi, M.; Vega, L.F. Molecular Dynamics Simulations of the Interfacial Tension and the Solubility of Brine/H_2/CO_2 Systems: Implications for Underground Hydrogen Storage. *Int. J. Hydrogen Energy* **2024**, *78*, 1344–1354. [CrossRef]
149. Mohammadian, E.; Liu, B.; Riazi, A. Evaluation of Different Machine Learning Frameworks to Estimate CO_2 Solubility in NaCl Brines: Implications for CO_2 Injection into Low-Salinity Formations. *Lithosphere* **2022**, *2022*, 1615832. [CrossRef]
150. Ratnakar, R.R.; Chaubey, V.; Dindoruk, B. A Novel Computational Strategy to Estimate CO_2 Solubility in Brine Solutions for CCUS Applications. *Appl. Energy* **2023**, *342*, 121134. [CrossRef]
151. Zou, X.; Zhu, Y.; Lv, J.; Zhou, Y.; Ding, B.; Liu, W.; Xiao, K.; Zhang, Q. Toward Estimating CO_2 Solubility in Pure Water and Brine Using Cascade Forward Neural Network and Generalized Regression Neural Network: Application to CO_2 Dissolution Trapping in Saline Aquifers. *ACS Omega* **2024**, *9*, 4705–4720. [CrossRef]
152. Chabab, S.; Kerkache, H.; Bouchkira, I.; Poulain, M.; Baudouin, O.; Moine, É.; Ducousso, M.; Hoang, H.; Galliéro, G.; Cézac, P. Solubility of H_2 in Water and NaCl Brine under Subsurface Storage Conditions: Measurements and Thermodynamic Modeling. *Int. J. Hydrogen Energy* **2024**, *50*, 648–658. [CrossRef]
153. Young, C.L. (Ed.) *Hydrogen and Deuterium*, 1st ed.; Solubility Data Series; Pergamon Press: Oxford, UK, 1981; ISBN 978-0-08-023927-9.
154. Wiebe, R.; Gaddy, V.L. The Solubility of Hydrogen in Water at 0, 50, 75 and 100° from 25 to 1000 Atmospheres. *J. Am. Chem. Soc.* **1934**, *56*, 76–79. [CrossRef]
155. Crozier, T.E.; Yamamoto, S. Solubility of Hydrogen in Water, Sea Water, and Sodium Chloride Solutions. *J. Chem. Eng. Data* **1974**, *19*, 242–244. [CrossRef]
156. Braun, L. Über die Absorption von Stickstoff und von Wasserstoff in wässerigen Lösungen verschieden dissociierter Stoffe. *Z. Für Phys. Chem.* **1900**, *33*, 721–739. [CrossRef]
157. Torín-Ollarves, G.A.; Trusler, J.P.M. Solubility of Hydrogen in Sodium Chloride Brine at High Pressures. *Fluid Phase Equilibria* **2021**, *539*, 113025. [CrossRef]
158. Bunsen, R. Ueber Das Gesetz Der Gasabsorption. *Justus Liebigs Ann. Chem.* **1855**, *93*, 1–50. [CrossRef]
159. Bohr, C.; Bock, J. Bestimmung Der Absorption Einiger Gase in Wasser Bei Den Temperaturen Zwischen 0 Und 100°. *Ann. Phys.* **1891**, *280*, 318–343. [CrossRef]
160. Winkler, L.W. Die Löslichkeit Der Gase in Wasser. *Berichte Dtsch. Chem. Ges.* **1891**, *24*, 89–101. [CrossRef]
161. Steiner, P. Ueber Die Absorption Des Wasserstoffs Im Wasser Und in Wässerigen Lösungen. *Ann. Phys.* **1894**, *288*, 275–299. [CrossRef]
162. Geffcken, G. Beiträge Zur Kenntnis Der Löslichkeitsbeeinflussung. *Z. Für Phys. Chem.* **1904**, *49U*, 257–302. [CrossRef]
163. Knopp, W. Über Die Löslichkeitsbeeinflussung von Wasserstoff Und Stickoxydul in Wässerigen Lösungen Verschieden Dissoziierter Stoffe. *Z. Für Phys. Chem.* **1904**, *48U*, 97–108. [CrossRef]

164. Huefner, G. Study of the Absorption of Nitrogen and Hydrogen in Aqueous Solutions. *Z Phys Chem Stoechiom Verwandtschaftsl* **1907**, *57*, 611–625.
165. Findlay, A.; Shen, B. CLVI.—The Influence of Colloids and Fine Suspensions on the Solubility of Gases in Water. Part II. Solubility of Carbon Dioxide and of Hydrogen. *J Chem Soc Trans* **1912**, *101*, 1459–1468. [CrossRef]
166. Müller, C. Die Absorption von Sauerstoff, Stickstoff Und Wasserstoff in Wässerigen Lösungen von Nichtelektrolyten. *Z. Für Phys. Chem.* **1913**, *81U*, 483–503. [CrossRef]
167. Ipat'ev, V.; Teodorovich, V. Solubility of Hydrogen in Water under Pressure at Elevated Temperatures. *Zh Obshch Khim* **1934**, *4*, 395–397.
168. Morrison, T.J.; Billett, F. The Salting-out of Non-Electrolytes. Part II. The Effect of Variation in Non-Electrolyte. *J. Chem. Soc.* **1952**, *730*, 3819–3822. [CrossRef]
169. Pray, H.A.; Schweickert, C.; Minnich, B.H. Solubility of Hydrogen, Oxygen, Nitrogen, and Helium in Water at Elevated Temperatures. *Ind. Eng. Chem. Res.* **1952**, *44*, 1146–1151. [CrossRef]
170. Zoss, L. A Study of the Hydrogen and Water and Oxygen and Water Systems at Various Temperatures and Pressures. Ph.D. Thesis, Purdue University, West Lafayette, IN, USA, 1952.
171. Stephan, E.F.; Hatfield, N.S.; Peoples, R.S.; Pray, H.A. *Ignition Reactions in the Hydrogen-Oxygen-Water System at Elevated Temperatures*; Springer: Berlin/Heidelberg, Germany, 1956; p. BMI-1138, 4356429.
172. Wet, W.J. De Determination of Gas Solubilities in Water and Some Organic Liquids. *S. Afr. J. Chem.* **1934**, *17*, 9–13.
173. Ruetschi, P.; Amlie, R.F. Solubility of Hydrogen in Potassium Hydroxide and Sulfuric Acid. Salting-out and Hydration. *J. Phys. Chem.* **1966**, *70*, 718–723. [CrossRef]
174. Shoor, S.K.; Walker, R.D.; Gubbins, K.E. Salting out of Nonpolar Gases in Aqueous Potassium Hydroxide Solutions. *J. Phys. Chem.* **1969**, *73*, 312–317. [CrossRef]
175. Longo, L.; Delivoria-Papadopoulos, M.; Power, G.; Hill, E. Forster Re Diffusion Equilibration of Inert Gases between Maternal and Fetal Placental Capillaires. *Am. J. Physiol.-Leg. Content* **1970**, *219*, 561–569. [CrossRef]
176. Power, G.G.; Stegall, H. Solubility of Gases in Human Red Blood Cell Ghosts. *J. Appl. Physiol.* **1970**, *29*, 145–149. [CrossRef]
177. Gerecke, J.; Bittrich, H. The Solubility of H_2, CO_2 and NH_3 in an Aqueous Electrolyte Solution. *Wiss. Z. Tech. Hochsch. Chem. Carl Shorlemmer Leuna Mersebg.* **1971**, *13*, 115–122.
178. Jung, J.; Knacke, O.; D, N. Solubility of Carbon Monoxide and Hydrogen in Water at Temperatures up to 300 Degrees C. *Chem. Ing. Tech.* **1971**, *43*, 112. [CrossRef]
179. Schröder, W. Untersuchungen Über Die Temperaturabhängigkeit Der Gaslöslichkeit in Wasser. *Chem. Ing. Tech.* **1973**, *45*, 603–608. [CrossRef]
180. Gordon, L.I.; Cohen, Y.; Standley, D.R. The Solubility of Molecular Hydrogen in Seawater. *Deep Sea Res.* **1977**, *24*, 937–941. [CrossRef]
181. Devaney, W. *High Temperature VLE Measurements for Substitute GAS Components*; Gas Processors Association: San Antonio, TX, USA, 1978.
182. Cargill, R.W. Solubility of Helium and Hydrogen in Some Water + Alcohol Systems. *J. Chem. Soc. Faraday Trans. 1 Phys. Chem. Condens. Phases* **1978**, *74*, 1444. [CrossRef]
183. Meyer, M.; Tebbe, U.; Piiper, J. Solubility of Inert Gases in Dog Blood and Skeletal Muscle. *Pflüg. Arch.* **1980**, *384*, 131–134. [CrossRef]
184. Gillespie, P.C.; Wilson, G.M. *Vapor-Liquid and Liquid-Liquid Equilibria: Water-Methane, Water-Carbon Dioxide, Water-Hydrogen Sulfide, Water-Npentane, Water-Methane-Npentane*; Gas Processors Association: San Antonio, TX, USA, 1982.
185. Choudhary, V.R.; Parande, M.G.; Brahme, P.H. Simple Apparatus for Measuring Solubility of Gases at High Pressures. *Ind. Eng. Chem. Fundam.* **1982**, *21*, 472–474. [CrossRef]
186. Dohrn, R.; Brunner, G. Phase Equilibria in Ternary and Quaternary Systems of Hydrogen, Water and Hydrocarbons at Elevated Temperatures and Pressures. *Fluid Phase Equilibria* **1986**, *29*, 535–544. [CrossRef]
187. Alvarez, J.; Crovetto, R.; Fernandez-Prini, R. The Dissolution of N_2 and of H_2 in Water from Room Temperature to 640 K. *Ber. Bunsenges. Phys. Chem.* **1988**, *92*, 935–940. [CrossRef]
188. Kling, G.; Maurer, G. The Solubility of Hydrogen in Water and in 2-Aminoethanol at Temperatures between 323 K and 423 K and Pressures up to 16 MPa. *J. Chem. Therm.* **1991**, *23*, 531–541. [CrossRef]
189. Jáuregui-Haza, U.J.; Pardillo-Fontdevila, E.; Wilhelm, A.M.; Delmas, H. Solubility of Hidrogen and Carbon Monoxide in Water and Some Organic Solvents. *Lat. Am. Appl. Res.* **2004**, *34*, 71–74.
190. Harvey, A.H. Semiempirical Correlation for Henry's Constants over Large Temperature Ranges. *AIChE J.* **1996**, *42*, 1491–1494. [CrossRef]
191. Fernández-Prini, R.; Alvarez, J.L.; Harvey, A.H. Henry's Constants and Vapor–Liquid Distribution Constants for Gaseous Solutes in H2O and D2O at High Temperatures. *J. Phys. Chem. Ref. Data* **2003**, *32*, 903–916. [CrossRef]
192. Trinh, T.-K.-H.; De Hemptinne, J.-C.; Lugo, R.; Ferrando, N.; Passarello, J.-P. Hydrogen Solubility in Hydrocarbon and Oxygenated Organic Compounds. *J. Chem. Eng. Data* **2016**, *61*, 19–34. [CrossRef]
193. Akinfiev, N.N.; Diamond, L.W. Thermodynamic Description of Aqueous Nonelectrolytes at Infinite Dilution over a Wide Range of State Parameters. *Geochim. Cosmochim. Acta* **2003**, *67*, 613–629. [CrossRef]

194. Khoshraftar, Z.; Ghaemi, A. Prediction of CO_2 Solubility in Water at High Pressure and Temperature via Deep Learning and Response Surface Methodology. *Case Stud. Chem. Environ. Eng.* **2023**, *7*, 100338. [CrossRef]
195. Zhang, H.; Thanh, H.V.; Rahimi, M.; Al-Mudhafar, W.J.; Tangparitkul, S.; Zhang, T.; Dai, Z.; Ashraf, U. Improving Predictions of Shale Wettability Using Advanced Machine Learning Techniques and Nature-Inspired Methods: Implications for Carbon Capture Utilization and Storage. *Sci. Total Environ.* **2023**, *877*, 162944. [CrossRef]
196. Nagulapati, V.M.; Raza Ur Rehman, H.M.; Haider, J.; Abdul Qyyum, M.; Choi, G.S.; Lim, H. Hybrid Machine Learning-Based Model for Solubilities Prediction of Various Gases in Deep Eutectic Solvent for Rigorous Process Design of Hydrogen Purification. *Sep. Purif. Technol.* **2022**, *298*, 121651. [CrossRef]
197. Xie, J.; Liu, X.; Lao, X.; Vaferi, B. Hydrogen Solubility in Furfural and Furfuryl Bio-Alcohol: Comparison between the Reliability of Intelligent and Thermodynamic Models. *Int. J. Hydrogen Energy* **2021**, *46*, 36056–36068. [CrossRef]
198. Hadavimoghaddam, F.; Ansari, S.; Atashrouz, S.; Abedi, A.; Hemmati-Sarapardeh, A.; Mohaddespour, A. Application of Advanced Correlative Approaches to Modeling Hydrogen Solubility in Hydrocarbon Fuels. *Int. J. Hydrogen Energy* **2023**, *48*, 19564–19579. [CrossRef]
199. Longe, P.O.; Davoodi, S.; Mehrad, M.; Wood, D.A. Combined Deep Learning and Optimization for Hydrogen-Solubility Prediction in Aqueous Systems Appropriate for Underground Hydrogen Storage Reservoirs. *Energy Fuels* **2024**. [CrossRef]
200. Dehghani, M.R.; Nikravesh, H.; Aghel, M.; Kafi, M.; Kazemzadeh, Y.; Ranjbar, A. Estimation of Hydrogen Solubility in Aqueous Solutions Using Machine Learning Techniques for Hydrogen Storage in Deep Saline Aquifers. *Sci. Rep.* **2024**, *14*, 25890. [CrossRef] [PubMed]
201. Ansari, S.; Safaei-Farouji, M.; Atashrouz, S.; Abedi, A.; Hemmati-Sarapardeh, A.; Mohaddespour, A. Prediction of Hydrogen Solubility in Aqueous Solutions: Comparison of Equations of State and Advanced Machine Learning-Metaheuristic Approaches. *Int. J. Hydrogen Energy* **2022**, *47*, 37724–37741. [CrossRef]
202. Cao, Y.; Ayed, H.; Dahari, M.; Sene, N.; Bouallegue, B. Using Artificial Neural Network to Optimize Hydrogen Solubility and Evaluation of Environmental Condition Effects. *Int. J. Low-Carbon Technol.* **2022**, *17*, 80–89. [CrossRef]
203. Debye, P.; Hückel, E. The Theory of Electrolytes. I. Freezing Point Depres Sion and Related Phenomena [Zur Theorie Der Elektrolyte. I. Gefrierpunktserniedrigung Und Verwandte Erscheinungen]. Translated and Typeset by Michael J. Braus (2020). *Phys. Z.* **1923**, *24*, 85–206.
204. Langelier, W.F. The Analytical Control of Anti-Corrosion Water Treatment. *J. AWWA* **1936**, *28*, 1500–1521. [CrossRef]
205. Chabab, S.; Cruz, J.L.; Poulain, M.; Ducousso, M.; Contamine, F.; Serin, J.P.; Cézac, P. Thermodynamic Modeling of Mutual Solubilities in Gas-Laden Brines Systems Containing CO2, CH4, N2, O2, H2, H2O, NaCl, CaCl2, and KCl: Application to Degassing in Geothermal Processes. *Energies* **2021**, *14*, 5239. [CrossRef]
206. Truche, L.; Bazarkina, E.F.; Berger, G.; Caumon, M.-C.; Bessaque, G.; Dubessy, J. Direct Measurement of CO2 Solubility and pH in NaCl Hydrothermal Solutions by Combining In-Situ Potentiometry and Raman Spectroscopy up to 280 C and 150 Bar. *Geochim. Cosmochim. Acta* **2016**, *177*, 238–253. [CrossRef]
207. Guo, H.; Chen, Y.; Hu, Q.; Lu, W.; Ou, W.; Geng, L. Quantitative Raman Spectroscopic Investigation of Geo-Fluids High-Pressure Phase Equilibria: Part I. Accurate Calibration and Determination of CO2 Solubility in Water from 273.15 to 573.15 K and from 10 to 120 MPa. *Fluid Phase Equilibria* **2014**, *382*, 70–79. [CrossRef]
208. Pruess, K.; Oldenburg, C.M.; Moridis, G. *TOUGH2 User's Guide Version 2*, Lawrence Berkeley National Laboratory: Berkeley, CA, USA, 1999.
209. Reagan, M.T.; Moridis, G.J.; Seim, K.S. Fast Parametric Relationships for the Large-Scale Reservoir Simulation of Mixed CH4-CO2 Gas Hydrate Systems. *Comput. Geosci.* **2017**, *103*, 191–203. [CrossRef]
210. Chen, Q.; Tian, Y.; Li, P.; Yan, C.; Pang, Y.; Zheng, L.; Deng, H.; Zhou, W.; Meng, X. Study on Shale Adsorption Equation Based on Monolayer Adsorption, Multilayer Adsorption, and Capillary Condensation. *J. Chem.* **2017**, *2017*, 1–11. [CrossRef]
211. Longe, P.; Sanni, K.; Okotie, S. New Production Rate Model of Wellhead Choke for Niger Delta Oil Wells. *J. Pet. Sci. Technol.* **2020**. [CrossRef]
212. Marcus, Y. Effect of Ions on the Structure of Water: Structure Making and Breaking. *Chem. Rev.* **2009**, *109*, 1346–1370. [CrossRef] [PubMed]
213. Ben-Naim, A.Y. Hydrophobic Interactions, An Overview. In *Solution Behavior of Surfactants*; Mittal, K.L., Fendler, E.J., Eds.; Springer: Boston, MA, USA, 1982; pp. 27–40, ISBN 978-1-4613-3493-4.
214. Springer, R.D.; Wang, Z.; Anderko, A.; Wang, P.; Felmy, A.R. A Thermodynamic Model for Predicting Mineral Reactivity in Supercritical Carbon Dioxide: I. Phase Behavior of Carbon Dioxide–Water–Chloride Salt Systems across the H_2O-Rich to the CO_2-Rich Regions. *Chem. Geol.* **2012**, *322*, 151–171. [CrossRef]
215. Sander, R. Compilation of Henry's Law Constants (Version 4.0) for Water as Solvent. *Atmos. Chem. Phys.* **2015**, *15*, 4399–4981. [CrossRef]
216. Carroll, J.J.; Slupsky, J.D.; Mather, A.E. The Solubility of Carbon Dioxide in Water at Low Pressure. *J. Phys. Chem. Ref. Data* **1991**, *20*, 1201–1209. [CrossRef]
217. Kaur, H.; Abedi, S.; Chen, C.-C. Estimating CO_2 Solubility in Aqueous N^{a+}–K^+–Mg^{2+}–Ca^{2+}–Cl^-–SO_4^{2-} Solutions with Electrolyte NRTL–PC-SAFT Model. *J. Chem. Eng. Data* **2022**, *67*, 1932–1950. [CrossRef]

218. O'Sullivan, T.D.; Smith, N.O. Solubility and Partial Molar Volume of Nitrogen and Methane in Water and in Aqueous Sodium Chloride from 50 to 125.Deg. and 100 to 600 Atm. *J. Phys. Chem.* **1970**, *74*, 1460–1466. [CrossRef]
219. Prausnitz, J.M.; Lichtenthaler, R.N.; de Azevedo, E.G. *Molecular Thermodynamics of Fluid-Phase Equilibria*, 3rd ed.; Prentice-Hall International Series in the Physical and Chemical Engineering Sciences; Prentice Hall PTR: Upper Saddle River, NJ, USA, 1999; ISBN 978-0-13-977745-5.